

## MECHANISM OF SOLUTE RETENTION IN SUPERCRITICAL FLUID CHROMATOGRAPHY

C. R. Yonker, S. L. Frye, H. R. Udseth, R. W. Wright, and R. D. Smith

Chemical Methods and Kinetics Section, Pacific Northwest Laboratory,  
(Operated by Battelle Memorial Institute), Richland, Washington 99352

### Introduction

Retention in supercritical fluid chromatography (SFC) is determined by solute solubility in the fluid and solute interaction with the stationary phase. The functional relationship between retention and pressure at constant temperature has been described by Van Wassen and Schneider (1). The trend in retention is shown to depend on the partial molar volume of the solute in the mobile and stationary phase coupled with the isothermal compressibility of the fluid mobile phase.

The solubility of the solute in a fluid has been discussed by Gitterman and Procaccia (2) and solute solubility has been described over the entire region of pressures of interest. The combination of solute solubility in a fluid with the equation for retention as a function of pressure derived by Van Wassen and Schneider allows one to determine the effect of solubility on solute retention.

The purpose of this work was to determine the relationship between solubility and retention. A thermodynamic model was developed which predicts the trend in retention as a function of pressure, given the solubility of the solute in the fluid mobile phase. From this model, solute retention behavior can be examined by theory and experiment in order to gain some insight into the complicated dependence of retention on the thermodynamic and physical properties of the solute and the fluid, providing a basis for consideration of more subtle effects unique to SFC.

### Theory

In SFC, the basic assumption of infinitely dilute solutions of the solute in the mobile and stationary phases is valid. The concentration of the solute in these phases respectively is  $C_i = X_i/V_m$ , where  $X_i$  is the mole fraction of solute (i) and  $V_m$  is the molar volume of the pure mobile or stationary phase (1). Solute retention is calculated from a dimensionless retention factor,  $k$ , where,

$$k = (C_i^{\text{stat}}/C_i^{\text{mob}}) \cdot (V^{\text{stat}}/V^{\text{mob}}) \quad 1)$$

$C_i^{\text{stat}}$  and  $C_i^{\text{mob}}$  are the concentration of solute (i) in the stationary and mobile phases respectively,  $V^{\text{stat}}$  and  $V^{\text{mob}}$  are the volumes of the stationary and mobile phase. Substituting for concentration into equation 1,

$$k = (X_i^{\text{stat}}/X_i^{\text{mob}}) \cdot (V_m^{\text{mob}}/V_m^{\text{stat}}) \cdot (V^{\text{stat}}/V^{\text{mob}}) \quad 2)$$

Taking the natural logarithm of both sides of equation 2 one obtains,

$$\ln k = \ln (X_i^{\text{stat}}/X_i^{\text{mob}}) + \ln (V_m^{\text{mob}}/V_m^{\text{stat}}) + \ln (V^{\text{stat}}/V^{\text{mob}}) \quad 3)$$

At equilibrium, the solute chemical potential in the respective phases are equal  $\mu_i^{\text{stat}} = \mu_i^{\text{mob}}$  (3). Therefore,

$$\mu_i^{\text{stat}} = \mu_i^{\text{mob}} = \mu_i^{\text{stat}} + RT \ln X_i^{\text{stat}} = \mu_i^{\text{mob}} + RT \ln X_i^{\text{mob}} \quad (4)$$

where  $\mu_i^\infty$  is the chosen standard state of infinite dilution of solute (i) in the two phases. Rearranging equation 4,

$$\ln (X_i^{\text{stat}}/X_i^{\text{mob}}) = (\mu_i^{\text{mob}} - \mu_i^{\text{stat}})/RT \quad (5)$$

Substituting equation 5 into 3,

$$\ln k = (\mu_i^{\text{mob}} - \mu_i^{\text{stat}}) / RT + \ln (V_m^{\text{mob}} V_m^{\text{stat}} / V_m^{\text{stat}} V_m^{\text{mob}}) \quad (6)$$

An assumption can be made that the second term on the right-hand side (RHS) of equation 6 is independent of pressure except for  $V_m^{\text{mob}}$ , the molar volume of the fluid mobile phase. Therefore differentiation of equation 6 with respect to pressure at constant temperature yields,

$$(\partial \ln k / \partial P)_T = 1/RT [(\partial \mu_i^{\text{mob}} / \partial P)_T - (\partial \mu_i^{\text{stat}} / \partial P)_T] + (\partial \ln V_m^{\text{mob}} / \partial P)_T \quad (7)$$

The partial molar volume of a solute is defined as  $(\partial \mu_i / \partial P)_T$  (3) and on rearranging the second term on the RHS of equation 7 one obtains the isothermal compressibility of the fluid mobile phase (4). Thus on substitution equation 7 reduces to,

$$(\partial \ln k / \partial P)_T = 1/RT [\bar{V}_i^{\text{mob}} - \bar{V}_i^{\text{stat}}] - K \quad (8)$$

where  $\bar{V}_i^{\text{mob}}$  and  $\bar{V}_i^{\text{stat}}$  are the partial molar volume of the solute (i) in the mobile and stationary phases at infinite dilution respectively and K is the isothermal compressibility of the fluid mobile phase. Equation 8 is the same as obtained by Van Wassen and Schneider (1) in their derivation of the trend in retention as a function of pressure for SFC.

The solubility of a solid in a supercritical fluid has been described by Gitterman and Procaccia (2). The region of interest chromatographically will be for infinitely dilute solutions whose concentration is far removed from the lower critical end point (LCEP) of the solution. Therefore the solubility of the solute in a supercritical fluid at infinite dilution can be approximated as,

$$(\partial \ln X_i^{\text{mob}} / \partial P)_T = 1/RT [V^S - \bar{V}_i^{\text{mob}}] \quad (9)$$

where  $V^S$  is the molar volume of the pure solid solute. This is the same as equation 2.5 in Gitterman and Procaccia (2), describing solute solubility for dilute solutions far from criticality. Solving equation 9 for  $V_i^{mob}$ .

$$\bar{V}_i^{mob} = -RT (\partial \ln X_i^{mob} / \partial P)_T + V^S \quad (10)$$

Equation 10 can be substituted into equation 8 and upon rearrangement,

$$(\partial \ln k / \partial P)_T = (V^S - \bar{V}_i^{stat}) / RT - (\partial \ln X_i^{mob} / \partial P)_T - K \quad (11)$$

Equation 11 should be the relationship between retention-solubility and pressure at constant temperature for infinitely dilute solutions. The RHS of equation 11 consists of three terms, the first term will be a constant whose value depends on the partial molar volume of the solute in the stationary phase. The second term can be determined experimentally from bulk solubility measurements of the solute in the supercritical fluid mobile phase. The last term, the solvent isothermal compressibility, can be reasonably predicted from a two-parameter, cubic equation of state (EOS) such as the Redlich-Kwong EOS or the Peng-Robinson EOS (5,6).

The fluid mobile phases isothermal compressibility was determined using the Redlich-Kwong EOS to evaluate the derivative  $(\partial V_m^{mob} / \partial P)_T$  in equation 12,

$$(\partial \ln V_m^{mob} / \partial P)_T = (1/V_m^{mob}) \cdot (\partial V_m^{mob} / \partial P)_T = -K \quad (12)$$

From the Redlich-Kwong EOS,

$$(\partial V_m^{mob} / \partial P)_T = \frac{V_m^{mob} T^{0.5} (b^2 - (V_m^{mob})^2)}{P T^{0.5} (3 (V_m^{mob})^2 - b^2) - RT^{3/2} (2V_m^{mob} + b) + a} \quad (13)$$

where R is the gas constant, P is pressure, and T is temperature in K. The constants a and b of the Redlich-Kwong EOS are,

$$a = 0.4278 R^2 T_C^{2.5} / P_C \quad (14a)$$

$$b = 0.0867 RT_C / P_C \quad (14b)$$

where  $P_C$  and  $T_C$  are the critical pressure and temperature of the fluid. The molar volume of the fluid was determined by the Peng-Robinson EOS, thus allowing one to solve for the isothermal compressibility of the fluid.

Therefore from equation 11, the trend in retention as a function of pressure at constant temperature can be determined and it is related to the solubility of the solute in the supercritical fluid, the isothermal compressibility of the solvent and the partial molar volume of the solute in the stationary phase at infinite dilution.

## Experimental

The experimental apparatus and technique has been described in detail elsewhere (7,8). The retention factors of selected solutes under isothermal conditions at various pressures were obtained using capillary columns coated with a cross-linked phenyl polymethylphenylsiloxane stationary phase with carbon dioxide as the fluid mobile phase. A Varian 8500 syringe pump was operated under computer control providing accurate, pulsefree control of the fluid pressure. The retention times of the solute as a function of pressure were determined by a reporting integrator with an accuracy of a tenth of a second. Solubility data for the solutes in CO<sub>2</sub> was obtained from the literature ((9) and references therein).

## Results and Discussion

Solute retention as a function of pressure has been determined experimentally for a wide number of solutes over a range of temperatures and pressures (1,10-12). The trend in retention of a solute with pressure can be predicted from the simple thermodynamic model upon which equation 11 is predicted. Experimental data for the retention of naphthalene in CO<sub>2</sub> at 35°C over a pressure range was reported by Van Wasen and Schneider (12). The solubility of naphthalene in CO<sub>2</sub> is given by McHugh and Paulaitis at 35°C, 55.0°C, 60.4°C, and 64.9°C (13). This data allows the trend in retention to be predicted from the calculation of the slope of  $(\partial \ln k / \partial P)_T$  for naphthalene at 35°C in CO<sub>2</sub>.

A plot of  $\ln X_1^{\text{mob}}$  versus pressure is shown in Figure 1 based on the data from McHugh and Paulaitis (13). The slope  $(\partial \ln X_1^{\text{mob}} / \partial P)_T$  at 35°C was obtained by interpolation between the data points, also the data range was extended to lower pressures than given in reference (13) by fitting the data using the method outlined by Reid et al. (14). This allowed the modeling of the trend in retention for a wider range of pressure. The fluids isothermal compressibility can be easily calculated for any temperature and pressure range of interest. The solute partial molar volume in the stationary phase was assumed constant and independent of pressure (15). Available data suggests that for a highly cross-linked stationary phase coated in a capillary column solvation is very small or negligible (16), therefore  $V^{\text{stat}}$  and  $V_1^{\text{stat}}$  would be independent of pressure. The above simplifying assumptions allow one to calculate the trend in solute retention based on the solubility of the solute in the mobile phase. Figure 2 shows the fit of equation 11 to the experimental data of Van Wasen and Schneider (12). The partial molar volume of the solute naphthalene in the stationary phase was determined to be ~180 cm<sup>3</sup>/mole, this gave the best fit to the experimental data (naphthalene's molar volume is ~130.8 cm<sup>3</sup>/mole). The simple thermodynamic model fits the retention data very satisfactorily. More experimental data for CO<sub>2</sub> in coated capillary columns is being undertaken in our laboratory at the present time but preliminary results with the model are promising.

On closer examination of equation 11, one can deduce that as the isothermal compressibility of the solvent becomes less important (temperature and pressure further removed from the critical temperature and pressure),  $(\partial \ln k / \partial P)_T$  is proportional to the solubility of the solute in the fluid phase. Therefore, if solubility is found to be a linear function of density then retention will mirror this behavior and also be a linear function of density. Further, the farther one is from the critical pressure and temperature of the solvent the more likely one obtains a constant slope  $((\partial \ln k / \partial P)_T = \text{constant})$ .

## Conclusion

The simple thermodynamic relationship developed in this work has been shown to adequately describe the features of solute retention as a function of pressure at constant temperature for supercritical fluid chromatography. The importance of this model is the relationship drawn between solute solubility in the fluid mobile phase to the trend in solute retention. The trend in solute retention is demonstrated to be dependent on isothermal compressibility, solubility in the fluid and the partial molar volume of the solute in the stationary phase. The dependence of  $V_1$  on pressure is being examined and will be discussed in a future work. This change and further experimental investigations over the relevant ranges of temperature and pressure are in progress and will serve to guide future experimental and theoretical developments.

## Acknowledgments

The authors acknowledge the financial support of the U.S. Department of Energy, Office of Basic Energy Science, under Contract DE-AC06-76RL0 1830.

## References

- (1) Van Wasen, U.; Schneider, G. M., *Chromatographia*, (1975), 8, 274.
- (2) Gitterman, M.; Procaccia, I., *J. Chem. Phys.*, (1983), 78, 2648.
- (3) Klote, I. M.; Rosenberg, R. M., "Chemical Thermodynamics," 3rd Ed. W. A. Benjamin, Inc. (1972).
- (4) Van Ness, H. C.; Abbott, M. M., "Classical Thermodynamics of Mon Electrolyte Solutions with Applications to Phase Equilibria," McGraw-Hill Book Company (1982).
- (5) Redlich, O.; Kwong, J. N. S., *Chem Rev.*, (1949), 44, 233.
- (6) Peng, D. Y.; Robinson, D. R., *Ind. Eng. Chem. Fundam.*, (1976), 15, 59.
- (7) Wright, B. W.; Smith, R. D., *Chromatographia*, (1984), 18, 542.
- (8) Smith, R. D.; Kalinoski, H. T.; Udseth, H. R.; Wright, B. W., *Anal. Chem.*, (1984), 56, 2476.
- (9) Paulaitis, M. E.; Krukonis, V. J.; Kurnik, R. T.; Reid, R. C., *Rev. Chem. Eng.*, (1983), 1, 179.
- (10) Sie, S. T.; Rijnders, G. W. A., *Sep. Sci.*, (1967), 2, 729.
- (11) Semonian, B. P.; Rogers, L. B., *J. Chromatogr. Sci.*, (1978), 16, 49.
- (12) Van Wasen, U.; Schneider, G. M., *J. Phys. Chem.*, (1980), 84, 229.
- (13) McHugh, M.; Paulaitis, M. E., *J. Chem. Eng. Data*, (1980), 25, 326.
- (14) Reid, R. C.; Kurnik, R. T.; Holla, S. J., *J. Chem. Eng. Data*, (1981), 26, 47.

(15) Wicar, S.; Novak, J., *J. Chromatogr.*, (1974), 95, 1.

(16) McHugh, M.; Private communication.

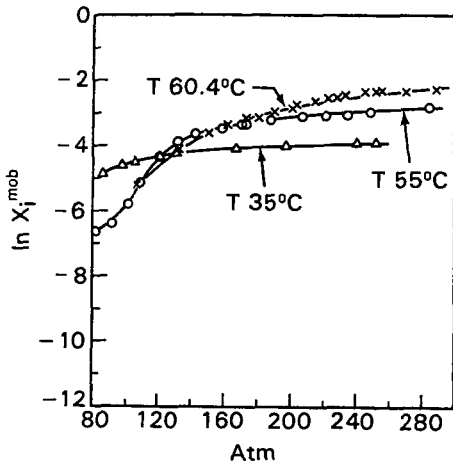


Figure 1. Plot of  $\ln X_1^{mob}$  against pressure in atmospheres at 35°C, 55°C, and 60.4°C. Data from McHugh and Paulaitis (13).

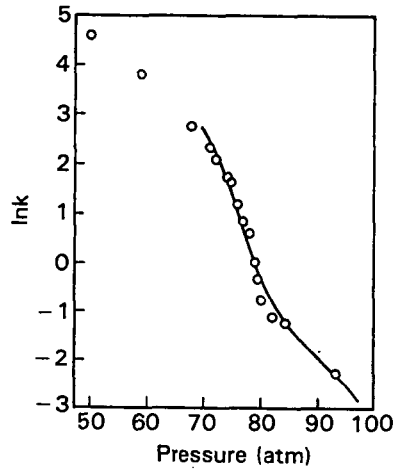


Figure 2. Experimental data for naphthalene with CO<sub>2</sub> (ref. 12) at 35°C and theoretical model (solid line).

## SEMI-PREPARATIVE SUPERCRITICAL FLUID EXTRACTION/FRACTIONATION

R.M. Campbell and M.L. Lee

Department of Chemistry, Brigham Young University, Provo, Utah 84602 USA

Supercritical fluids have been used with considerable success both as mobile phases in chromatography and as solvents in extraction processes. While packed columns have been used in chromatography with greatly reduced analysis times (1), ease of solvent removal has been one of the major benefits of extractions with supercritical CO<sub>2</sub> (2). The supercritical fluid extraction of caffeine from coffee and of nicotine from tobacco are only a few of the many uses of supercritical fluids for separations which have been reported. These have been reviewed previously (2). In several studies, packed columns were used to improve the separation of closely related compounds. For example, supercritical fluid fractionation (SFF) methods were used to isolate several polycyclic aromatic hydrocarbons (PAH) in an automobile exhaust extract (3). These studies have shown that the ability to instantaneously vary the solvating power of a supercritical fluid by changing its pressure (or density) can be used to great advantage. Using the selectivity of the mobile phase, compounds were resolved in SFC which would have required many more theoretical plates to resolve in gas chromatographic systems (4). This mobile phase selectivity can only be preserved by avoiding large pressure drops across the column which can occur in columns packed with very small particles or in systems operated at very high flow rates (5). In the present study, columns packed with silica materials of intermediate particle sizes (30 to 70  $\mu$ m) were used to prevent large pressure drops and allow dynamic pressure programming to achieve semi-preparative scale separations.

### EXPERIMENTAL

A supercritical fluid extraction/fractionation system was constructed to provide separations and fraction collection on a semi-preparative scale. A schematic diagram of this system is shown in Figure 1. The system included a 375-mL syringe pump (Isco, Lincoln, NE) modified for pressure control at flow rates of up to 8 mL/min (liquid), a chromatographic oven (Varian, Walnut Creek, CA), and four 125-mL fraction collection vessels which were fitted with cooling jackets. During fraction collection, the vessels were cooled to  $3 \pm 2^\circ\text{C}$  via a circulating cooling bath (Grant Science/Electronics, Dayton, OH). A six-port switching valve (Valco Instrument Co., Houston, TX) was used to collect successive fractions in different collection vessels. The collection vessels were pressurized with N<sub>2</sub> from a high pressure tank in conjunction with appropriate valving. A micrometering valve (Autoclave Engineering, Erie, PA) was used to control the flow when the effluent was vented directly to atmosphere. An extraction column (10 cm x 4.6 mm i.d.) and a separation column (25 cm x 4.6 mm i.d.) were placed in the oven, and effluents were monitored with a UV-absorbance detector (Hitachi, Model 100-10, Tokyo, Japan) equipped with a high pressure cell (Hewlett-Packard, Avondale, PA). All parts of the extraction/fractionation apparatus were constructed of stainless steel.

A coal tar was fractionated by adding 1 mg of the tar in 50  $\mu$ L of methylene chloride to the top of the extraction column which had been dry-

packed with 40-63  $\mu\text{m}$  silica (Sigma, No. S-0507, St. Louis, MO). The column end fittings (equipped with 2  $\mu\text{m}$  frits) were tightened and the column was installed in the oven by tightening the appropriate fittings. The separation column was dry-packed with  $\text{NH}_2$ -Adsorbosil (Applied Science, Deerfield, IL, 30 - 70  $\mu\text{m}$ ). The oven temperature was raised to 40°C and held there for the duration of the fractionation. The pressure was brought to 72 atm, then immediately raised to 95 atm at 8 atm/min. The pressure was held at 95 atm until phenanthrene began to elute (Fraction 3), whereupon it was raised at 1.5 atm/min to 98 atm. As soon as the fluoranthene/pyrene peak (Fraction 4) started eluting, the pressure was again programmed at 1.5 atm/min to 130 atm. At this point, as the chrysene peak (Fraction 5) was finishing, the pressure was programmed at 5 atm/min to 198 atm and held for about 10 min. Fractions were collected as marked on the chromatogram in Figure 3. Fractions were analyzed by capillary gas chromatography with an HP 5880 gas chromatograph equipped with a 20 m x 0.2 mm i.d. fused silica capillary column coated with SE-54 stationary phase which was crosslinked with azo-t-butane.

## RESULTS AND DISCUSSION

In 1977, Wise *et al.* (6) reported the separation of PAH according to number of aromatic rings using an HPLC system with a chemically bonded aminosilane stationary phase. This was very important because each of the ring-number cuts could then be analyzed by reversed phase HPLC, which provides resolution of closely related isomers. More recently, ring-number fractions of complex mixtures of PAH have been sought for analysis by GC with a liquid crystalline stationary phase, which exhibits excellent selectivity for the separation of geometric isomers (7,8).

Figure 2 shows the UV chromatogram of the fractionation of a number of standard PAH using the SFF system. A similar pressure program was used to fractionate a coal tar sample as shown in Figure 3. Figure 4 shows the capillary gas chromatograms of typical fractions of the coal tar extract obtained on the SFF system. The polar amino bonded phase provided good selectivity for separations by ring number. Alkylated species tended to elute at or near the same time as their parent compounds, while compounds of different ring structure were widely separated.

Samples were best introduced into the SFE system by applying the solutes in a small amount of solvent to the head of the column with a syringe. This method resulted in narrower bands than are obtained when the sample is distributed over the entire extraction column. An external sample loop injection valve was not used in the system because at the lower pressures used at the beginning of a fractionation run, all sample components were not dissolved, resulting in plugging of the frits at the head of the separation column.

Adsorbents of intermediate particle size (30-70  $\mu\text{m}$ ) were found to give the best separations. The trade-off between column efficiency and pressure drop was at or near optimum with this particle size. Smaller particles resulted in large pressure drops, while larger particles resulted in poor efficiency and large column dead volumes.

In addition, standard compounds were used to study the effect of mobile phase density on resolution of closely related compounds. The resolution of biphenyl and acenaphthalene was measured at a number of different mobile phase densities. Results of this study are listed in Table I. It was found that, in general, the resolution of a pair of closely related isomers could be improved by as much as 100% by decreasing the mobile phase pressure at

constant temperature on a given column. However, it was also concluded that the particle size of the packing in the column has a large effect on resolution as well. Column efficiency, which is solely dependent on the particle size of the column packing material, may have a greater effect on resolution than the selectivity of the mobile phase. Also, by going to smaller particle diameter of the column packing, analysis times can be shortened. However,

Table 1. Resolution of Acenaphthalene and Biphenyl at Various Pressures of CO<sub>2</sub> at 40°C and using a 35-70 μm NH<sub>2</sub>-silica column.

<u>Pressure</u>	<u>Resolution</u>
85	1.1
90	1.1
100	0.8
120	0.9
140	0.9
160	0.9
180	0.7
198	0.5

large pressure drops across columns packed with very small particles cause significant selectivity losses. For some solutes, the gain in efficiency is greater than the loss in selectivity on going to a smaller diameter packing. It was concluded that particles in the 35-80 μm range were best for the separations we have attempted thus far.

UV monitoring of the column effluents was essential to enable precise cuts during fractionation on a routine basis as well as during development. Solute in the fractions were best collected by cooling the collection vessels to 2 to 5°C. This created a two-phase (gas/liquid) region in the collection vessels, causing the solutes to precipitate out of the gas phase. In this way, the solutes were removed from the CO<sub>2</sub> before it decompressed through the fused silica restrictors. The cooling was not enough to cause precipitation of very volatile solutes such as naphthalene. Therefore, fractions containing very volatile components were collected by bubbling the effluents through methylene chloride or *n*-pentane.

With our current pumping system, the maximum sample capacity appears to be about 10 to 20 mg per run. Figure 5 shows the UV SFF chromatogram of 8 mg of coal tar extract obtained on a 25 cm x 6.2 mm i.d. column with a 10 cm x 6.2 mm i.d. sample introduction column. The NH<sub>2</sub>-Adsorbosil stationary phase was used in this case as well. Fractions were again collected as marked on the chromatogram. Typical analysis times for separations of components ranging from 2 to 5 rings was between 1 and 1.5 h.

Overall, it was found during this study that semi-preparative supercritical fluid fractionation shows great potential for high quality separations with easy solvent removal.

## REFERENCES

1. Gere, D.R.; Board, R.; McManigill, D. Anal. Chem. **1982**, 54, 736-740.
2. Randall, L.G. Sep. Sci. Tech. **1982**, 17, 1-118.
3. Jentoft, R.E.; Gouw, T.H. Anal. Chem. **1976**, 48, 2195-2200.
4. Sie, S.T.; Rijnders, W.A. Sepr. Sci. **1967**, 2, 755.
5. Peaden, P.A.; Lee, M.L. J. Lig. Chromatogr. **1982**, 5 (Suppl. 2), 179-221.
6. Wise, S.A.; Chesler, S.N.; Hertz, H.S.; Hilpert, L.R.; May, W.E. Anal. Chem. **1977**, 49, 2306.
7. Kong, R.C.; Lee, M.L.; Tominaga, R.; Pratap, M.; Iwao, M.; Castle, R.N. Anal. Chem. **1982**, 54, 1802.
8. Markides, K.E.; Nishioka, M.; Tarbet, B.J.; Bradshaw, J.S.; Lee, M.L. Anal. Chem., in press.

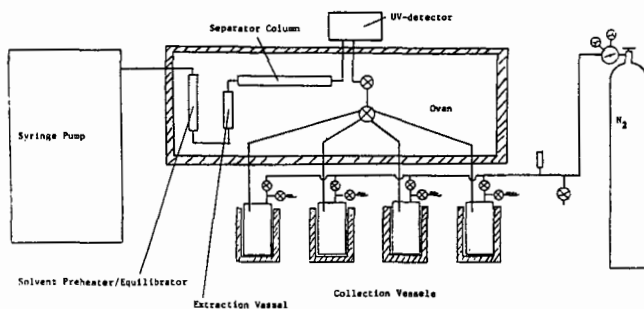


Figure 1. Schematic diagram of the supercritical fluid extraction/fractionation system.

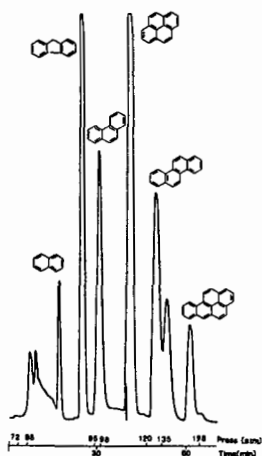


Figure 2. UV chromatogram of the supercritical fluid fractionation of a number of standard compounds with  $\text{CO}_2$  at  $40^\circ\text{C}$ .

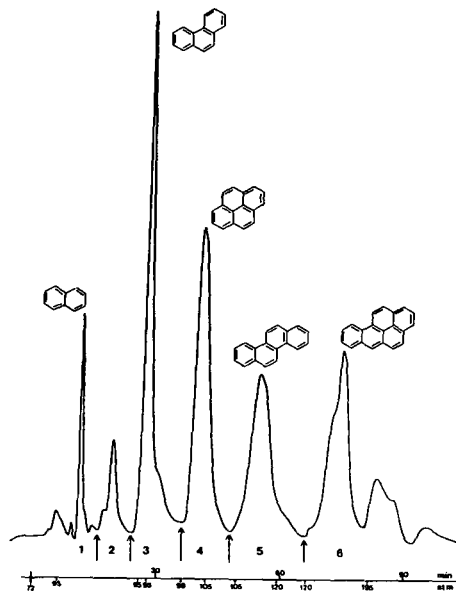


Figure 3. UV chromatogram of the supercritical fluid fractionation of 1 mg of a coal tar extract with  $\text{CO}_2$  at  $40^\circ\text{C}$ . The numbers 1-6 indicate the fractions that were collected.

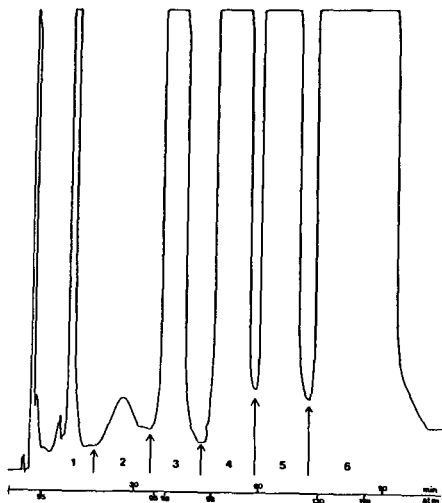


Figure 5. UV chromatogram of the supercritical fluid fractionation of 8 mg of the coal tar extract with  $\text{CO}_2$  at  $40^\circ\text{C}$ .

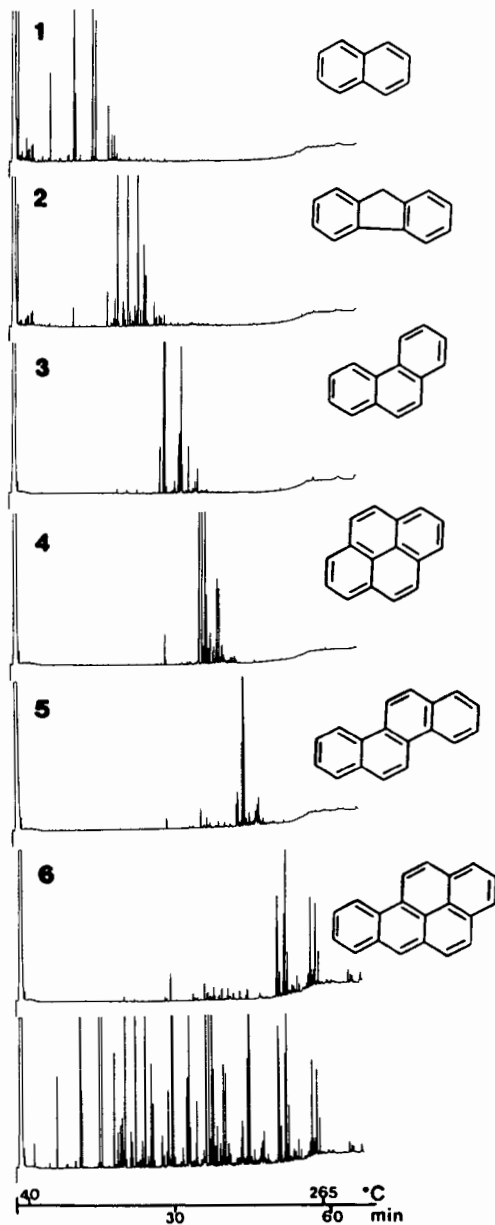


Figure 4. Capillary gas chromatograms of the six fractions collected during the supercritical fluid fractionation of the coal tar extract. The numbers refer to the fractions shown in Figures 3 and 5. The bottom chromatogram shows the total unfractionated coal tar for comparison.

## Supercritical Carbon Dioxide Extraction of Lemon Oil

Steven J. Coppella and Paul Barton\*

Department of Chemical Engineering  
The Pennsylvania State University  
University Park, PA 16802

In 1983-1984, Arizona and California produced annually over 10<sup>6</sup> kg of cold-pressed lemon oil. After being concentrated by distillation or liquid extraction, lemon oil is used as flavoring and/or fragrance agent in beverages and cosmetics. Distillation thermally degrades lemon oil. Extraction with organic solvents only partially reduces thermal degradation (since the solvents must be recovered by distillation) and introduces solvent contamination. Extraction with nonfermentative supercritical carbon dioxide near its critical point (304.3 K, 7.38 MPa, 0.467 g/cm<sup>3</sup>) offers a cheap, nontoxic solvent that does not impart flavors nor thermally degrade the product. It can handle feedstocks with high wax content because these constituents can be solubilized in supercritical carbon dioxide. Supercritical extraction is a hybrid unit operation in the domain between extractive distillation and liquid extraction. Solvent recovery is accomplished by depressurization at ambient temperature.

Processes for supercritical extraction of oils have been described in numerous literature references. Several recent ones are Paulaitis et al. (1983), Ely and Baker (1983), Gerard (1984), Stahl et al. (1984), and Robey and Sunder (1984). The literature lacks detailed data on multicomponent essential oils with supercritical solvents in the proximity of the solvent critical temperature. Accurate prediction of data in this region by equations of state is limited to binary and ternary systems.

The purpose of our research is threefold: evaluate the feasibility of supercritical carbon dioxide extraction of lemon oil near ambient temperature, generate equilibrium data with carbon dioxide and multicomponent essential oil constituents, and evaluate the ability of the Peng-Robinson equation of state to model a reduced multicomponent supercritical system.

### CONCENTRATING LEMON OIL

Staroscik and Wilson (1982) have quantitated various lemon oils and identified 38 compounds. These compounds can be subdivided into three major classifications: terpenes (C<sub>10</sub> hydrocarbons), oxy's (oxygenated C<sub>8</sub>-C<sub>12</sub> hydrocarbons), and sesquiterpenes (C<sub>15</sub> hydrocarbons). A usual goal in concentrating lemon oil is to remove the terpenes and sesquiterpenes from the desired oxy fraction.

When concentrating the lemon oil by multistage fractional distillation under vacuum, column operability coupled with condenser pressure, column pressure drop, reboiler design, and mode of operation (batch or continuous) dictate the degree of thermal exposure. Overhead temperatures increase in the range of 320 to 340 K, reboiler temperatures increase in the range of 330 to 370 K, and exposure times of 15 to 20 hours may be expected during batch distillation. In continuous distillation, exposure times are lower but reboiler temperature may be higher.

In extractive distillation with supercritical solvent, volatility amplification by the solvent rather than vacuum is used to get the components into the extract or vapor phase. Operating temperature can be made lower than in conventional distillation, and the heart-cut product will have been subjected to less thermal degradation. Carbon dioxide has a critical temperature that meets this goal.

In order to make data correlation tractable in supercritical carbon dioxide extraction, it is convenient to represent each major chemical classification by a single compound. Each select compound should have available good vapor pressure data and should be a predominant constituent in its group with regard to structure and concentration. For correlation purposes, we selected limonene, geranial, and  $\beta$ -caryophyllene. Their structures are shown in Figure 1.

Stahl et al. (1984) presented solubility data for limonene and caryophyllene with carbon dioxide; Gerard (1984) included carvone. Temperatures in the range of 279 to 377 K, and pressures in the range of 1.5 to 11 MPa were covered. Robey and Sunder (1984) provided solubility and relative volatility data for carbon dioxide with folded lemon oil and with limonene and citral (geranial/neral) at 323 to 353 K and 9.4 to 10.6 MPa.

Gerard (1984) describes a continuous multistage column process for carbon dioxide extraction (distillation) of essential oils at ambient temperature and 8 MPa, with solvent recovery at 273 K and 3 MPa. Robey and Sunder (1984) propose a lemon oil fractionator operated at 333 K and 10 MPa with an efficiency equivalent to 12 stages, with solvent recovery at 293 K and 5.5 MPa.

#### EXPERIMENTAL SECTION

Cold-pressed oil from Arizona early desert lemons was supplied by A. M. Todd Company, Kalamazoo, MI. Degassed lemon oil and dry carbon dioxide were charged into the one-liter isothermal constant volume cell shown in Figure 2. After the operating temperature was reached, the system was stirred for one hour, then allowed to settle for 15 minutes before sampling. Experiments were performed at 303 to 313 K and 4 to 9 MPa. Parallel phase visualization experiments were conducted in a sight gauge to insure operation in the two-phase region.

A sample of the equilibrated liquid phase was removed (after purging) by depressurization through a valve and hypodermic tubing into a two-stage trap cooled by dry ice - acetone. A wet test meter measured the carbon dioxide off-gas. A sample of the vapor phase was then similarly removed. Purge and sample sizes were kept small to minimize disturbance of equilibrium. Pressure changes in the cell were 0-0.1 MPa during sampling of liquid phase and 0-1.2 MPa during sampling of vapor phase. Special high-pressure sample valves with microliter-sized traps were tried in an effort to reduce pressure disturbance, but reliability was inadequate.

Estimated relative errors are 0.2% for temperature, 5% for pressure, 4% for carbon dioxide mole fraction in the liquid phase, and 10% for lemon oil mole fraction in the vapor phase.

The recovered lemon oil samples were analyzed by gas chromatography. A 0.5 mm i.d. x 30 m thin film (0.1  $\mu$ m) SE-30 glass capillary column (Supelco, Inc., Bellefonte, PA) was used with a flame ionization detector in a F&M 810 chromatograph. The unit was fitted with a temperature programmer (F&M Scientific Model 240), glass-lined inlet splitter (J&W Scientific, Inc.), and integrator (Hewlett-Packard Model 3370B). No reference column was used. The following conditions were employed: 27 cm/s He carrier gas; 250 cm<sup>3</sup>/min air, 40 cm<sup>3</sup>/min N<sub>2</sub>, and 55 cm<sup>3</sup>/min H<sub>2</sub> to detector; 0.4  $\mu$ l sample size, 27/1 split ratio; temperature program 348 K hold 8 minutes, 4 K/min, 473 K hold 15 minutes; injection port temperature 523 K; detector temperature 523 K; attenuation X1, range 10 $\times$ ; slope sensitivity 0.01 mV/min; manual baseline reset; chart speed 1.3 cm/min. Baseline drift was 0.02 mV/125 K. Peak areas from the integrator were within 5% of those determined by cutting and weighing the peaks.

Peak identification was based on information of Supelco, Inc., A. M. Todd Company, and Staroscik and Wilson (1982). Staroscik (1984) provided us with the response values used in his work and we assumed that our detector would give proportionate response. Staroscik found in his work that relative standard deviations were generally less than 3%.

## RESULTS

Lemon oil-carbon dioxide equilibrium was measured at 303, 308, and 313 K and in the pressure range of 4 to 9 MPa. Below 6 MPa, there was insufficient lemon oil in the vapor phase to attain good samples for analysis. Above 9.0 MPa at 313 K, above 7.8 MPa at 308 K, and above 7.4 MPa at 303 K, the system reverted to a single phase. Nine experiments provided two-phase, vapor-liquid equilibrium data suitable for correlations and generating coefficients for the Peng-Robinson equation. Detailed experimental data can be found in Coppella (1985).

The results of an experiment at 308 K and 6.98 MPa are detailed here. The liquid phase contained 48 wt% (74 mole %) carbon dioxide and the vapor phase contained 99.5 wt% (99.8 mole %) carbon dioxide. A gas chromatogram for the lemon oil from the liquid phase sample is shown in Figure 3. A chromatogram for the lemon oil in the vapor phase is shown in Figure 4. Peak identification, retention, response value, and concentration for these traces are given in Table I. Average molecular weight of lemon oil is 137.9 in liquid and 136.4 in vapor.

The relative volatility in the presence of carbon dioxide, or selectivity factor, for each component with respect to limonene is also given in Table I. Relative volatility is defined as the ratio of equilibrium vaporization  $K$  for component 1 to equilibrium vaporization  $K$  for limonene. Equilibrium vaporization  $K_1$  is defined as mole fraction 1 in the vapor (extract) phase to mole fraction 1 in the liquid (raffinate) phase.

By comparing the relative volatilities of various components, the ease of separation between these components can be determined. The chromatographic column employed separates components in the order of volatility; thus, the first cut point in the separation should be between terpinolene and adjacent oxygenated compounds. The chromatograph doesn't separate terpinolene from linalool or nonanal, so the separability of these compounds couldn't be determined. The next adjacent separation involves terpinolene with a relative volatility with respect to limonene of 0.7 and citronellal with a relative volatility with respect to limonene of 0.4. The relative volatility of terpinolene to citronellal is then 0.7/0.4 or 2. For the limonene/geranial pair, the relative volatility is 1.0/0.2 or 5. These separation factors for the terpene-oxy split are adequate.

The second cut point in the separation is between geranylacetate and  $\beta$ -caryophyllene. This separation factor is 0.06/0.07, or 0.9. This is opposite that of 0.2/0.07 or 3 for geranial to  $\beta$ -caryophyllene.

There is some overlap in the volatilities of  $C_{12}$  oxy and sesquiterpenes, which means that for extractions of lemon oil with supercritical carbon dioxide, some  $\beta$ -caryophyllene will be extracted into the heart-cut oxy product. This is the result of the nonpolar carbon dioxide preferentially extracting the less polar of the lemon oil constituents.

## SOLUBILITY AND SELECTIVITY

Solubility diagrams were prepared for the phases that separated in the lemon oil extractions performed in this study with carbon dioxide. Such diagrams can serve

only as guides, since solubility is composition-dependent and is a function of extraction severity. The data are shown in Figures 5, 6, and 7 at 303, 308, and 313 K, respectively.

Extractions or extractive distillations with supercritical solvent need to be performed at as high as possible a solubility of oil in the extract or vapor phase in order to reduce the solvent or carrier gas requirement. From our lemon oil-carbon dioxide phase diagrams, it appears that the highest practical solubility level is 0.9 mole % (2.8 wt.%) essential oil. This is attainable at 313 K. At lower temperature, sensitivity of solubility to pressure requires that solubility be lower (e.g., 0.3 mole % at 308 K).

At 313 K and 8.4 MPa, slope of extract phase solubility versus pressure is 0.06 weight fraction oil/MPa. For a 15 m tall extraction tower operated at a density of 0.5 g/cm<sup>3</sup>, the pressure at the bottom is higher than that at the top by 0.025 MPa. The solubility at the bottom will then be 0.15 wt.% higher at the bottom (ignoring composition effects). At 308 K and 7.69 MPa, an increase in pressure of 0.14 MPa causes the two-phase system to revert to a one-phase system. It is imperative that temperature and pressure profiles in the supercritical extraction tower be maintained accurately. Windows are recommended to confirm that operation remains in the two-phase domain.

The selectivities in supercritical carbon dioxide extraction of terpenes from oxs, and oxs from sesquiterpenes, for lemon oil are shown in Figures 8 and 9, respectively. Figure 8 shows the relative volatility, or selectivity factor, of limonene to geranial as a function of oil solubility in the vapor phase. Operation of the extractor at 308 K and 1 wt.% solubility provides a relative volatility of 2. Operation at 313 K provides a relative volatility of 1.4. The selectivity factors, though adequate, are an order of magnitude lower than the vapor pressure ratio.

Figure 9 shows the relative volatility of geranial to  $\beta$ -caryophyllene as a function of oil solubility in the vapor phase. At 313 K and 1 wt.% volatility, relative volatility is 1.4. At 308 K and 1 wt.% solubility, these constituents are inseparable by supercritical carbon dioxide extraction. The ratio of vapor pressures for this pair is in the vicinity of 2.

#### MODELING OF EQUILIBRIA

The carbon dioxide:lemon oil P-x behavior shown in Figures 5, 6, and 7 is typical of binary carbon dioxide:hydrocarbon systems, such as those containing heptane (Im and Kurata, 1971), decane (Kulkarni et al., 1972), or benzene (Gupta et al., 1982). Our lemon oil samples contained in excess of 64 mole % limonene; so we modeled our data as a reduced binary of limonene and carbon dioxide. The Peng-Robinson (1976) equation was used, with critical temperatures, critical pressures, and acentric factors obtained from Daubert and Danner (1983), and Reid et al. (1977). For carbon dioxide,  $\omega = 0.225$ ; for limonene  $\omega = 0.327$ ,  $T_c = 656.4$  K,  $P_c = 2.75$  MPa. It was necessary to vary interaction parameter with temperature in order to correlate the data satisfactorily. The values of  $d_{12}$  are reasonable (0.1135 at 303 K, 0.1129 at 308 K, 0.1013 at 313 K). Comparisons of calculated and experimental results are given in Figures 5, 6, and 7.

Attempts to model the relative volatilities of the minor organic constituents to limonene using the Peng-Robinson equation proved unfruitful.

### PROPOSED PROCESS

Lemon oil can be concentrated by supercritical carbon dioxide extraction in the temperature range of 308 to 313 K. Pressure in the extractor will be in the range of 7.7 to 8.5 MPa. Solubilities of oil in the extract, or vapor, phase will range from 1 to 3 wt.%. Selectivity factors near 1.4 will be attained for the terpene-oxy split and oxy-sesquiterpene split. The operation is performed in a multistage extractor with reflux. Operation can be either in the batch or continuous mode. Solvent recovery is performed at conditions slightly below the critical point of carbon dioxide.

Solubility limitations require that the solvent treat be high; an economic analysis is needed to establish process feasibility.

### REFERENCES

Coppella, S. J.; M.S. Thesis, The Pennsylvania State University, University Park, PA, 1985.

Daubert, T. E.; Danner, R. P.; eds. "Technical Data Book - Petroleum Refining," 4th ed., American Petroleum Institute, Washington, DC (1983).

Ely, J. F., Baker, J. K., NBS Technical Note 1070, 1983.

Gerard, D., Chem., Ing. Tech., 1984, 56, 794.

Gupta, M. K.; Li, Y. H.; Hulsey, B. J.; Robinson Jr., R. L., J. Chem. Eng. Data, 1982, 27, 55.

Im, U. K.; Kurata, F., J. Chem. Eng. Data, 1971, 16, 412.

Kulkarni, A.A.; Zarah, B. Y.; Luks, K. D.; Kohn, J. P., J. Chem. Eng. Data, 1972, 19, 92.

Paulaitis, M. E.; Krukonis, V. J.; Kurnik, R. T.; Reid, R. C., Reviews in Chemical Engineering, 1983, 1, 179.

Peng, P. Y.; Robinson, D. B., I.E.C. Fund., 1976, 15, 59.

Reid, R. C.; Prausnitz, J. M.; Sherwood, T. K., "The Properties of Gases and Liquids," 3rd ed., McGraw-Hill Book Co., New York (1977).

Robey, R. J.; Sunder, S., 1984 Annual Meeting American Institute of Chemical Engineers, San Francisco, CA, 1984.

Stahl, E.; Quirin, K. W.; Glatz, A.; Gerard, D.; Rau, G., BBPCA, 1984, 88, 900.

Staroscik, J. A., Sunkist Growers, Inc., Ontario, CA, personal communication, 1984.

Staroscik, J. A.; Wilson, A. A., J. Agric. Food Chem., 1982, 30, 507, 835.

TABLE I  
LEMON OIL VAPOR-LIQUID ANALYSES AT EQUILIBRIUM IN CO<sub>2</sub>

PEAK NO.	COMPOUND	RETENTION <sup>a</sup> RELATIVE TO LIMONENE	WEIGHT <sup>b</sup> RELATIVE RESPONSE	MOLE %		VOLATILITY RELATIVE TO LIMONENE
				VAPOR	LIQUID	
ref	acetone	0.00	-	-	-	-
1	$\alpha$ -thujene	0.55	0.75	0.61	0.35	1.8
2	$\alpha$ -pinene	0.58	0.75	2.80	1.68	1.7
3	camphene	0.63	0.70	0.09	0.06	1.6
4	sabinene } $\beta$ -pinene }	0.76	0.74	17.27	13.06	1.34
5	myrcene	0.79	0.73	1.87	1.59	1.2
6	octanal } phellandrene }	0.86	1.17	0.09	0.07	1.3
7	$\alpha$ -terpinene	0.92	1.19	1.21	1.10	1.1
8	limonene	1.00	0.75	67.14	68.22	1.0
9	$\gamma$ -terpinene	1.09	0.78	7.59	8.45	0.91
10	terpinolene } linalool } nonanal }	1.19	0.78	0.47	0.67	0.7
11	citronellal	1.40	1.06	0.02	0.04	0.4
12	terpinenen-4-ol	1.51	0.92	0.02	0.04	0.4
13	$\alpha$ -terpineol	1.55	0.92	0.06	0.20	0.3
14	decanal	1.60	0.97	0.01	0.08	0.1
15	neral	1.70	0.96	0.24	0.92	0.3
16	geranial	1.80	0.96	0.29	1.45	0.2
17	nonylacetate	1.95	0.24	0.00	0.03	-
18	nerylacetate	2.12	1.02	0.03	0.25	0.1
19	geranylacetate	2.18	1.02	0.009	0.15	0.06
20	$\beta$ -caryophyllene	2.36	0.78	0.013	0.18	0.07
21	<i>trans</i> - $\alpha$ -bergamotene	2.40	0.78	0.016	0.26	0.06
22	$\alpha$ -humalene	2.53	0.71	0.00	0.05	-
23	$\beta$ -bisabolene	2.60	0.77	0.013	0.38	0.03

<sup>a</sup> Retention time for limonene averaged 8.7 minutes

<sup>b</sup> Peak area multiplier

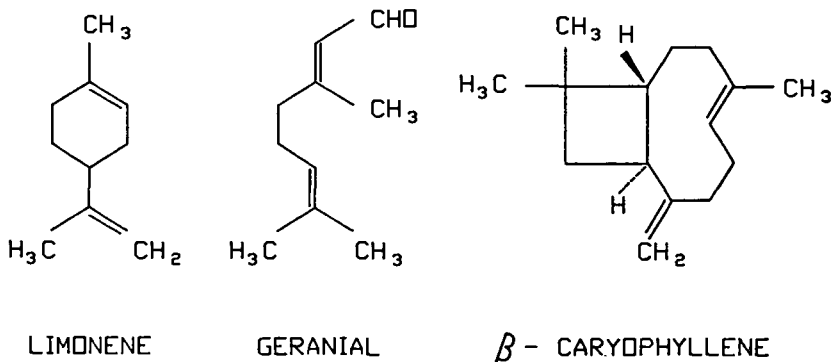


Fig. 1. Key constituents in lemon oil.

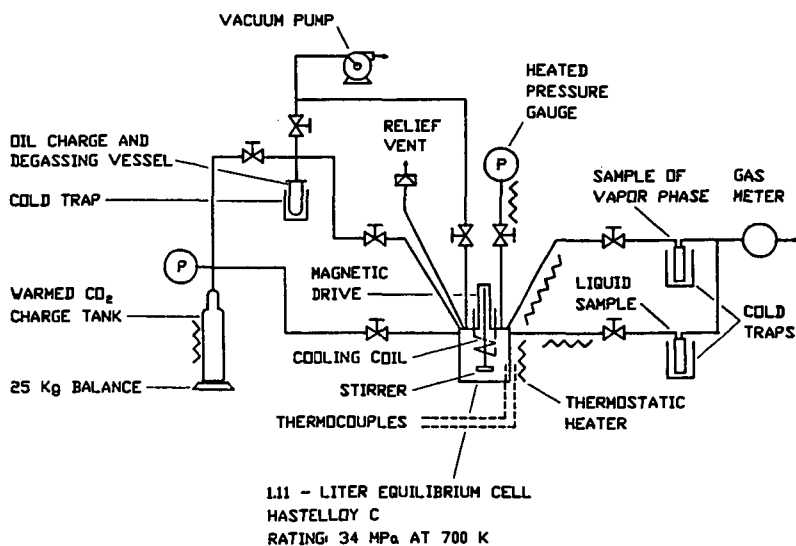


Fig. 2. Vapor-liquid equilibrium apparatus

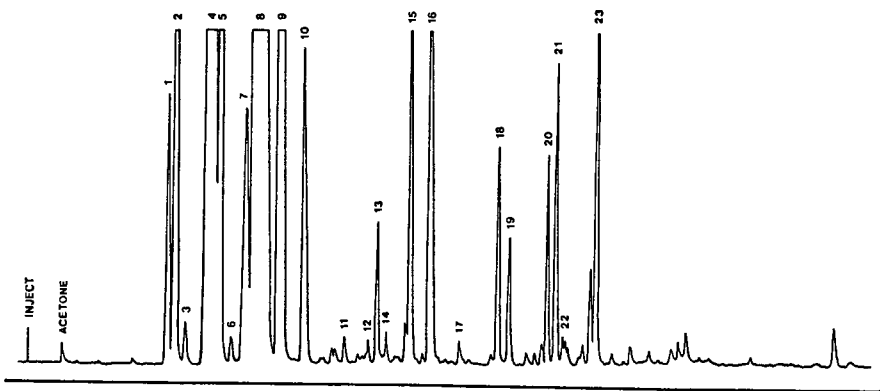


Fig. 3. Gas chromatogram of lemon oil in liquid phase sample

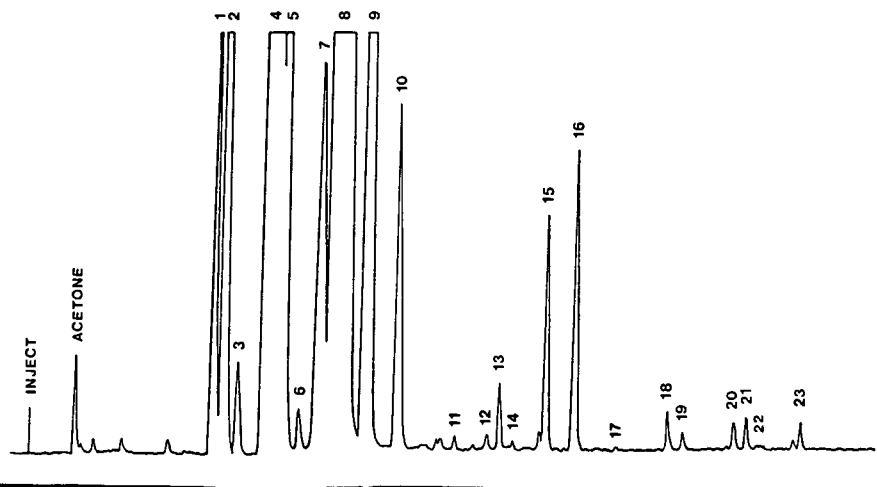


Fig. 4. Gas chromatogram of lemon oil in vapor phase sample

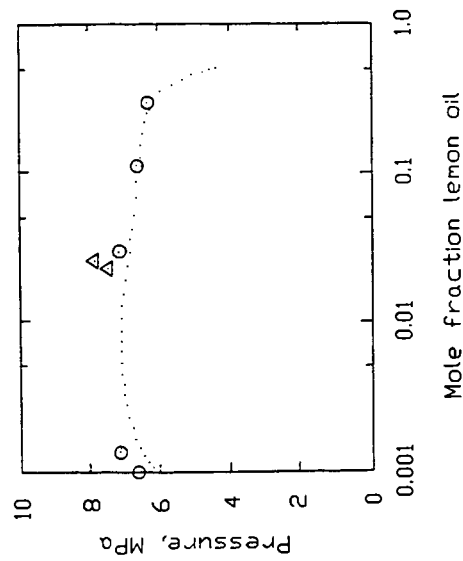


Fig. 5. Phase equilibrium for carbon dioxide : lemon oil at 303 K.  
 o - experimental two-phase  
 Δ - experimental one-phase  
 . . . Peng-Robinson eq.

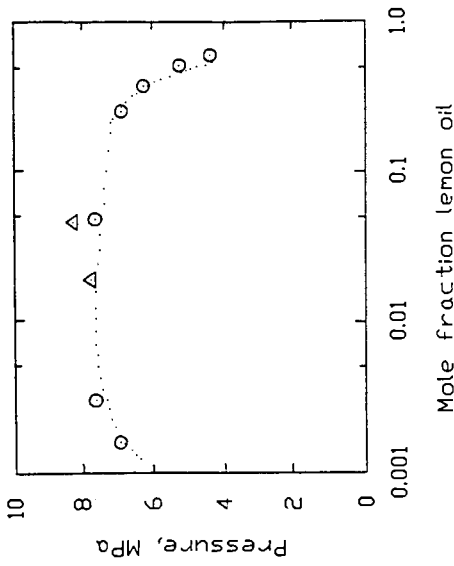


Fig. 6. Phase equilibrium for carbon dioxide : lemon oil at 308 K.  
 o - experimental two-phase  
 Δ - experimental one-phase  
 . . . Peng-Robinson eq.

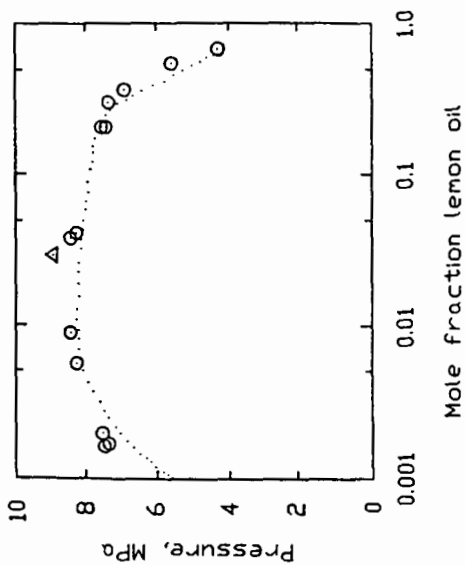


Fig. 7. Phase equilibrium for carbon dioxide : lemon oil at 313 K.  
 o - experimental two-phase  
 Δ - experimental one-phase  
 ... Peng-Robinson eq.

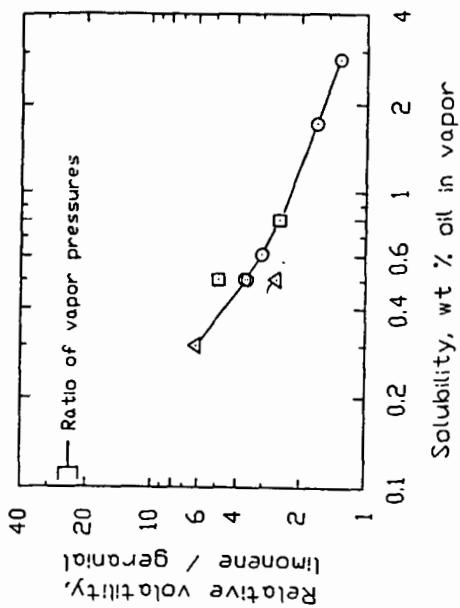


Fig. 8. Lemon oil : carbon dioxide vapor-liquid equilibria. Δ - 303 K.  
 □ - 308 K. o - 313 K.

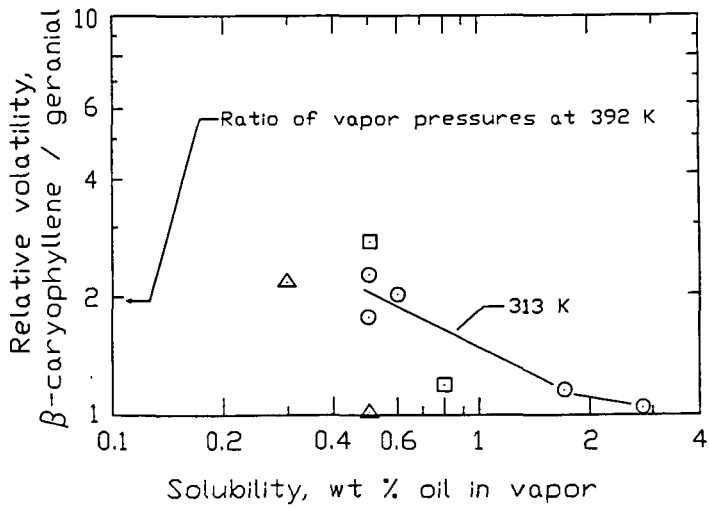


Fig. 9. Lemon oil : carbon dioxide vapor-liquid equilibria.  $\Delta$  - 303 K.  $\square$  - 308 K.  $\circ$  - 313 K.

## FRACTIONATION OF ETHYL ESTERS FROM FISH OIL

by Dr. Wilhelm O. Eisenbach

Max-Planck-Institut für Kohlenforschung 4330 Mülheim-Ruhr West Germany

### 1. Introduction

In this paper the efficiency of supercritical fluid extraction as a separation procedure will be presented, as an example the fractionation of a mixture of high boiling substances is described. Generally the product dissolved in a supercritical fluid can be separated either by increasing the temperature at constant pressure (isobaric method) or by lowering the pressure at constant temperature (isothermal method). Both phenomena can be used in fractionation procedures.

#### 1.1 Variation of Pressure

Discontinuous variation of the pressure in either the extraction vessel or in the separator can lead to fractionation. In the first case the pressure and hence the density of the extraction agent is increased in a stepwise manner with the result that material is taken up into the supercritical phase in order of increasing boiling point or molecular weight. The dissolved material can be isolated then in either an isobaric or isothermal manner. In practice the pressure is generally raised after extraction at the lower pressure is completed.

Alternatively the extraction can be carried out at a constant pressure in the extraction vessel and the loaded supercritical phase will be expanded in a step-wise manner whereby the least volatile components are deposited first, while the better volatile components remain dissolved in the supercritical phase.

#### 1.2 The Hot Finger

The other application of fractionation by increasing the temperature is shown in Figure 1. The extraction vessel has been combined with a rectification column consisting of a pressure tube packed with stainless steel packings. A heated head of column, the so-called Hot Finger, is fitted onto the top of the column and is held at a higher temperature than the rest of the apparatus. On contact with the Hot Finger the density of the supercritical loaded phase decreases and the less volatile components condense and drop back into the column and are subjected to rectification in the same manner as in a conventional distillation. The product still dissolved in the supercritical phase after passing the Hot Finger is isolated by decreasing the pressure as already described.

### 2. Fractionation of Fatty Acid Ethyl Esters

As an example of various applications which are investigated at the Max-Planck-Institut für Kohlenforschung in Mülheim-Ruhr in this paper the fractionation of a mixture of ethyl esters of fatty acids is

described. This investigation was concerned with the separation of eicosapentaenoic acid (EPA) out of a mixture of fatty acid ethyl esters from codfish oil. The starting material consisted of ethyl esters of saturated and unsaturated fatty acids from C(14) to C(22) partly containing up to 6 double bonds. In order of the high boiling points of these esters a conventional vacuum distillation needs relatively high temperatures so that, first, decomposition cannot be excluded and, second, a separation into single components is hardly possible.

In co-operation with the NIPPON SUISAN KAISHA, LTD - TOKYO (Japan) it was tried to fractionate such a mixture, the composition is shown in table 1, by using supercritical carbon dioxide to isolate a C(20-5)-rich fraction. (x-y) means the ethyl ester of a fatty acid with x carbon atoms and y double bonds.

Table 1 Composition of the Codfish Oil

Acid	%	Acid	%
14-0	5.80	20-1	11.43
15-0	0.19	20-4	0.50
16-0	12.88	20-5	14.46
16-1	9.79	22-1	8.64
18-0	2.66	22-4	0.43
18-1	23.25	22-5	0.49
18-2	0.16	22-6	5.74
18-4	2.19		

In a series of experiments carried out in an equipment similar to that shown in figure 1 various conditions were investigated to optimize this procedure, mainly the following:

1. The increase of the temperature of the Hot Finger in order to increase the reflux ratio.
2. The increase of the pressure to get a higher loading of the supercritical phase.
3. Variation of the length of the column and of the packings

In all these experiments the temperature of the extraction vessel, column and separator was kept constant at 50°C, the supercritical loaded phase was expanded to 25 bar in the separator and the flow rate of the supercritical carbon dioxide amounted to about 25 l/h. Samples of the loaded supercritical phase after passing the Hot Finger were analyzed each hour by gaschromatography.

## 2.1 Variation of the Temperature of the Hot Finger

### 2.11 Without the Hot Finger

The first experiment was carried out without the influence of the Hot Finger that means, the temperature of the Hot Finger was kept also at 50°C. The starting material was divided into 10 fractions by SCF extraction with supercritical carbon dioxide. It shows that no separation comes off, only an enrichment of the lower boiling esters C(14) and C(16) in the first fractions and of C(20) and C(22) in the later fractions according to their boiling points.

## 2.12 With the Hot Finger

The variation of the temperature of the Hot Finger really led to an increase of the reflux ratio but the selectivity decreased by exceeding the temperature of 90°C.

The curves in figure 2 show the difference in selectivity at the two temperatures 90 and 100°C. Here out of the whole mixture only the content of two components in the supercritical loaded phase, that are the sum of C(16)- and C(20)-esters analyzed by GC, are plotted versus the extraction time. To get a high purity combined with a yield as high as possible at 90°C one is able to collect a fraction amounting to 13.5% of the starting material containing 50% of the C(20)-esters of the feed-stock with a purity of 96.2%. At 100°C it is only possible to collect 25.7% of the C(20)-esters with a maximum concentration of 85.5%.

## 2.2 Variation of Pressure

The loading of the supercritical carbon dioxide depends on the pressure of the system. Under constant conditions of temperature and flow rate of the supercritical carbon dioxide the increase of the loading with raising the pressure can be demonstrated by the extraction rate: at 150 bar 15 g/h extract could be isolated, at 170 bar the amount was 55 g/h and at 200 bar 140 g/h. But the higher extraction rate was accompanied by a decrease in selectivity, at 200 bar no fractionation could be realized.

## 2.3 Results of Optimization

The results of these optimization experiments suitable only for the equipment we used are listed in table 2.

Table 2 Conditions and Results of Optimization

Nr	Temperature Hot Finger (°C)	Pressure (bar)	Rate of Extraction (g/h)	Max. Content (%) *	50 % Yield Extract (%) **	C(20)-esters Purity (%)
01	80	120	8.2	84.2	17.2	75.0
02 ***)	80	120	13.1	92.2	14.4	86.8
03 ****)	80	120	12.8	55.6	25.1	50.3
04	90	200	138.5		no fractionation	
05	90	170	55.3		no fractionation	
06	90	150	14.7	98.9	13.5	96.2
07	120	200	38.2	45.3	42.8	33.0
08	120	170	12.4	89.3	15.7	80.7
09	120	150	7.8			
10	100	150	15.8	92.7	14.7	84.5

- \* ) of C(20)-esters in the loaded supercritical phase (without CO<sub>2</sub>)  
 \*\* ) related to the starting material  
 \*\*\* ) with smaller packings  
 \*\*\*\* ) without packings

In all these experiments the extraction temperature, the length of the column and the flow rate of the supercritical carbon dioxide were kept constant. Besides the reaction conditions in this table the results of the fractionation are listed in relation to the isolation of the sum of C(20)-esters. In this table the maximum content means the maximum concentration of C(20)-esters in the supercritical loaded phase during the extraction, analyzed by GC. Next to the last column of the table shows the amount of extract including 50 % of the C(20)-esters, related to the starting material. The last column shows purity of this fraction.

The best result was obtained in the experiment O6 with a temperature of the Hot Finger of 90°C and a pressure of 150 bar. Both at higher temperatures and higher pressures the selectivity of the fractionation decreases.

## 2.4 Two-step Extraction

The last experiments have shown that it is impossible to get a higher yield than 50 % with a purity of more than 90 %. Under the best conditions described above it should be tried to raise the yield of C(20)-esters by a two-step extraction procedure.

### 2.41 First Fractionation Step

In this experiment the codfish oil was extracted with supercritical carbon dioxide and by means of the hourly GC-analyses of the loaded supercritical phase several fractions were collected. In the first fraction all extracts were joined in which no C(20)-esters could be detected. In the second fraction the extracts up to 10 % C(20)-esters were collected and in the third fraction the extracts which contain the last traces of C(16)-esters. The next fraction contained only C(18)- and C(20)-esters of different composition. After the content of C(20)-esters of more than 90 % in the supercritical phase was reached the main fraction was collected until the content again reached 90 % after passing a maximum content of about 99 %. The next fraction consisted only of C(20)- and C(22)-esters in various combinations. When the value of the C(20)-esters was lower than 2 %, then the rest of the inserted material was extracted without using the Hot Finger. This last fraction besides C(22)-esters contained some not identified higher molecular components. Figure 3 shows the fractionation curves where the composition of the mixture dissolved in the supercritical phase is plotted versus the extraction time respectively versus the amount of extract in percent of the starting material.

The main fraction contains 48.2 % of the C(20)-esters which have been containing in the original starting material with a purity of 95.8 %, this is the first part of the desired product.

### 2.42 Second Fractionation Step

The fractions got in the first fractionation step containing only C(18)- and C(20)-esters respectively C(20)- and C(22)-esters were combined to give the new starting material for the second fractionation step. The first and the last fraction which contained only C(14)- to C(18)-esters respectively C(22)-esters were rejected.

Fraction 2 with the highest concentration of C(18)-esters was stored separate. This new starting material amounted of 24.5 % of inserted material of the first fractionation step. The composition, analyzed by gaschromatography, was as followed:

C(16)-esters	traces
C(18)-esters	23.56 %
C(20)-esters	45.28 %
C(22)-esters	28.74 %

This mixture was fractionated into 5 fractions under the same conditions as used in the first step. In table 3 the results of the GC-analyses are listed.

**Table 3** Composition of the Fractions of the Second Step

Nr	% Extract	% C14	% C16	% C18	% C20	% C22
01	25.5	----	1.3	76.1	20.8	----
02	17.3	----	----	25.3	73.3	----
<b>03</b>	<b>21.2</b>	----	----	<b>1.6</b>	<b>97.5</b>	<b>0.6</b>
04	10.8	----	----	----	48.6	51.3
05	24.3	----	----	----	0.6	98.0

In this fractionation step it was impossible to get a fraction without C(20)-esters. Therefore the first fraction was collected until the content in the supercritical phase reached about 50 %, in this fraction the main portion of C(18)-esters was found. Fraction 3 was collected in the same manner as the main fraction in the first step, herein all extracts were combined in which the content of C(20)-esters was higher than 90 %. The last fraction, a very clean C(22)-ester mixture, was extracted without the Hot Finger.

Fraction 3 consists of 45.7 % of the C(20)-esters in the starting material of the second step, respectively about 20 % related to the original Codfish oil with a purity of 97.5 %. If fraction 2 and 3 are mixed the yield of C(20)-esters raises up to 73.8 % in course of which the purity decreases to 86.6 %.

#### **2.43 Results of the Two-step Fractionation**

If the main fraction from the first step and fraction 3 from the second are mixed one gets a portion of extract which contains 67.7 % of the C(20)-esters in the original ester mixture with a very high purity of 96.3 %. Including fraction 2 from the second step, the yield increases to 80 % with the sufficient purity of 92 %. This mixture contains 77 % of the C(20-5)-ester of the inserted codfish oil.

### 3. Conclusions

It could be demonstrated that it is possible to separate a mixture of high boiling fatty acid ethyl esters into single components by fractionation using supercritical carbon dioxide at an extraction temperature of 50 °C. Regarding the areas of the single C-numbers a rather sharp separation could be achieved. In the case of the C(20)-esters the best results were obtained but also the C(18)-esters and the C(22)-esters could be isolated with a high purity.

In the experiments described the fractions containing only C(18)- and C(22)-esters besides the desired C(20)-esters were fractionated separately in a second extraction step. The better procedure would be to recycle this portion to the starting material to enrich the concentration of the desired esters in order to increase the yield of these esters in one extraction step. Such a procedure could be carried out in the following manner: In a discontinuous process the fractions containing only C(14)- and C(16)-esters respectively C(22)-esters were rejected, the fraction with the highest concentration of the desired esters would be the final product and all other fractions would be recycled to the process.

The main assignment of these investigations was to separate most of the C(20)-esters in high yield and high purity. It seems that it is possible to enrich the C(20-5)-ester by a suitable fractionation. But these experiments have also shown that it will be rather difficult to achieve a clean separation of C(18-1)-, C(20-5)- and C(20-1)-esters because of their similarity, the C(20-5)- and the C(20-1)-esters differ only in 8 H-atoms, i.e. 2.4 % in molecular weight related to the molecular weight of 332.6 for eicosapentaenoic acid ethyl ester.

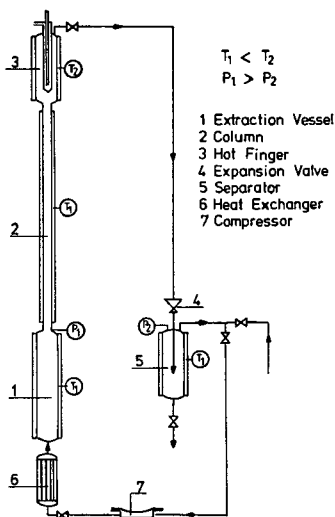


Figure 1 Fractionation Apparatus with Hot Finger

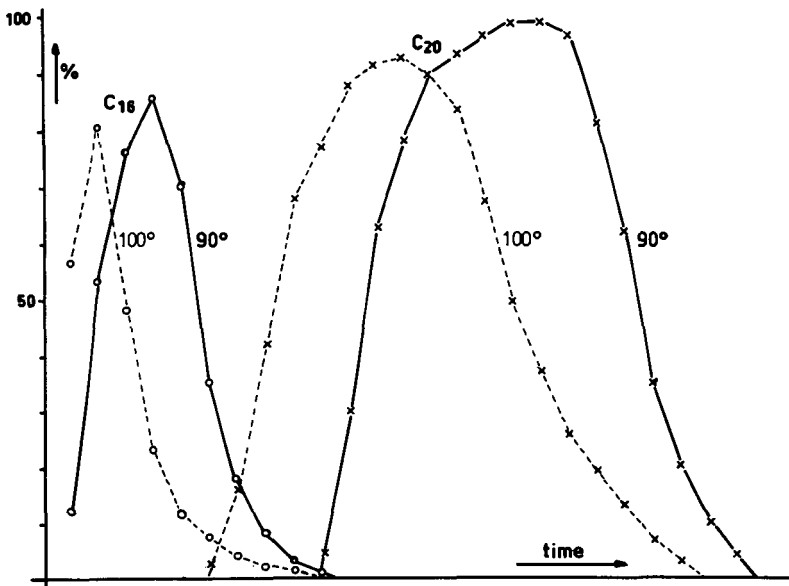


Figure 2 Separation Curves at 90 and 100°C

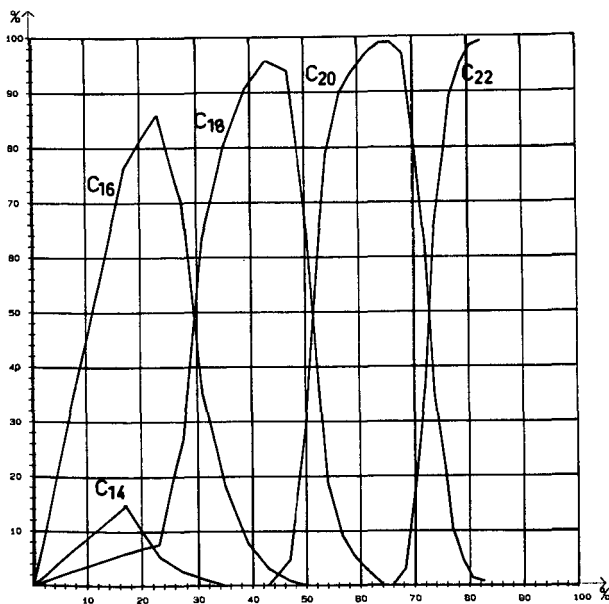


Figure 3 Separation Curves (Composition in Supercritical CO<sub>2</sub>)

SEPARATION OF BUTADIENE BUTENE MIXTURE WITH MIXTURES OF  
AMMONIA AND ETHYLENE IN NEAR CRITICAL CONDITIONS

D.S. Hacker, Amoco Chemicals, Naperville, Il., 60566

Abstract

We describe the results of an investigation into the separation of mixtures of 1,3-butadiene and 1-butene conducted at near critical conditions. Selected solvents and solvents containing ammonia as an entrainer are compared with respect to their selectivity in removing 1-butene from this close boiling mixture. Separation factors of 1.4 to 1.8 at a pressure of 600 psig and a temperature of 20 C are observed for mixtures containing 5%-8% ammonia in ethylene. Pure solvent gases, on the other hand, such as ethane, ethylene, and carbon dioxide show no selectivity. This is also true for ethane /ammonia mixtures which also appear poor as separating agents for this mixture. Experimental results are compared with values predicted by a modified two parameter corresponding states equation with reasonably good agreement. A case is made for the choice of an entraining component to be made on the basis that it contributes a chemical property to the system enabling the same selection criteria described by Elgin to be used in SC processes as are in liquid-liquid extraction or extractive or azeotropic distillation processes.

Introduction:

An alternative separation process is much to be desired to replace the more conventional azeotropic or extractive distillation used in the separation of closely boiling mixtures. There is a need to reduce both the energy costs associated with solvent recovery and costs due to loss of the expensive solvent. Ideally suited to the task would be a separating agent that could be readily flashed off, leaving a relatively pure product behind, assuring almost complete recovery of the solvent with a minimum expenditure of energy. Supercritical and near critical extraction where retrograde condensation and vaporization occur may be candidates for this task.

The separation of liquid mixtures by near critical solvents is still a relatively new technology. The lack of experimental phase equilibria data for many liquid systems and the dearth of solubility data for either critical gaseous solvents in liquid mixtures or for solutes dissolved in critical solvents makes any realistic design difficult. Some estimate can be obtained from an understanding of the general physical chemical principles involved, but ultimately each system must be addressed individually and its characteristics determined experimentally. In the discussion that follows, an experimental investigation was undertaken to determine the applicability of mixed solvents, near their critical conditions to the separation of butadiene from mixtures with 1-butene. These results are compared with predictions obtained from a representative equation of state in the region of the solvent-solute critical solution envelope.

### Theoretical Discussion:

The recovery of butadiene from a mixed C<sub>4</sub> olefin stream has all of the characteristics of an energetically difficult separation resulting from the almost pinched VLE conditions existing in this mixture. As is shown in Table I, the physical properties of these components are almost identical with the exception of the large dipole moment of the 1-butene. Conventional distillation is impractical since the relative volatility of many of the C<sub>4</sub> compounds are reasonably close to unity. A separation, nevertheless, can be effected provided a suitably polar solvent is used to selectively remove the butene. The influence of polarity can be exploited in this separation by "salting out" the more nonpolar compound(1).

As a result, virtually all industrial practice for the recovery of butadiene currently makes use of extractive distillation with an entrainer such as acetonitrile or some other strong organic base to enhance the relative volatility of the components. The potential of achieving an equally effective separation through the introduction of a mixture of a solvent and an entrainer exhibiting polar properties close to its critical solution conditions is intriguing. Ammonia, a polar gas, has already been shown to act as an effective solvent(2) for this separation although at pressures much below its critical. Its use as a supercritical solvent for this separation would be also feasible were it not for its very high critical temperature (405.45 K) which favors the polymerization of the butadiene. A method developed in this work and described in a recent publication (3) makes use of a supercritical mixture of solvents which in combination provides the chemical as well as the physical conditions for the most efficient extraction of the 1-butene solute in the mixture within the limitations imposed by the thermal stability of the system.

The ability to effect the separation of various liquid solutions in the presence of a supercritical or near critical component has been adequately demonstrated(4). In general, these solvents tend to be either inorganic gases or light hydrocarbons such as carbon dioxide, ammonia, ethane, ethylene, or propane. For example, Weinstock and Elgin (5) used pressurized ethylene to promote the separation a number of miscible aqueous-organic liquid mixtures. Through the introduction of a solvent at or near critical conditions one can effect separation by forming multiple phases. The distributed component may concentrate in either one of the newly created phases. More recently several practical processes have been developed that use carbon dioxide to efficiently dehydrate ethanol(6). Deashing and the physical separation of asphaltines by supercritical propane have been commercially developed(7). Starling et al recently applied this concept to the separation of light hydrocarbons such as n-butane and n-decane(8). The theory of separation of multicomponent mixtures by SC solvents is now of current research interest with several papers devoted to the application of concepts of continuous thermodynamics(9,10) to handle multicomponent mixtures as well.

Reid and others(11,12) have shown that supercritical solvents show varying degrees of selectivity towards a particular solute. This is not surprising since the same principle that applies in liquid solvent selection should apply in the case of SC solvents. Because of the limited number of SC solvents available, the application of SC extraction to a broad range of systems is very limited. One way of increasing the applicability of the technique is either to find ways of expanding the solvent category, which does not seem likely at this time, or to develop methods of modifying existing solvents. Since the maximum selectivity of the solvent occurs when its critical temperature matches the extraction temperature, a match between the solute and the SC solvent is not always possible with a single solvent.

To circumvent this difficulty, Brunner(13) introduced an entrainer whose function is to modify the chemical activity of the solute mixture sufficiently to enhance the separation. This was put to use in the extraction of triglycerides from a mixture of polyglycerides using carbon dioxide with acetone as an entrainer. The entrainer served as a source of hydrogen bonding to augment the separation of the desired component. The principle of the entrainer in improving separation has been widely known in liquid extraction processes and described by Treybal(14).

A ternary nonideal solution, for example, will generally exhibit a minimum in one of the pairs of activity coefficients. The addition of a second solvent, if properly selected, may further lower the activity coefficient of the solute and increase its concentration in a given phase(15). The addition of a second component to an SC solvent will result in configurational effects that enhance the extraction of a pure solid. It can be shown theoretically that a binary SC solvent at pressures close to the critical envelope will also have a strong influence on the solubility of the solid solute(16). How well this principle can be extrapolated to multicomponent solids or liquid systems is still to be determined.

In this study, we have measured the degree of extraction of butene from a binary mixture of butadiene/ butene with various solvents eg. ethane, carbon dioxide, ethylene, ammonia and ethylene and ammonia and ethane solvent mixtures in the region of critical solution pressure of the solvent mixture. The experimental results are then compared with the VLE calculations for this system using a newly developed corresponding states equation devised by Ely and Mansoori(17).

The primary features of the equation are a new generalization for the shape factors and the use of propane as its reference component. The equation allows for the inclusion of multicomponent mixtures. The model has been successfully used with non-polar compounds and for a small number of selected polar compounds. It correctly represents liquid-vapor phase relations in the region of the critical, but does not specify the formation of a second liquid phase. The mixing rules, defined as  $a_{ij} = (a_{ix}a_{jy})^{1/2} (1-k_{ij})$  and  $b_{ij} = \{(b_{i1}^{1/3} + b_{j1}^{1/3})/2\}^3$ , are then adjusted to account for the enhanced polar contribution of ammonia-butene through the interaction parameters,  $k_{ij}$ , and  $b_{ij}$ . All other interaction coefficients were set to  $k_{ij} = 0$  and  $b_{ij} = 1$ . It is recognized that such a simplified model is in serious error since the polar and hydrogen bonding contributions are ignored. Nevertheless, it does permit one to obtain a "ball park" estimate of the separation likelihood. The results of these VLE flash calculations are then compared with our experimental results.

#### Experimental

Near-critical extraction experiments were carried out in a one-liter, stirred, stainless steel Autoclave (MR #7331), rated at 5000 psig at 600 F. Phase separations were monitored through an attached 50 cc Jerguson sight gauge (rated at 5000 psig at 72 F) which also served as a level indicator. A complete schematic of the assembly is shown in Fig. 1. The autoclave was maintained at constant temperature by means of an external heating tape and an internal cooling coil. Cooling was furnished by a circulating water Freon refrigeration unit. An Autoclave magnetic stirring unit powered by an air motor was used to ensure adequate mixing of the sample volume. All lines were heat traced with electrothermal heating tapes. The reactor was depressurized before each experiment by venting the system and then evacuating the chamber under reduced pressure to ensure the complete removal of residual mixture and air from the system. Filling of the vessel was accomplished through a feed port at the base of the reactor. The samples of the upper and lower phases was removed through small bore (1/8 ") tubing through the head of the reactor and at the bottom of the reactor. No provision was made to sample any second liquid phase that may appear during an experiment.

Volumetric measurements obtained from observations through the sight glass of the Jerguson gauge and were used to determine the the molar volume of all liquid components used to make up the charge. A calibrated platinum thermocouple was used to measure the temperature of the contents of the autoclave reactor. The pressure of the system and of each of the receiver vessels were measured with calibrated high pressure precision Bourdon tube gauges of appropriate range. The gauge glass window was calibrated to give a direct reading of the volumes of the liquids added. When ammonia was used in the solvent makeup, it was added to the contents before the addition of the pressurizing solvent gas.

Ammonia was fed through a second Whitey pump into a storage cylinder that could be independently cooled to ensure minimum vaporization of the ammonia before admitting it to the reactor. The ammonia was added under a slight helium pressure to minimize liquid vaporization at the surface and to allow for a measurement of a quiescent interface.

The solvent gases, ethylene, carbon dioxide, or ethane, were fed by a Haskel gas compressor, Model AG-62, a 25-l air driven compression pump with a maximum outlet pressure of 9000 psig. The quantity of these gases introduced into the autoclave was determined by measuring the weight change of the gas cylinder and separately by a measurement of the change of the liquid level resulting from gas dissolving in the liquid during pressurization. The difference between the liquid level and the total volume of the vessel was measured and the second phase volume determined.

Chemically pure grade butene and butadiene were supplied in cylinders by Matheson Co. and used as received without further purification. The hydrocarbons were fed to the reactor through an LP10 Whitey laboratory positive displacement pump. A 30-pound nitrogen head was added to each hydrocarbon cylinder to maintain adequate pumping efficiency.

Heating controls were manually adjusted and the temperatures were indicated on a 10-point Acromag. The heating zones of the reactor were controlled by three Eurotherm 103 with voltage controlled manually by Variacs. The remaining sections were heat traced with self-limiting autotrace heating tapes to prevent condensation in the lines.

#### Sample Analysis:

The contents of the reactor were sampled before and after the introduction of the solvent gas and entrainer by trapping approximately 1 cc of the mixture from the reactor volume in a precalibrated volume of sample line located between two high pressure valves, adjacent to the vessel. The volume of the sample withdrawn was sufficiently small to minimize any changes in the pressure of the main contents of the vessel. Once trapped, the high pressure sample was further expanded into a pre-evacuated 300 cc Hoke cylinder to about 5 atm. This volume of sample was again expanded into a final 70-cc Hoke cylinder to about 1 atm. Portions of this volume were introduced into the Valco valve located at the Varian 920 Gas Chromatograph. All sample loops were heat traced as well to prevent condensation in the lines. This procedure was followed in sampling the lower portion of the liquid phase as well. An additional sample port was installed in the low pressure cylinder for syringe sampling to provide an additional check on the accuracy of sampling procedures.

The pressure of the gas was slowly increased until the liquid interface disappeared, indicating the attainment of the critical region. The gas pressure was then reduced by slightly depressurizing the chamber until the interface just reappeared. It was established that this procedure permitted the contents to be within 2 to 3 psi below the region of the critical. After stirring for about five minutes, the system was allowed to equilibrate before vapor and liquid phases were sampled.

Samples withdrawn from the upper and lower sections of the reactor autoclave were analyzed in the G.C. using a thermoconductivity detector with a 20', 1/8" VZ-7 packed column with helium used as the carrier gas. The G.C. was run with the injector set at 115 C, the column oven temperature at 60 C, and the detector set at 115 C. Filament current to the detector was set at 150 ma.

Samples were injected into the column by an air-operated Valco valve, which was controlled by a timer- controlled solenoid. The detector output was integrated and a concentration analysis was performed by an Autolab System. A Leeds and Northrup recorder was used to monitor the condition changes, and peak shapes, and composition analysis. The larger volume of solvent to solute required a change in sensitivity to adequately monitor the butadiene and butene peaks. A typical record of the GC output is shown in Fig.2 and indicates the integrated values of the represented peaks of the solvent gas, and butene and butadiene. The equilibrium compositions for each run are obtained in this manner and with the initial mixture composition tie lines of the system can be generated. The entrainer-solvent gas are considered as a pseudosolvent of fixed composition. The results of the measurements obtained for the 5% ammonia/ethylene are represented in the ternary diagram in Fig.3. Butene is represented as the distributed component with the butadiene as the heavy component.

**Results:**

The ratio of the integrated peaks for butene(i) and butadiene(j) was used to determine the separation factor, B, where the separation factor is defined as

$$B = \frac{\{y_i/x_i\}\text{solvent phase}}{\{y_j/x_j\}\text{heavy phase}} \quad (1)$$

The results shown in Table II and III are representative of the data collected for the studies conducted with ethylene and ethylene/ammonia and ethane and ethane/ammonia solvent mixtures. Table IV shows some selected data for other solvents and solvent mixtures as well. The results of extraction conducted with pure ethylene, carbon dioxide, and ethane in all cases showed no evidence of appreciable separation. In each set of experiments with single solvents, the same ratio of butadiene to butene was obtained in both phases. The butadiene/butene mixture is distributed in each phase in amounts that are primarily a function of the extracting gas and the temperature and pressure of the system.

Runs were made with several mixtures of ammonia/ethylene and ammonia/ethane with varying concentrations of ammonia. For both of these mixtures a separation of the butadiene was achieved, but the effect of the ethylene as a preferred solvent is most pronounced. The butene appears to be concentrated in the vapor phase in agreement with the findings of the earlier pure ammonia study(2). A series of experiments were also conducted to determine the temperature and pressure conditions in which maximum separation could be attained. For the ethylene/ hydrocarbon/ 8 % ammonia mixtures, this was found to be at 20 C and 600 psia. The maximum occurs at a pressure below the critical solution temperature determined by Lentz(18) for the ethylene/ammonia binary ( Fig.4). The experimental selectivity was observed to decrease with an increase in pressure with an accompanying increase in the loading in the solvent phase. The selectivity is also reduced as the temperature rises all other things being equal(Fig.5).

## Discussion

The results obtained in this study are by no means comprehensive and cover only a narrow range of variables. However, they indicate the maximum effect of entrainer enhancement on the relative volatility of an otherwise close-boiling mixture through the addition of 8% ammonia/ethylene solvent mixture close to its critical solution conditions. The relatively large selectivity achieved of 1.4 to 1.8 is to be considered in light of the value obtained for pure liquid ammonia of 1.63 reported by Poffenberger(2). Moreover, it is shown that the use of a solvent and an entrainer solvent permits the separation to be effected at temperatures and pressures lower than would have been otherwise predicted had pure critical ammonia been used, a result also observed by Fong et al(19) in studies of mixed solvent extraction of coal. An explanation for the lower than expected pressure for the separation is the likely formation of a Class IV mixture according to Van Konynenburg(20). It has been observed in

several systems containing ammonia and aromatics that a second liquid phase is formed under lower pressures than expected if the mixture behaved as an ideal Class I system. The P-T projection for these classes of mixtures is shown in Fig.6. A lower critical solution temperature (LCST) and an upper critical solution temperature (UCST) are the boundaries for the VLL phases observed to be present in these experiments. The critical points are the values for the two pseudo-components. Despite the fact that these phase relations are similar to those observed for a number of binary mixtures, one can consider the present mixture as a pseudo-binary system in which the solvent mixture, comprising ammonia and excess ethylene/ or ethane and a hydrocarbon phase of butadiene and butene exhibiting very similar vapor pressures.

The enhanced solubility of the solvent in the solution phase is evidenced in Table II by the large concentration of the ethylene present in both phases. An estimate of the volume of solvent added to the hydrocarbon mixture was obtained by calculating the difference in the liquid level before and after gas solvent addition. This is approximately the volume of gas dissolved in the liquid phase. This value is added to the volume above the liquid interface to obtain the total solvent added to the system. The volume of ethylene/ammonia solvent mixture added to the volume of butadiene/butene solution was approximately 5:1.

A comparison of the calculated selectivities obtained for the ethylene mixtures given in Table II can be made with the results in Table III obtained for the ethane system. These differences cannot be explained solely in terms of the critical properties of the respective gases. Usually the efficiency of extraction of a given solvent towards a particular solute is related to the proximity of the extraction temperature to the critical temperature of the solvent. The ratio of the two temperatures,  $T_{ext}/T_c$ , or the effective reduced temperature should be unity or somewhat greater to maximize separation. For a gas of given critical temperature, the reduced temperature is inversely proportional to the solubility of the solute in the solvent. Since ethane has a reduced temperature more nearly equal to unity at the extraction conditions at 20 C ( $T_r = .98$ ) as compared with ethylene ( $T_r = 1.47$ ), one would expect the ethane mixtures to be a better solvent for the butene. That this is not the case suggests an alternative explanation would be that the ethylenic double bond structure has a greater chemical affinity for the olefins in the solution phase which may account for the enhanced solubility of the butene in the ethylene phase. This is in addition to the chemical synergistic effect exerted by the ammonia which further increases the solubility of the butene in the vapor phase.

These results are also compared with calculated values obtained from the equation of state using  $k_{ij} = 0.8$ . Solvent to feed ratios as well as the effect of ammonia concentration in the solvent were independently varied to match the experimental data. The effect increasing ammonia concentration at constant pressure and temperature in both ethylene/ammonia and ethane/ammonia solvent mixtures are shown in Table V. The separation factor increases proportionally to an increase in entrainer concentration and appears to have a more important influence than either temperature or pressure. This is in contrast to the experimental observations in which the selectivity achieves a maximum at an ammonia composition of 8%. A comparison of these experimental findings with both the predictions of the present model and the Prausnitz model for the solubility of solute in mixed SC solvents suggests that chemical factors such as synergistic effects cannot be ignored and are likely to have a greater effect than anticipated. The vapor liquid equilibrium predictions are, in general, in fair agreement with the results of these experiments.

#### Conclusions:

1. The information presented in this study indicates the degree of mixing critical solvents with an appropriate component whose hydrogen bonding or polarity will enhance the separation of a close boiling mixture of butene-butadiene.
2. A maximum value in the selectivity of 1.4 - 1.8 can be achieved with a 5 - 8% ammonia concentration in ethylene for the butadiene - butene separation. This is in agreement with the predictions of the Ely-Mansoori equation of state. However, the presence of a maximum in the selectivity is not predicted by the model, suggesting the synergistic effect of the ammonia in the solvent rather than a concentration effect which is proportional to the added entrainer.
3. Ethylene/ammonia mixtures are more effective solvents for the separation of this mixture than is ethane/ammonia mixture with the same concentration of ammonia. It is suggested that ethylene because of its greater chemical similarity in the butene/butadiene solution exerts a greater influence on the binary activity coefficients of the system.

TABLE I  
PROPERTIES OF C4 COMPONENTS

PROPERTY	1-BUTENE	1,3-BUTADIENE
Molecular Wt.	56.11	54.09
Critical Temp, C	146.4	152.20
Critical Press.MPa	4.019	4.329
Critical Vol. cc/mole	4.276	4.083
Normal BP.C	-6.25	-4.411
Solubility Param.	4.7504xE04	4.8694xE04
Dipole Mom. Debye	0.34	0.0
Acentric Factor	0.1867	0.1932 1

PROPERTIES OF SOLVENTS

PROPERTY	ETHANE	ETHYLENE	CARBON DIOXIDE	AMMONIA
Molecular Wt.	30.07	28.05	44.01	17.03
Critical Temp,C	32.27	9.21	31.04	132.50
Critical Press.				
MPa	4.88	5.03	7.38	11.27
Critical Vol. cc	4.919	4.601	2.136	4.255
Normal BP,C	-88.60	-103.7	-	-33.43
Solubility Coeff.				
	3.9134xE04	3.932xE04	4.605xE04	9.239xE04
Dipole Mom.Debye	0.0	0.0	0.0	1.47
Acentric Factor	0.09896	0.085	0.2276	0.2520

TABLE II

## BUTADIENE-BUTENE-ETHYLENE-AMMONIA EQUILIBRIUM COMPOSITION

NH <sub>3</sub> (%)	--- Solvent Phase (%) ---			---Butadiene Phase (%) ---			Beta
	C <sub>2</sub> H <sub>4</sub>	Butene	Butadiene	C <sub>2</sub> H <sub>4</sub>	Butene	Butadiene	
At T = 20° and P = 600 psia							
0	88.351	3.768	7.881	45.940	17.470	36.584	1.00
0	88.425	3.763	7.839	38.338	19.765	41.901	0.99
0	69.694	14.932	15.374	71.997	13.092	14.911	1.10
2.3	82.199	8.828	8.973	58.461	17.483	20.879	1.17
5.0	89.063	6.936	4.001	52.675	23.890	23.435	1.70
5.0	88.879	6.903	4.218	40.109	30.149	29.742	1.61
5.0	76.970	15.069	7.961	58.039	22.047	19.914	1.71
5.0	75.469	15.505	8.448	55.886	23.201	20.913	1.61
5.0	89.132	8.805	2.064	38.799	47.751	13.450	1.20
8.0	91.066	2.629	6.305	46.473	12.884	39.303	1.27
8.0	85.908	3.288	8.151	44.928	13.157	40.645	1.24
8.0	86.668	11.710	1.622	47.847	41.382	10.771	1.88
8.0	86.775	11.737	1.488	49.963	39.604	10.433	2.08
8.0	69.579	19.803	10.618	49.100	27.951	22.949	1.53
10.0	59.583	27.028	13.389	39.981	36.671	23.348	1.29
10.0	60.217	26.028	13.389	41.815	35.692	22.493	1.32
10.0	74.642	19.423	5.984	66.140	25.400	8.451	1.10
At T = 20°C and P = 800 psia							
2.3	70.166	13.873	15.960	34.716	28.791	36.493	1.10
2.3	69.498	14.112	16.389	43.984	24.539	31.477	1.10
5.0	76.947	12.740	10.312	74.065	14.520	11.415	1.05
5.0	77.599	12.566	9.835	74.093	14.494	11.413	1.00
10.0	81.026	7.044	11.930	67.741	11.236	21.021	1.10
10.0	80.266	3.354	12.183	67.009	11.767	21.224	1.12
At T = 20°C and P = 1100 psia							
0	69.694	14.932	15.374	71.997	13.092	14.911	0.90
0	81.759	8.583	8.713	73.607	12.124	14.270	0.86
5.0	84.760	8.380	6.860	77.316	11.457	11.227	0.84
5.0	84.074	8.457	7.451	74.816	12.849	12.335	0.92
At T = 40°C and P = 600 psia							
5.0	85.128	8.416	6.456	34.556	34.501	30.943	1.17
5.0	86.617	7.812	5.571	29.325	37.302	33.372	1.25
At T = 60°C and P = 600 psia							
5.0	75.099	11.814	8.756	19.215	42.621	38.163	1.21
5.0	74.163	12.412	9.471	20.693	41.856	37.451	1.17

TABLE III

## BUTADIENE-BUTENE-ETHANE-AMMONIA COMPOSITION

## EXPERIMENTAL VALUES

TEMP C	PRESSURE PSIA	NH3 %	SOLVENT PHASE			BUTADIENE PHASE			SELECTIVITY B
			C2H6 yi	BUTENE yJ	BUTADIENE yk	C2H6 xi	BUTENE xJ	BUTADIENE xk	
20	900	4.18	76.258	10.925	12.817	74.367	11.568	14.065	1.0
		4.18	76.505	10.834	12.661	74.993	12.079	12.929	1.09
		4.18	74.654	11.232	14.113	75.137	12.667	12.169	1.31
17	620	6.97	90.406	3.998	5.596	85.647	5.830	8.523	1.04
	640	6.97	90.107	4.123	5.770	83.324	6.804	9.871	1.03
	725	6.97	87.224	5.220	7.556	88.497	4.817	6.686	1.00
	725	6.97	87.387	5.181	7.432	88.766	4.497	6.737	1.05
	1060	6.97	88.840	4.489	6.689	93.178	2.751	4.071	1.00
	1060	6.97	88.90	4.443	6.657	93.086	2.801	4.113	1.00
19	675	6.97	85.525	7.426	7.229	88.073	6.047	5.879	1.00
	675	6.97	86.137	7.105	6.758	87.789	6.295	5.914	1.00
18	600	6.97	88.024	6.135	5.841	85.503	7.379	7.117	1.01
	600	6.97	87.722	6.201	6.077	85.812	7.185	7.002	1.00
16	550	6.97	95.867	2.252	1.977	76.208	11.624	12.168	1.19
18	600	6.97	83.134	10.507	6.358	80.277	11.959	7.577	1.05
	600	6.97	82.572	10.834	6.594	80.176	12.228	6.044	1.02
20	700	6.97	87.532	7.907	4.561	84.122	9.834	6.044	1.06
	700	6.97	87.295	8.009	4.696	83.794	10.026	6.180	1.05
22	525	1.85	89.169	5.166	5.664	69.808	15.252	14.939	1.0
	525	1.85	93.286	3.828	2.886	67.462	16.489	16.049	1.28
	525	1.85	92.362	3.900	3.737	78.235	11.064	10.701	1.01
	1100	1.85	88.100	6.345	5.555	78.508	11.205	10.288	1.04
	1100	1.85	87.700	6.328	5.973	78.581	11.078	10.341	1.00
23	550	0	82.754	8.164	3.668	53.113	22.449	24.438	1.00
	550	0	92.243	9.091	4.089	55.308	21.121	23.570	1.00
	1075	0	77.928	10.633	11.438	72.545	13.088	14.367	1.00
	1075	0	77.279	11.078	11.693	75.175	12.095	12.730	1.01

TABLE IV  
SEPARATION OF EQUIMOLAR MIXTURES OF BUTENE-BUTADIENE  
WITH VARIOUS SOLVENTS

EXPERIMENTAL VALUES			
TEMP. C	PRESSURE psia	SOLVENT	SELECTIVITY
6.0	750	C2H4	1.23
40.0	1100	CO2	1.0
22.0	1000	"	1.0
22.0	700	"	1.0
20.0	500	"	1.0
23.0	1100	C2H6/5% NH3	1.0
18.0	700	C2H6/7% NH3	1.06
20.0	900	C2H6/4% NH3	1.09
23.0	550	C2H6/	1.0

TABLE V  
EFFECT OF TEMPERATURE AND PRESSURE ON THE SEPARATION OF EQUIMOLAR BUTENE  
BUTADIENE SOLUTIONS USING NEAR CRITICAL AMMONIA-ETHYLENE MIXTURES  
AS SOLVENTS

CALCULATED VALUES BY ELY-MANSOORI MODEL

$k_{ij}=0.8$  , all others  $k_{ij}=0$

MIXTURE COMPOSITION S/F MOLE FRACTION		T K	P atm	$\gamma$ butene	K butene	B
NH3/C2H4						
0.25	20	300	50	0.011	0.405	1.54
		310	50	0.0208	0.460	1.87
0.50	10	300	50	0.0175	0.385	1.29
		305	50	0.024	0.393	1.37
	310	50	0.0317	0.407	1.40	
	320	50	0.0332	0.641	2.86	
	330	50	0.426	0.786	3.10	
	310	40	0.339	0.635	3.94	
		320	40	0.433	0.834	4.29
NH3/C2H6						
0.50	10	320	40	0.0250	0.544	1.96
		330	50	0.0252	0.606	1.65
		350	58	0.0348	0.931	1.10
	20	315	40	0.0129	0.579	2.26
		320	40	0.0173	0.679	2.48
1.0	10	390	81	0.0331	0.900	0.91
		370	65	0.3636	0.512	1.13
0.0	2	295	20	0.5501	0.228	1.04

#### References:

1. Prausnitz, J.M., "Molecular Thermodynamics of Fluid Phase Equilibria", Chap. 10, Prentice Hall, N.Y. (1969)
2. Poffenberger, N., Horsley, L.H., Nutting, H.S., Trans. AIChE, 42, 815, (1946)
3. Joshi, D.K., Prausnitz, J.M., AIChE Jour. 30, 522, (1984)
4. Todd, D.B., Elgin, AIChE Jour. 1, 20, (1955)
5. Weinstock, J.J., Elgin, J.C., Jour Chem Engr. Data, 4, 3, (1959)
6. Fogel, W. Arlie, J.P., Revue Franc. Petrole, 39, 617, (1984)
7. Brule, M.R., Corbett, J.C., Hydrocarbon Process. 73, (1984) June
8. Starling, K.E., Khan, M.A., Watanasiri, S., Fundamental Thermodynamics of Supercritical Extraction, Presented Annual Mtg AIChE, San Francisco, Ca. (1984)
9. Prausnitz, J.M., Fluid Phase Equil., 14, 1, (1983)
10. Cotterman, R.L., Dimitrelis, D., Prausnitz, J.M., Ber. Bunsen Gesch. Phy und Chem, 9, 796, (1984)
11. Reid, R.C., Schmitt, N.J., The Influence of Solvent Gas on the Solubility and Selectivity in SC Extraction, Presented Annual Mtg AIChE., San Francisco (1984)
12. Vasilakos, N.P., Dobbs, J.M., Parisi, A.S., IEC Process Design, 24, 121, (1985)
13. Brunner, G. Fluid Phase Equil, Part II, 10, 289, (1983)
14. Treybal, R.E., "Liquid Extraction" 2nd Ed. McGraw-Hill, N.Y. (1963)
15. Prigogine, I., Bull Soc. Chim, Belg., 52, 115, (1943)
16. Eckert, C.A., Greiger, R.A., IEC Process Design, 6, 250, (1967)
17. Mansoori, G.A., Ely, J.F., Density Expansion Mixing Rules, Unpublished (1984)
18. Lentz, H., Franck, E.U., Extraction by SC Gases, Ed. Schneider, G.M. Verlag Chemie, (1980)
19. Fong, W.s., et al, Experimental Observations on Systematic Approach to SC Extraction of Coal, Presented at National Mtg AIChE, New Orleans, La. (1981)
20. Van Konynenburg, P.H., Scott, R.L., Phil. Trans., Royal Soc., 298, 495, (1980)

#### Acknowledgement:

We are grateful to the AMOCO Chemical Corp. for their support for this work. In particular we express our appreciation for the interest shown in this work by D.E. Hannemann and P. Thornley and to Frank Brooks for his industry and care in carrying out these experiments.



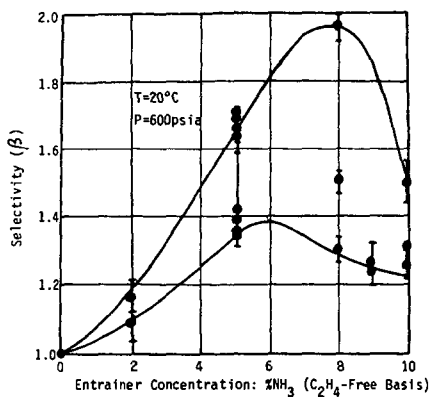


Figure 4. Influence of Entrainer Concentration on the Effectiveness of Solvent Ethylene.

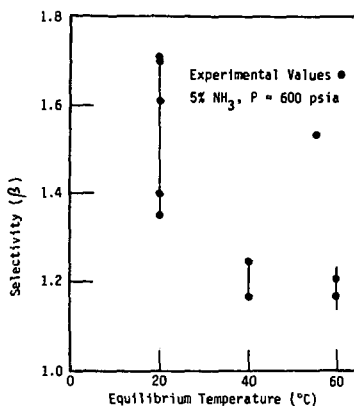


Figure 5. The Influence of Temperature on the Selectivity of Ethylene/Ammonia Solvent Mixtures on the Separation of  $C_4$  Hydrocarbons.

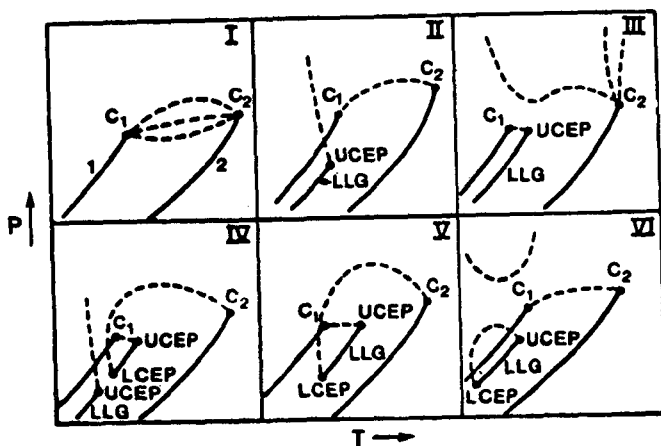


Figure 6. Classes of Different Binary Mixture Fluid Phase Behavior.

## BENEFICIATION OF WATER-SENSITIVE EASTERN OIL SHALES

C. A. Audeh

Mobil Research and Development Corporation  
Central Research Laboratory  
P. O. Box 1025  
Princeton, New Jersey, 08540

### INTRODUCTION

Development of the eastern oil shale deposits of the US has been considered of secondary importance when compared with the development of the western shale. The usual reason given for this assessment is the low oil yield of the eastern shales. For example, a typical eastern shale containing 12% organic carbon yields about 12-14 gallons per ton (G/T); in comparison a western shale with the same organic carbon percent yields about 28 G/T. Thus for eastern shales to be considered as an attractive alternative source of liquid fuels a higher yield of oil has to be achieved.

Techniques are known by which an oil shale may be beneficiated so as to increase the amount of oil that is generated by retorting. One such technique described for eastern shales is froth flotation.

Beneficiation by grinding and froth flotation is a well established procedure in the mineral dressing industry. Large scale ore beneficiation facilities have been developed and are commercially applied.

In froth flotation advantage is taken of the difference between the specific gravity of the organic and inorganic components in the shale. Thus if the organic-rich portion of the shale which has a lower density than the inorganic portion could be disengaged from the organic-poor portion, the two portions will exhibit a specific gravity difference that may allow for their separation by flotation.

Unlike western shale which has essentially a layered structure of magnesium and calcium marlstones interspaced with organic-rich kerogen, eastern shale has essentially a matrix structure. This matrix is typically composed of particles of quartzite, clay, organic-rich kerogen and pyrite. To achieve the separation of the organic-rich from the organic-poor components of an eastern shale, it is thus necessary to reduce the shale matrix to its components which could then be separated by flotation.

For eastern shales, size reduction by grinding (1) can bring about the separation of the desirable organic from the inorganic components of the shale. This has also been achieved by persistent milling in a rod mill (1), ball mill, or a rod and ball mill (2,3). It has also been reported (1-6) that the finer the particles, the more successful is the beneficiation. The grinding or milling process is a major contributor to the

cost of beneficiation. It has been estimated (7) that 45% of the cost of beneficiation accrues to the grinding step with energy the major component.

Although water has been used for dust control and lubrication during grinding, it has not been used as the main medium for size reduction. Earlier work at Mobil (8) has shown that when a water slurry of an eastern shale is stirred, the shale particles crumble and lose their shape and size. This suggested the use of agitated water slurries of the shale as a means of size reduction and flotation.

## EXPERIMENTAL

### Apparatus

The beneficiation apparatus consisted of two components, a flotation cell and a circulating pump. Figure 1 depicts the flotation cell used. A TEEL pump manufactured by Dayton Electric Co., Model IP 810, equipped with 2 1/4 inch diameter flexible impeller driven by a 1/4 HP electric motor was used to circulate the shale and reduce its size. The outlet of the flotation cell was attached to the inlet of the impeller pump and the pump outlet was attached to the inlet of the flotation cell. A 1/2 inch 25 micron frit was used to support the shale slurry and to supply the frothing gas.

A DuPont thermogravimetric analyzer (TGA) was used to determine the weight loss; heat up rate was 10°C/min. Air or argon was used to sweep the volatiles during thermal decomposition of the kerogen.

### Procedure

In a typical experiment about 750ml of water was placed in the flotation cell and the pump started. About 50g of 8-mesh shale was then added to the circulating water and the slurry was allowed to circulate for 30-60 minutes.

About 0.1g of sodium dodecylbenzenesulfonate was then added to the slurry and the mixture circulated for 10 minutes. Flotation gas was then turned on to generate a foam with small bubbles and the flow adjusted so as to achieve a steady flow of foam at the foam outlet of the flotation cell.

Samples of the foam were collected at predetermined intervals. Each sample was filtered, Büchner, and the collected solid washed well, and dried to constant weight at room temperature at a pressure of about 0.05 mm Hg, weighed and analyzed.

In TG analyses care was taken to use an amount of shale that gave a uniform layer of shale on the TGA balance. Usually a 20-25 mg sample was satisfactory.

## RESULTS AND DISCUSSION

### Shale Particle Size Reduction

Earlier work on eastern shale at Mobil (8) has shown that some shales are friable when wet. It was observed, for example,

that when a slurry of 8-mesh New Albany shale was stirred gently, most of the shale became smaller than the original 8-mesh size. It was clear that wet New Albany shales yield and crumble under the impact of the Teflon blade of a glass stirrer. This observation suggested to us the use of an impeller slurry pump as a means of size reduction. It was reasoned that when the impeller struck the wet shale particles, they would break down and crumble.

After several experiments with different impellers it was concluded that the impact of the impeller on the wet shale reduced the particle size of the shale but the particle size was not small enough to bring about flotation. However, when a slurry pump equipped with a flexible impeller was used, the shale size was sufficiently reduced for its flotation. This size reduction was brought about by the scraping action of the flexible impeller over the wet shale. As the impeller moved in its housing, the shale particles were trapped by the flexible vanes and scraped over the metal surface of the impeller housing; this scraping action brought about the size reduction.

### Shale Flotation

Several attempts were made to apply the sink/float procedure (9) for beneficiating the shale particles generated by the action of the impeller pump. The fine shale was mixed with brines of various densities and allowed to segregate into lighter and heavier portions. Brines containing calcium chloride or calcium bromide with densities in the range of 1.05-1.64 g/cc were used. In all sink/float attempts little or no beneficiation took place.

The same brines were also used as the liquid medium of the shale slurry and circulated by the impeller pump followed by flotation. Although size reduction was affected, little or no beneficiation took place. In one example a brine with a density of 1.105 g/cc produced a small fraction containing 41% more carbon than the raw shale; organic carbon was increased from 12.83% to 18.10% by weight.

After the unsuccessful experiments with the various brines a slurry composed of 50g, 8-mesh shale and 750 ml water containing 0.013% by weight (0.1g) sodium dodecylbenzenesulfonate was circulated and was successfully beneficiated. The shale used in all these studies was a well characterized New Albany shale containing little or no carbonate carbon. Table 1 presents the elemental analyses of the raw shale and shows the yields of products obtained in the Fischer assay and selected properties and elemental composition of the oil and spent shale. The carbon content of the oil represents a 33% conversion of the carbon of the raw shale to oil. This level of carbon conversion is typical of eastern shales (10) and serves to illustrate the need for beneficiation.

Table 2 shows the elemental analyses and amounts of the beneficiated fractions of the New Albany shale studied. About 17% by wt of the shale has over 32% by weight carbon, a 2.5 fold carbon beneficiation. This 17% fraction contains 45% of the total carbon contained in the 50g sample. About 5% of the

sample remained unground and essentially had the same composition as that of the raw shale. About 95% of the fractions collected by flotation passed a 200 mesh screen, however the fractions with the high carbon content had a "waxy" feel and were difficult to sieve. These particles stuck to the sieve opening and an accurate measure of their mesh size distribution could not be made. It is estimated that over 25% would pass a 325 mesh sieve.

The leanest fraction was a finely ground portion of the shale that remained in the flotation cell upon termination of the experiment and was separated from the 8-mesh residue by sieving. This finely ground residue passed a 200 mesh sieve and had a 3% by wt. carbon content.

#### Estimate of Oil Yield by TGA

Since these experiments were carried out on 50g samples of shale, Fischer assay (FA) yields could not be determined on any of the beneficiated shale fractions. Although all beneficiated fractions were analysed for carbon and hydrogen content, Table 2, it was considered necessary to estimate their oil yield potential.

It has been shown (11) that small samples, 1 or 2 mg, could be used in thermal decomposition studies for comparing the oil generating potential of shales. Also, thermogravimetric (TG) analysis techniques have been used to compare shales by determining relative weight loss profiles (12,13). Weight loss from three shales of known FA yield, including the shale used in this study, was determined by TGA, Table 3. The New Albany shales have similar weight loss in TGA and have FA yields consistent with such weight loss. Also the western shale which is known to produce more oil per percent organic carbon than the eastern shales shows the same trend in the TGA.

By combining elemental analyses of the beneficiated shale fractions with their TGA weight loss and using the data for shales with known FA yields an estimate of the FA yields of the fractions could be made, Table 4. The two fractions with the highest carbon contents also have the highest weight loss in argon. Weight loss in air was also determined, Table 5, and shows that the raw shale and the unground residue have the same weight loss. Considering the elemental composition and the TGA weight loss in argon of both samples, it was concluded that the unground residue is unbeneficiated shale. The recovered unground material was similar in appearance to the raw shale and crumbled when wet. It was reasoned that this material must have been trapped at the bottom of the flotation cell and was not carried into the pump housing where size reduction takes place.

TGA weight loss in air when compared to weight loss in argon is one measure of how well carbon conversion to oil takes place during thermal decomposition of a kerogen. A spent shale with a high char content will lose that char by oxidation when air is the sweep gas. A high char content is an indication of poor organic carbon conversion to oil. The beneficiated fractions do not generate char to the same extent as the raw shale. Whereas

the weight loss in argon of the raw shale is 36% of that in air, that of the beneficiated fractions is 65%. It is possible that the inorganic matrix, in the raw shale, especially the pyrite, contributes to the inefficient conversion of the kerogen to oil.

Although the sulfur content of the beneficiated shale increases relative to that of the raw shale, the ratio of carbon to sulfur is higher, 5.22 vs. 2.69, and that of sulfur to hydrogen is lower 2.30 vs 3.38. Pyrite in shales is a hydrogen consumer (14) and competes with carbon for the available hydrogen during thermal conversion of kerogen to product oil. Shales containing pyrite are known to produce significant amounts of hydrogen sulfide (15).

### CONCLUSIONS

A new approach to size reduction followed by froth flotation to beneficiate water-sensitive eastern shales coupled with thermogravimetric analysis has been investigated. Organic-rich fractions with 3.5 times the oil generating capacity of the raw shale were prepared by this procedure. It is suggested that this procedure be used as a screening test for the applicability of flotation to the beneficiation of shales.

### REFERENCES

1. H. S. Hanna and W. E. Lamont, AIChE 1982 Summer National Meeting, August 1982, Cleveland, Paper No. 35A.
2. U.S. D.O.E. Contract ET 78 Col 2628, December 31, 1982.
3. P. H. Fahstrom, 12th Oil Shale Symposium, Golden, Colorado, April 1979.
4. News Feature, Chemical Engineering, February 22, 1982, p. 37.
5. Synthetic Fuels Report, September 1982, p. 2-10.
6. Synthetic Fuels Report, June 1983, p. 2-28.
7. J. D. Miller, U.S. Patent No. 4,279,743, July 21, 1981.
8. C. A. Audeh, J. J. Dickert and P. E. Fowles, U.S. Patent 4,466,882, August 24, 1984.
9. C. J. Vadovic ACS Symposium Series #230, 1983, p. 385.
10. A. M. Rubel and T. T. Coburn, 1981 Eastern Oil Shale Symposium Proceedings, Lexington, Kentucky, November, 1984, p. 21.
11. J. W. Reasoner, L. Sturgeon, K. Naples and M. Margolis, 1981 Eastern Oil Shale Symposium Proceedings, Lexington, Kentucky, November, 1981, p. 11.
12. R. A. Addington, J. P. Humphrey, and E. M. Piper, 1983, IGT Symposium Synthetic Fuels from Oil Shale and Tar Sands, Louisville, Kentucky, May 17-19, 1983, P. 497.

13. M. Nakamura, R. Matsumotu, M. Sasaki, N. Yamagucki and N. Hirai, *ibid*, p. 167.
14. M. R. Abadi and R. W. Mickelson, AIChE 91st National Meeting, August, 1981, Detroit, Paper No. 16B.
15. C. A. Audeh, ACS, Division of Petroleum Chemistry, Inc. Preprints, Vol. 29, No. 1, p. 19.

Table I

Properties and Yields of Products Obtained by Fischer Assay Retorting a New Albany Raw Shale

Yields	
Oil, G/T	13.0
Oil, %wt	5.0
Spent Shale, %wt	90.2
Gas, liters/100 g	1.67
H <sub>2</sub> S, liters/100 g (%wt)	0.53(0.81)
Total Gas, liters/100 g	2.20
Water, %wt	1.9
Oil Properties	
Gravity, °API	22.6
Specific Gravity, 60/60°F	0.9182
Viscosity at 40°C, cS	8.94
Viscosity at 40°C, SUS	51.0
Carbon, %wt	85.26
Hydrogen, %wt	10.87
Nitrogen, %wt	1.13
Sulfur, %wt	1.62
Raw Shale Analysis, %wt	
Carbon	12.83
Hydrogen	1.41
Nitrogen	0.40
Sulfur	4.77
Ash	77.4
Spent Shale Analysis, %	
Carbon	8.05
Hydrogen	0.47
Nitrogen	0.34
Sulfur	3.78
Ash	86.6

Table II

Yields and Elemental Analyses of Beneficiated  
New Albany Oil Shale Fractions

Fraction No	Weight	% Wt	C	H	N	S
Raw Shale	50	100	12.83	1.41	0.40	4.77
1	2.8	5.6	32.20	2.74	0.83	6.30
2	6.0	12.0	33.01	2.70	0.78	6.19
3	16.0	32.0	9.69	0.56	0.26	2.82
4	20.0	40.0	7.19	0.37	0.18	2.58
Residue (ground)	2.7	5.4	3.04	0.33	0.06	1.27
Unground Residue	2.6	5.2	11.85	0.83	0.34	5.48

Table III

Fischer Assay Yield and Thermogravimetric Weight Loss in  
Argon in the 210-510°C Temperature Range of 3 Shales

Shale Sample	Carbon %wt	TGA Wt Loss % wt		Fischer Assay Oil Yield G/T
		Oil	Water	
Colorado	12.1	10.5	1.0	27.8
New Albany 1	11.8	4.3	2.5	11.1
New Albany 2	12.8	5.0	2.1	13.0

Table IV

Thermogravimetric Weight Loss in Argon in the 210-510°C  
Temperature Range of Beneficiated  
New Albany Oil Shale Fractions

<u>Fraction No</u>	<u>Loss, % Weight</u>	<u>G/T</u>
Raw Shale	6.5	13.0
1	22.0	45.0
2	22.0	45.0
3	4.0	8.0
4	3.0	6.0
Residue (ground)	1.0	-
Unground Residue	5.0	11.0

Table V

Thermogravimetric Weight Loss in Air of Beneficiated  
New Albany Oil Shale Fractions

<u>Fraction No</u>	<u>Loss, % Weight</u>
Raw Shale	18.3
1	34.0
2	34.0
3	5.0
4	5.0
Unground Residue	18.0

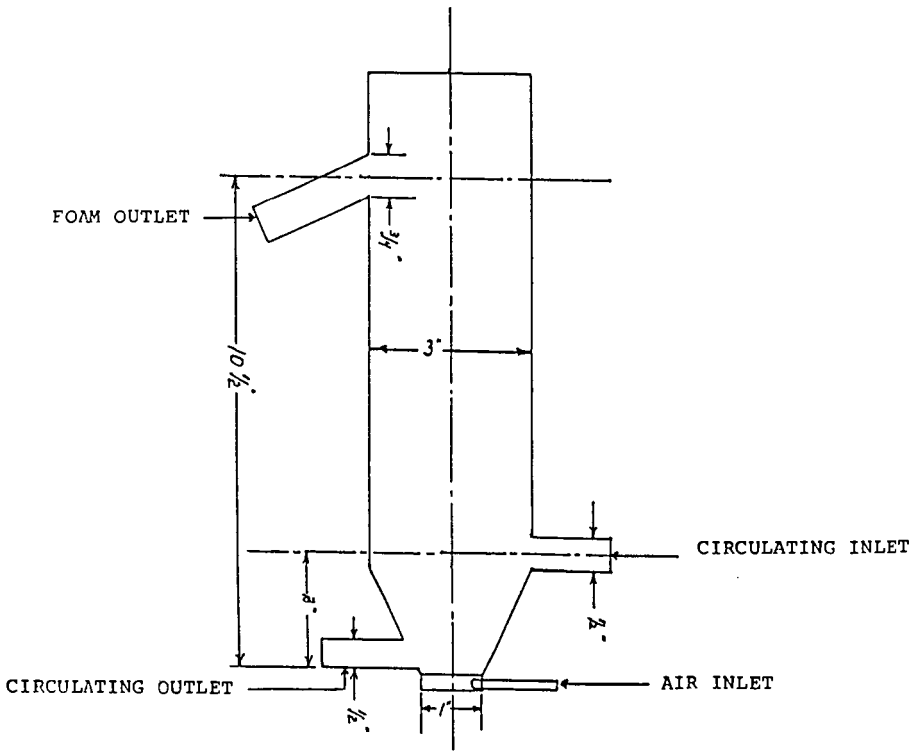


FIGURE 1

FLOTATION CELL

## COMBINED BENEFICIATION AND HYDRORETORTING OF OIL SHALE

R. Bruce Tippin, University of Alabama  
P. O. Box AY, University, AL 35486

and

Raymond C. Rex, HYCRUDE Corporation  
10 West 35th Street  
Chicago, Illinois 60616

### ABSTRACT

The Mineral Resources Institute (MRI) of The University of Alabama and Institute of Gas Technology subsidiary, HYCRUDE Corporation, are evaluating the potential benefits of combining pre-concentration of oil shale by froth flotation followed by hydroretorting to recover the oil. Exploratory laboratory testing of several oil shales has been completed in a continuing research program. To date the testing includes a sample of Upper Devonian New Albany shale from Indiana, an upper Chattanooga shale from Alabama and a Permian Irati shale from Brazil.

Results of flotation tests of the three samples showed that the oil content in the beneficiation concentrates was increased by a factor of 2 to 3 with recoveries up to 90 percent. After briquetting the products, the MRI beneficiated oil shales were submitted to HYCRUDE and subjected to bench scale HYTORT processing. The yield was improved further through hydroretorting by a factor between 3 and 5.5.

### INTRODUCTION

Until recent years most of the research and development work directed toward establishing a domestic oil shale industry has focused on the shales of the Green River Formation of Eocene age occurring in Colorado, Utah, and Wyoming. This is largely because the Western shales are relatively rich (in the range of 25-30 gal/ton) and respond favorably to oil production by simple thermal treatment, yielding 75-85% of their organic content (kerogen) as oil when pyrolyzed.

Recent developments in innovative retorting and fine particle technologies have altered this situation significantly. The HYTORT process, developed by HYCRUDE Corporation utilizes hydrogen rich gas during retorting to enhance oil yields from certain types of oil shales. It has provided a key to processing the Devonian-Mississippian shales of the Eastern United States to achieve oil yields comparable to those from Colorado shales. This technique permits the fullest possible recovery of oil from the kerogen present in the shale.

The range of potential oil shale resources available to HYTORT processing can be expanded by combining hydroretorting with The University of Alabama Mineral Resources Institute's (MRI) physical beneficiation process. The MRI process involves fine grinding the oil shale matrix followed by selective froth flotation of the kerogen. During flotation up to three quarters of relatively kerogen-free inorganic matter is rejected as waste.

By combining the HYTORT and MRI processes, the economics of treating oil shales can be improved, and the range of oil shales which can be processed is extended. Descriptions of the MRI and HYTORT processes, and typical results obtained on oil shales of low and moderate kerogen content are presented in this paper.

### BACKGROUND

#### The HYTORT Process

Oil shales vary significantly in their ability to produce oil. For example, the Green River oil shales of the Western U.S. contain a high hydrogen content in

proportion to organic carbon, and exhibit relatively complete conversion of kerogen to oil. When retorted by conventional thermal processes. However, many other oil shales including the Eastern U.S. Devonian shales, contain lesser amounts of hydrogen relative to organic carbon as shown in Table 1. This deficiency in hydrogen reduces the fraction of the kerogen which can be converted to hydrocarbon products by conventional retorting (1,2). Oil yields from these shales can be substantially improved by supplying hydrogen during retorting. Thus a significant larger fraction of the kerogen is converted to hydrocarbon products rather than remaining in the spent shale in the form of coke. The degree of oil yield enhancement for each particular oil shale depends upon the partial pressure of hydrogen used.

In 1980 HYCRUDE Corporation was formed to commercialize the HYTORT process. HYTORT is a process which utilizes a hydrogen-rich gas for the hydroretorting of oil shale kerogen to produce a synthetic crude oil. The hydroretorting is carried out in a hydrogen-rich atmosphere at elevated pressure, and enables attainment of the maximum possible oil yields from most oil shales. As a result of a Development Agreement with Phillips Petroleum Company, a feasibility study was conducted by HYCRUDE Corporation, Phillips Petroleum Company, Bechtel Group, Inc., and the Institute of Gas Technology. The HYTORT process development work during the feasibility study was divided into three basic areas:

- Chemistry of hydroretorting
- Experimental development work to support mechanical design of HYTORT reactors
- Process design, reactor mechanical design, and cost estimation work.

The HYTORT experimental work and process economics were completed in May 1983 and details are available in other publications (3,4).

Throughout the course of the feasibility study, the HYCRUDE Corporation and Bechtel Group, Inc. continually reviewed the experimental efforts to assure that the experimental programs addressed areas important to the design of commercial reactions (5). This study resulted in a conceptual commercial plant design for Eastern U.S. Devonian shale processing based on the results of the experimental program. The conceptual HYTORT plant flow diagram is shown in Figure 1. The plant contains all the process areas necessary to produce upgraded shale oil including by-product recovery of sulfur and ammonia. As designed, the HYTORT reactors can be constructed using currently available equipment. All other processes are within the sizing and operating constraints of commercial facilities. Implementation of the plant design can be achieved with current process technology.

Natural gas is utilized in the production of hydrogen and as an indirect heat source for hydroretorting. This is an economic optimum for areas such as the Eastern United States where inexpensive sources of natural gas area available. For plants located in areas lacking an inexpensive natural gas source, the HYTORT process conditions would be selected to provide sufficient by-product gas as a substitute.

Although most of the HYTORT process development effort has concentrated on Eocene oil shales of the Western U.S. and on Eastern U.S. Devonian oil shales (1,2), HYCRUDE Corporation in cooperation with the U.S. Geological Survey is conducting work on other oil shales from various locations worldwide. The primary goal of this on-going work is to determine the extent of oil yield enhancement which can be obtained using HYTORT processing. Test work is conducted in a Hydroretorting Assay unit (6), which is designed to serve the same function for HYTORT processing that the ASTM D3904-80 Fischer Assay test serves for conventional thermal retorting processes. Table 2 gives results

of Hydrotretorting Assay tests on some of the samples. The data show that HYTORT processing had a wide range of effects on the shales tested, with oil yield enhancements varying from no improvement to oil yields over four times those obtained in Fischer Assay tests. No trend of behavior with geological age is evident. Further details of these test results are available in a previous publication (4).

#### The MRI Oil Shale Beneficiation Process

Physical beneficiation techniques have long been used in the mineral and coal industries to obtain a product more enriched in the economical mineral than the run-of-mine ore. A prerequisite for physical separation is to free the valuable constituent from the associated impurities. This is normally achieved by comminution of the raw material to sizes finer than their natural particle size consist. The degree of grinding may dictate certain separation approaches. This is particularly important in the case of oil shales, which are fine grained sedimentary rocks composed of 10 micron particles (7). Thus ultrafine grinding of the shale is required to achieve reasonable liberation of oil-bearing kerogen from the intimately associated inorganic mineral matter.

Ultrafine grinding and physical beneficiation of finely disseminated ores were once considered impractical. This is because of the general belief that the grinding costs are prohibitive and that most separation techniques at sizes finer than 74 microns (200 mesh) are ineffective (8). However, this belief has been dispelled with the continuing engineering advancement in beneficiation equipment and recent advances in fine particle technology. This is evidenced by the non-magnetic taconite flotation plant of the Cleveland-Cliffs Iron Company in the Lake Superior Region (9). In this large tonnage plant the hard taconite ore is ground to a particle size finer than 30 microns (500 mesh) prior to flotation to recover high grade iron oxide products. The technical practicality and economic feasibility of extremely fine grinding of the hard, tough taconite suggests that fine grinding and flotation of the oil shale should be equally effective.

During the past six years of continuing research, MRI has developed a beneficiation process which successfully concentrates the Devonian oil shales of the Eastern U.S. The MRI process involves wet grinding the raw shale to minus 20 microns followed by froth flotation to recover a kerogen rich concentrate. Details of the development of this process are available in previous publications (10-12).

MRI test results have been used to formulate a process flowsheet for an oil shale beneficiation plant (Figure 2). The plant is designed to recover concentrates yielding 2 to 3 times as much recoverable oil per ton as can be obtained from the raw untreated shale. Unit operations of this plant are within the limits of current commercial practice. In the process, at least 50% to as much as 70% of the raw shale will be rejected as a substantially barren waste which need not be retorted.

The beneficiation plant includes the following standard mineral processing unit operations:

- Fine grinding of shale to mineral particle liberation size
- Classification
- Kerogen flotation
- Thickening and filtration
- Agglomeration or briquetting of the flotation concentrate
- Disposal of the flotation tailing

Most of the beneficiation research investigations has been directed to the Eastern oil shale deposits, particularly the Devonian shales outcropping in Northern Alabama, but several samples from the Western United States and foreign countries also have been tested in a cursory way. Typical results are shown in Table 3. Plans are to evaluate additional types of oil shales as they become available.

#### EXPERIMENTAL

The combined beneficiation and hydrotretorting studies were conducted on two Eastern oil shale samples (Alabama and Indiana) and one foreign sample (Brazil). The Indiana sample was collected by HYCRUDE Corporation from the Upper Devonian New Albany shale formation near Henryville, Indiana. The Alabama shale sample was part of a 5-ton lot of Upper Chattanooga shale collected by MRI from the Hester Creek area in Madison County, Alabama. The Brazilian oil shale represents a typical shale from the Irati formation in the south of Brazil. Analyses and Fischer Assay oil yields from the three samples and a Western shale are shown in Table 1.

#### Procedures and Techniques

The beneficiation tests were conducted at the Mineral Resources Institute at the University of Alabama. In these tests the raw shale samples were stage crushed dry to minus 2 mm (10 mesh) and wet ground in a 20 x 30 cm stainless steel rod mill operated at 78% of critical speed using 26 stainless steel rods of 1.7 cm diameter as the grinding medium. A 500-gram charge of each flotation test sample was ground at 50% solids in Tuscaloosa tap water for two hours to reduce the particles to 90% minus 10 microns. Bench scale flotation tests were conducted using a Denver Model D-12 laboratory flotation machine for the conditioning, roughing and cleaning steps. The flotation products were filtered, dried at 50° C, weighed and assayed for oil yield using the modified Fischer Assay method. Samples for hydrotretorting were produced from the flotation concentrate using a uniaxial compression briquetting unit to make 1.25 cm diameter by 1 cm high specimens.

Hydrotretorting tests were conducted at the Institute of Gas Technology at Chicago, Illinois under the sponsorship of HYCRUDE Corporation using a Hydrotretorting Assay unit designed to evaluate the hydrotretorting characteristics of oil shale samples. Details of the apparatus and the test procedure have been previously published (6). In this unit a 100-gram sample of material is reacted with hydrogen gas under the following conditions.

- 1000 psig pressure
- 1000° F temperature
- 4 SCF/hr gas flow
- 25 degree/minute heat-up rate
- 30 minutes reaction time

#### RESULTS AND DISCUSSION

##### Beneficiation of Raw Oil Shale

Response of the oil shale samples to beneficiation by ultrafine grinding and flotation are given in Table 4. All three samples responded favorably to beneficiation. Good flotation of the kerogen-enriched fractions was obtained from the ground shale which indicated that reasonable liberation of the kerogen and the mineral components was achieved. As compared to the flotation feed, the concentrates recovered from the Alabama and Indiana samples were upgraded in kerogen by factors of 2.4 and 2.8,

respectively. Flotation of the Brazilian shale yielded a concentrate assaying 33.5 gallons per ton, but the ratio of concentration (1.7) was less than that of the American oil shale samples. The variations in the response of the samples to flotation are attributed to differences in their origin, mineral substrate, and composition. The oil recoveries in all cases were comparable. Only the Alabama oil shale has been investigated extensively at MRI and improvements in the flotation results of the other shales would be expected by further research. Even with the limited number of samples evaluated, it appears reasonable to assume that beneficiation of oil shales can be accomplished with good results.

Experimental testwork is continuing on this research program at The University of Alabama to further define the beneficiation variables in an effort to optimize the process. The goal of the research is to establish the technical parameters of the process in a continuous pilot plant operation to define the process economics. The pilot testing will also produce a reasonably large quantity of kerogen enriched concentrate which will be used in more extensive hydroretorting tests.

#### Hydroretorting of Raw Oil Shale

Results of Hydroretorting Assay tests on the three raw shale samples are given in Table 5. Results of the tests of the U.S. samples indicate that the HYTORT process can produce oil yields of 222 to 226% of those obtained by conventional thermal retorting. The oil yield from the Brazilian sample was less, only 156%. The hydroretorting data shows that oil yields of 27 to 29 gallons per ton can be produced from oil shale resources which would be considered too lean for commercialization by conventional retorting.

#### Combined Beneficiation and Hydroretorting of Oil Shale

Combined MRI beneficiation-HYTORT processing was tested on a laboratory scale by hydroretorting the flotation concentrates of three oil shale samples. Test results are shown in Table 6. The concept proved to be technically successful in substantially increasing the extraction of oil. The data indicate that the combined technique can improve the overall level of oil yield from the raw shale by a factor of 2.9 to 5.6.

#### CONCLUSIONS

Based on the above results, the potential of the combined beneficiation-hydroretorting approach is evident in the following areas:

- Reduction in the capital and operating costs for oil shale production should be possible by substituting atmospheric pressure, ambient temperature, grinding and froth flotation equipment for some of the elevated pressure and temperature HYTORT reactor units. Further, because of the enhanced shale oil yields, energy savings should result in a lower cost per barrel of shale oil.
- Pre-retorting concentration of kerogen from lean shales should extend the range of oil shales which can be considered for commercial processing.
- Rejection of inorganic sulfur (i.e., pyrite) may be possible either by flotation or high-intensity magnetic separation. By removing the pyrite, not only will the kerogen content increase but the overall quality of the concentrate will be enhanced.
- During grinding, trace elements are solubilized into the process water. As a result, the tailings rejected during beneficiation and the spent shale produced by HYTORT processing should be less prone to the natural leaching of harmful metals and elements. Thus, surface and groundwater contamination after disposal should be substantially reduced.

#### ACKNOWLEDGEMENTS

HYCRUDE Corporation would like to acknowledge the interest and support of the Institute of Gas Technology, particularly Dr. F. S. Lou, and Mr. M. J. Roberts, in conducting the hydrotorting assay testwork. The Brazilian oil shale sample was graciously provided by Mr. Lauro Carta of Petrobras, Petroleo Brasileiro, S.A.

#### REFERENCES

1. Janka, J. C. and J. M. Dennison, "Devonian Oil Shale: A Major American Energy Resource," Presented at the IGT Symposium on Synthetic Fuels from Oil Shale, Atlanta, Georgia, December 3-6, 1979. Published in Proceedings, April 1980, pp. 22-116.
2. Matthews, R. D., J. C. Janka, and J. M. Dennison, "New Insights into Devonian Oil Shale Resources of the Eastern United States," AAPG Bulletin, Vol. 65, No. 5 (May 1981), pg. 53. Paper presented at the following meetings: AAPG Eastern Section Meeting, October 1-3, 1980, Evansville, Indiana (AAPG Bulletin), Vol. 64, No. 8, August 1980, pg. 1285). AAPG Annual Convention, San Francisco, May 31 - June 3, 1981.
3. Rex, R. C., P. A. Lynch, M. J. Roberts, and H. L. Feldkirchner, "Experimental Test Program of the HYTORT Feasibility Study." Presented at the 1983 Eastern Oil Shale Symposium, Lexington, Kentucky, November 13-16, 1983. Published in Proceedings, February 1984, pp. 391-229.
4. Janka, J. C., and R. C. Rex, "Application of the HYTORT Process to Oil Shales Throughout the World," Paper presented at the Summer National Meeting of the American Institute of Chemical Engineers, Philadelphia, Pennsylvania, August 19-22, 1984.
5. Rex, R. C., et al., "Selection of a Commercial Plant Design for the HYTORT Process." Presented at the 3rd IGT Symposium on Synthetic Fuels from Oil Shale and Tar Sands, Louisville, Kentucky, May 17-19, 1983. Published in Proceedings, July 1983, pp. 531-544.
6. Lynch, P. A., et al., "The Hydrotorting Assay - A New Technique for Oil Shale Assessment," Paper presented at the Joint Fuel/Petroleum Division Meeting of the American Chemical Society, St. Louis, Missouri, April 8-13, 1984.
7. Nowack, P., Oil Shale Technical Data Handbook, Noyes Data Corporation, Park Ridge, New Jersey (1981).
8. Somasundaran, P., Ed. Fine Particles Processing, Pub. AIME, New York, 1, 2 (1980).
9. Villar, J. W. and G. A. Dawe, "The Tilden Mine - A New Processing Technology for Iron Ore," Mining Congress. 40-48 (1975).
10. Hanna, H. S., and W. E. Lamont, "Physical Beneficiation Studies of Eastern Oil Shales," Proceedings of the Symposium on Synthetic Fuels from Oil Shale and Tar Sands, Louisville, Kentucky, May 17-19, 1983. Published IGT, pp. 295-321, July 1983.
11. Lamont, W. E., "Beneficiation of the Kerogen Content of Eastern Devonian Oil Shales by Flotation," Paper No. 83-621, presented at the SME-AIME Annual Meeting, Atlanta, Georgia 6-10, 1983.
12. Hanna, H. S. and C. Rampacek, "Eastern Oil Shale Investigations at The University of Alabama." Presented at the 1981 Shale Symposium, Lexington, Kentucky, November 15-17, 1981. Published in Proceedings, dated November 1981, pp. 24-25.

Table 1. Analysis and Fischer Assay Oil Yield of Selected Oil Shales

Oil Shale Sample	Alabama	Indiana	Brazil	Colorado
<b>ULTIMATE ANALYSIS (wt. %)</b>				
Organic Carbon	14.20	12.53	13.70	13.60
Organic Hydrogen	1.03	0.93	1.37	2.10
Sulfur	8.02	4.41	4.98	0.50
Carbon Dioxide	2.90	2.30	N.A.	15.90
Nitrogen	0.48	0.48	0.44	0.50
Ash	79.70	77.83	80.00	66.80
Atomic H/C Ratio	0.87	0.94	1.2	1.85
<b>FISCHER ASSAY</b>				
Yield (wt. %)	4.9	4.6	7.1	11.4
Yield (gal/ton)	11.6	12.0	18.6	29.8
Carbon Conversion (%)	31.2	32.9	50.0	84.0

Table 2. Selected Hydroretorting Assay Test Results

Oil Shale Sample	Oil Yield (gal/ton)		
	Fischer Assay	Hydroretorting Assay	Percent of Fischer Assay
Sweden - Billingen	3.8	17.5	440
Sweden - Naerke	10.9	32.3	300
Sicily	4.4	12.2	280
Indiana - New Albany	12.5	28.2	230
Montana - Heath Formation	16.2	33.6	210
Canada - Kittle	10.0	21.1	210
Jordan - El Lajjun	32.8	57.0	170
Brazil - Lower Irati	19.4	32.7	170

Table 3. Selected Beneficiation Test Results

Oil Shale Sample	Fischer Assay (gal/ton)		Percent Oil Recovered	Ratio of Concentration
	Flotation Feed	Flotation Concentrate		
Eastern U.S.				
Alabama	12	37	87	3.1
Kentucky	17	31	81	1.8
Indiana	12	35	81	2.9
Western U.S.				
(Lo-grade)	14	34	90	2.4
(Hi-grade)	46	88	80	1.9
Canadian	8	16	52	2.0
Brazil	20	34	89	1.7

Table 4. Flotation Response of Raw Oil Shales

Oil Shale Sample	Flotation Products	Weight Percent	Fischer Assay Yield (gal/ton)	Distribution of Oil (%)
Alabama Chattanooga Shale	Concentrate	27.0	34.3	80.0
	Reject	73.0	3.2	20.0
	Feed	100.0	11.6	100.0
Indiana New Albany Shale	Concentrate	35.5	27.2	79.0
	Reject	64.5	4.4	21.0
	Feed	100.0	12.5	100.0
Brazil Irati Shale	Concentrate	48.9	33.5	88.2
	Reject	51.1	4.3	11.8
	Feed	100.0	18.6	100.0

Oil Shale Sample	Original Sample Fischer Assay (gal/ton)	Hydroretorted Sample Assay (gal/ton)	Oil Yield Percent of Fischer Assay
Alabama - Chattanooga	11.6	27.8	220
Indiana - New Albany	12.5	27.2	230
Brazil - Irati	18.6	29.0	160

Oil Shale Sample	Oil Yield (gal/ton)			Overall Percent of Fischer Assay
	Original* Sample	Flotation* Concentrate	Hydroretorted Concentrate**	
Alabama - Chattanooga	11.6	34.3	65.0	560
Indiana - New Albany	12.5	27.2	54.4	430
Brazil - Irati	18.6	33.5	53.3	290

\* Fischer Assay

\*\* Hydroretorting Assay

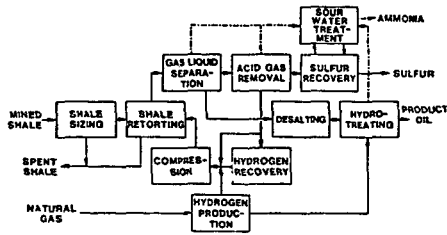


Figure 1. CONCEPTUAL COMMERCIAL HYTORT PLANT BLOCK FLOW DIAGRAM

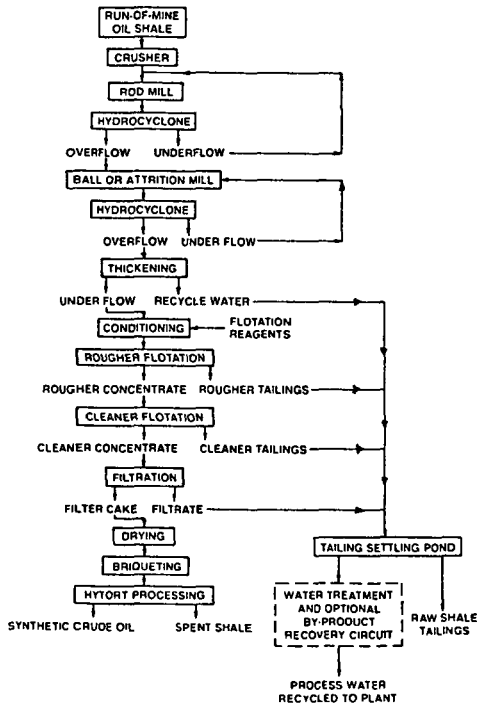


FIGURE 2. SCHEMATIC FLOWSHEET FOR MRI OIL SHALE BENEFICIATION PLANT

INVESTIGATION OF THE REACTION MECHANISMS FOR PYROLYSIS OF  
RUNDLE OIL SHALES BY DYNAMIC  $^1\text{H}$  NMR TECHNIQUES

T. Parks, L.J. Lynch and D.S. Webster

CSIRO Division of Fossil Fuels, P.O. Box 136, North Ryde,  
NSW, 2113, Australia

ABSTRACT

Dynamic proton nuclear magnetic resonance ( $^1\text{H}$  NMR) techniques were used to study the pyrolysis behaviour of a suite of Rundle oil shale ore types. Experimental results were obtained by monitoring the  $^1\text{H}$  NMR transverse relaxation signal for both the shales and their kerogen concentrates during their pyrolysis by heating at a uniform rate in open glass tubes in an inert atmosphere provided by flowing nitrogen gas.

These results indicate that while the Rundle ore types have variable pyrolysis behaviour, all of the demineralized shales pyrolyse similarly. The differences observed in the behaviour of the shales are thought to be a consequence of variations in the permeability of the inorganic matrices to evolving volatile species. Enhancement of molecular mobility marks two transitions of the specimen during pyrolysis. The first, which occurs between room temperature and  $\sim 500$  K and involves most of the structure, is probably a "glass to rubber" type transition and the second, which occurs near 600 K indicates the presence of a relatively thermally stable component in the kerogen. The results show that the pyrolysis residue formed above 750 K is contributed to by material that passes through a transient mobile state.

INTRODUCTION

Studies over many years of the pyrolytic decomposition of oil shales have led to a variety of kinetic models which invoke intermediate species referred to as pyrobitumens (1-3) and sometimes also as rubberoid (4) and polyoil (5) species. These intermediate species are at best only loosely defined and while it is expected that such intermediate states do occur during pyrolysis their delineation in composition and occurrence are still matters for investigation. In these models the original kerogen is usually treated as being homogeneous but recently kerogen pyrolysis has been analysed in terms of the chemically distinct aromatic and aliphatic fractions (6-8).

Dynamic measurement techniques have an advantage over equilibrium measurement techniques in such investigations because of their potential to monitor transient states of the reacting system. The adaptation of proton nuclear magnetic resonance ( $^1\text{H}$  NMR) as a dynamic measurement technique has been described previously (9-11). The hydrogen specificity of the  $^1\text{H}$  NMR experiment aids in the distinction of thermal processes associated with the organic kerogen from those of the inorganic matrix of the shale. For organic solids the most important factors governing their  $^1\text{H}$  NMR behaviour are the concentration and distribution of protons and unpaired electrons in the structure and the molecular dynamics. To this extent uncoupled or "broadline" NMR can provide information on the complex interactions which determine the molecular properties and form of the bulk material. These NMR measurements will detect molecular mobility changes associated with melting and other "softening" transitions and likewise transitions of the molecular lattice back to the rigid lattice state, the loss of hydrogen from the specimen during decomposition and changes in free radical concentrations related to bond rupture and condensation reactions. The results reported here are all derived from dynamic measurements of the  $^1\text{H}$  NMR transverse relaxation signal  $I(t)$ . Parameters are derived from these measured signals which (a) represent the residual specimen as consisting of two

components, one containing rigid hydrogen and the other mobile hydrogen, (b) characterize the molecular mobility of the structure containing the mobile hydrogen, (c) estimate the residual hydrogen content and (d) characterize the  $^1\text{H}$  NMR transverse relaxation signal  $I(t)$  and therefore the total residue in terms of its average molecular mobility. The temperature dependences of these parameters form a set of pyrograms reflecting changes in the specimen during the pyrolysis.

## EXPERIMENTAL

The shales studied were a suite of the ore types distinguished and characterized in the Rundle deposit by Coshell (12). Specimens in the form of -100 mesh powders were supplied by ESSO Australia together with chemical analysis and Fischer assay oil yield data (Table I). A composite Rundle shale has been reported as having a  $^{13}\text{C}$  CP-MAS aromaticity value of about 0.22 (13). Kerogen concentrates were prepared by HCl/HF digestion of the mineral matter and subsequent analysis showed them to contain large quantities of fluorine and to have total ash contents in the range 17 to 38% (13).

Predried shale and kerogen concentrate specimens of ~ 400 mg contained in 8 mm O.D. open glass tubes were used for the  $^1\text{H}$  NMR thermal analysis experiments which were conducted under nitrogen gas flowing at  $5\text{ ml min}^{-1}$ . Comparative studies of the shale ore types and their kerogen concentrates were made in a series of pyrolysis experiments at a uniform heating rate of  $4\text{ K min}^{-1}$ . The  $^1\text{H}$  NMR measurements were made using the two pulse ( $90^\circ\text{-}\tau\text{-}90^\circ$ ) sequence to generate the solid-echo form of the  $^1\text{H}$  NMR transverse relaxation signal  $I(t)$ . A sequence repetition time of 1 s avoided saturation effects which indicates that the shales are free of inorganic hydrogen with much longer  $^1\text{H}$  NMR spin-lattice relaxation times that have been found to occur in Green River oil shales (14).

## RESULTS AND ANALYSIS

The peak signal amplitude  $I(2\tau)$  normalized per gram of sample at room temperature (which is a measure of the hydrogen concentration contributing to the NMR signal of the specimens) shows a linear correlation with elemental percent hydrogen (w/w) as shown in figure 1 for both the whole and the demineralized shales used in the study. The fact that both the whole and demineralized shales gave the same linearity of  $I(2\tau)$  with elemental hydrogen further indicates that the  $^1\text{H}$  NMR signals are representative of all the hydrogen in the shales. It is important therefore to know the relative contributions to the  $^1\text{H}$  NMR signals of the organic kerogen and the inorganic matrix. Figure 2 compares the temperature variation of the relative  $^1\text{H}$  NMR signal amplitudes (normalized per gram of shale) for three shales of different grade with that for a predried montmorillonite sample pyrolysed at  $6\text{ K min}^{-1}$ . Analyses of these shales (15) have shown that clays which account for ~ 35% of the inorganic matter are the only significant source of inorganic hydrogen with montmorillonite being the most abundant clay variety. The data in Figure 2 therefore show that the inorganic hydrogen signal is a minor fraction of the total shale signal except for the relatively kerogen-poor ore types such as claystone (ore type III in figure 2). The mineral matter analysis data of Loughnan (15) identified montmorillonite, kaolinite, and illite clays in Rundle shales. From the experimentally determined  $^1\text{H}$  NMR signal contributions of montmorillonite and kaolinite and an estimated signal contribution of illite, the calculated signal contributions of the clays in the ore types studied range from ~ 13% for the type III claystone to ~ 6% for the most kerogen-rich type I ore.

A selection of  $^1\text{H}$  NMR relaxation signals  $I(t)$ , recorded at various stages of pyrolysis of a predried shale and its kerogen concentrate are shown in figures 3(a) and 3(b) respectively. These data are typical for all the shales studied. At room temperature the signals for both materials are dominated by a rapidly decaying component, which comprises about 90% of the total signal intensity in the case of

the raw shale. This rapidly decaying component is characteristic of a rigid lattice or "glassy" structure devoid of molecular mobility on a time scale less than  $\sim 10^{-5}$  s. The more slowly relaxing minor component of each signal indicates that parts of the structure have a degree of molecular mobility on this time scale, consistent either with extended structural domains being above their glass transition temperature or with a distribution of isolated mobile molecular segments in the structure. As the temperature is raised above room temperature the slower relaxing component increases in intensity at the expense of the rapidly decaying "rigid" signal, suggesting a gradual transition of the structure from the glassy to the mobile state. This occurs earlier and to a greater extent for the demineralized shale. However, even for the shale above  $\sim 600$  K the mobile component accounts for almost all of the signal intensity of the residual specimen. At higher temperatures the total signal intensity falls rapidly as a result of pyrolytic loss of volatile material from the specimen and there is a regrowth of a rapidly decaying signal intensity consistent with the formation of the rigid char residue.

These data were reduced to provide a number of largely independent parameters: (i) The percentage of the total initial signal intensity that is contributed by the rapidly decaying or rigid component (% rigid) is estimated. This estimate is made by fitting an exponential function to the slowly relaxing tail of the signal and extrapolating to the echo peak time of the signal to obtain the mobile signal intensity. The time constant  $T_2$ , of the exponential function is a second parameter which is a measure of the average molecular mobility of the mobile component. These two parameters - % rigid and  $T_2$  - are plotted together against temperature in figures 4a and 4b for a shale and its kerogen concentrate respectively.

(ii) The apparent hydrogen content of the specimen ( $\%H$ ), obtained by calibration of the total  $^1H$  NMR signal intensity  $I(2\tau)$  for its sensitivity to temperature, is a semi-quantitative parameter useful for monitoring the pyrolytic decomposition and loss of volatile products from the sample. Its temperature dependence for the shale and kerogen concentrate are plotted in figures 5(a) and 5(b) respectively. Also shown in these figures are the differential hydrogen contents computed from these data.

(iii) The analytical second moment  $M_2^*$  of the frequency power spectrum representation of the  $^1H$  NMR signal (11) which is characteristic of the total signal and enables a qualitative measure of the average molecular mobility of the total specimen to be monitored during the pyrolysis. The temperature variations of  $M_2^*$  for the whole and demineralized specimens are also recorded in figures 5(a) and 5(b) respectively.

The apparent hydrogen loss pyrolysis profiles at  $4 \text{ K min}^{-1}$  for all of the shales were found to be similar. Two outlying profiles of this set are compared in figure 6, and in figure 7 the corresponding  $M_2^*$  pyrograms are compared. The temperature of maximum rate of loss of hydrogen as defined by the minimum in the differential percent hydrogen content curve, and the total percentage loss of hydrogen from room temperature to 875 K did not vary significantly (see Table I) between the ore types. This small variation in the total percentage loss for the shale ore types and the linear correlation between this loss when expressed as  $^1H$  NMR signal loss normalized per gram of shale and Fischer assay oil yield (figure 8) show that the hydrogen loss during the pyrolysis is predominantly organic.

Previous (16)  $^1H$  NMR second moment profiles presented by us on the pyrolysis of Rundle oil shale identified two regions of enhanced molecular mobility of the kerogen during pyrolysis. The first event occurred on heating from room temperature to  $\sim 500$  K and was attributed to a possible glass to rubber transition. This observation is similar to Maddadin and Tawarah's (17) interpretation of an endotherm they detected for a Jordanian oil shale, peaking in the region 433-443 K, as a physical softening and molecular rearrangement of the kerogen, and is also

consistent with Rogers and Cane's (4) description of a "rubberoid" material present after heating to 523 K for a Permian Torbanite. The second less obvious event commenced just prior to onset of the main pyrolysis at ~ 600 K and was attributed to the mobilization of a relatively thermally stable component of the kerogen. These events occurred for all but one of the shales of the present study and in the case of this exception no second softening event was noticeable. Further as illustrated in figure 7 there are considerable variations apparent in details of the  $^1\text{H}$  NMR second moment profiles for these ore types which occur above 450 K and which cannot simply be accounted for by differences in the kerogen concentration of the ores. Differences are most apparent above ~ 600 K where there is a wide range of behaviours in the total data for the ore suite as represented in figures 6 and 7 by the extreme examples. These differences certainly do not correlate with kerogen concentration. The temperature at which  $M_2^*$  reaches its maximum high temperature value is however very similar, at ~ 780 K for all ores. For those where the onset of increase in  $M_2^*$  is delayed (e.g. ore type I) the rate of increase is greater compared to that of ore types (e.g. ore type XI) where the increase commences earlier.

It can be concluded from these experiments on whole shales that although the behaviour of the different Rundle ore types is similar during heating at the lower temperatures, at higher temperatures and in the zone of main pyrolytic decomposition there are significant differences in the nature of the reacting residues that are particularly evident when the second moment pyrograms are compared. This would suggest the likelihood of corresponding differences in the pyrolysis products of these ore types.

In figures 9 and 10 respectively the sets of  $^1\text{H}$  NMR hydrogen loss and  $M_2^*$  pyrograms for the demineralized ore types are superimposed for comparison. Clearly there is a close similarity in the pyrolysis behaviour of the kerogens of the various ore types. One conspicuous dissimilarity is at low temperatures where in contrast the raw shales are similar. These low temperature differences are possibly the result of variations in the effect of the demineralization treatment on the different ore types in which some degree of structural degradation occurs however it has not been possible to establish any correlation with the analytical data. The more rapid fall in  $M_2^*$  immediately above room temperature for the demineralized as compared to the shale specimens shows lesser inhibition to thermal activation of molecular mobility for the demineralized specimens. This could be contributed to both by covalent bond rupture in the kerogen structure and by reduction of binding interactions at the molecular level between the organic kerogen and the mineral matter. Most of the kerogen structure is transformed from an immobile or rigid lattice state to one of considerable molecular mobility by this low temperature transition during which there is little loss of hydrogen. This low value of  $M_2^*$  attained is sustained on further heating until about 650 K while there is only gradual loss of volatile matter to a total loss represented by 15-20% of the hydrogen at 650 K.

The  $M_2^*$  pyrograms of all the kerogen concentrates are strikingly similar above 500 K. They all show evidence of the secondary softening event and all the residues undergo a rapid transition from their highly mobile state to a rigid state between 750 K and 770 K. This rapid transition in  $M_2^*$  is not reflected in the hydrogen loss programs as a sharp increase but as a sharp decrease in the rate of hydrogen loss at ~ 760 K (figure 10). This is clear evidence of the transition of parts of the mobile material existing in the residue below 750 K by condensation reactions to a rigid state above 770 K. This present evidence for the existence of a transient fluidity in the intermediate kerogen residue complements the microscopic evidence for mesophase formation during the pyrolysis of similar materials by Villey et al (18, 19).

## CONCLUSIONS

Notwithstanding the differences in the  $M_n^*$  pyrograms at low temperatures these  $^1\text{H}$  NMR thermal analysis experiments on the demineralized ore types clearly demonstrate the close similarity of all the Rundle oil shale kerogens tested. These Rundle kerogens all exhibit two "softening" events. The first occurs on heating above room temperature and involves the bulk of the structure. The second occurs above 650 K and involves a minor component. There is slow evolution of volatiles between 450 K and 650 K and rapid evolution between 650 K and 750 K. A rapid solidification of the residue occurs between 750 K and 770 K which identifies the secondary softening as a thermoplastic transient event akin to that of bituminous coals.

Given the similarity of the kerogens of all the ore types and the similar mineralogy of the inorganic matrices (15), the differences detected in the pyrolysis behaviour of the ore types must be related to either the concentration differences, or possible variations in the degree of dispersion and/or the nature of the interactions that occur between the organic and inorganic structures. Any of these factors could for example affect the permeability of the shale matrix to evolving molecular species. Thus it can be concluded that the differences observed in shale pyrolysis above 600 K result from differences in the rates of molecular diffusion and losses of mobile pyrolysis products.

## ACKNOWLEDGEMENTS

This work was carried out in collaboration with and financially supported by Esso Australia and Southern Pacific Petroleum.

## REFERENCES

1. Allred, V.D. Chem. Eng. Progress 62, 55 (1966).
2. Finucane, D., George, J.H. and Harris, H.G. Fuel 56, 65 (1977).
3. Rajeshwar, K. Thermochemica Acta 45, 253 (1981).
4. Rogers, L.J. and Cane, R.F. Aust. Chem. Inst. J. & Proc. 12, 159 (1945).
5. Wen, C.S. and Kobylinski, T.P. Fuel 62, 1269 (1983).
6. Miknis, F.P., Szeverenyi, N.M. and Maciel, G.E. Fuel 61, 341 (1982).
7. Hershkowitz, F., Olmstead, W.N., Rhodes, R.P. and Rose, K.D. In "Geochemistry and Chemistry of Oil Shales", ACS Symposium Series 230 (Eds. F.P. Miknis and J.F. McKay) 301 (1983).
8. Burnham, A.K. and Happe, J.A. Fuel 63, 1353 (1984).
9. Webster, D.S., Cross, L.F. and Lynch, L.J. Rev. Sci. Instrum. 50, 390 (1979).
10. Lynch, L.J. and Webster, D.S. In "Geochemistry and Chemistry of Oil Shales", ACS Symposium Series 230 (Eds. F.P. Miknis and J.F. McKay) 353 (1983).
11. Lynch, L.J., Webster, D.S., Bacon, N.A. and Barton, W.A. In "Magnetic Resonance Introduction, Advanced Topics and Applications to Fossil Energy". (Eds. L. Petrakis and J.P. Fraissard) NATO ASI Series, C 124, 617, Reidel, Dordrecht (1984).
12. Coshell, L. Proc. First Australian Workshop on Oil Shales, Lucas Heights, 25 (1983).
13. Wilson, M.A., Lambert, D.E. and Collin, P.J. Fuel (in press) (1985).
14. Miknis, F.P., Decora, A.W. and Cook, G.L. In "Science and Technology of Oil Shales" (Ed. T.F. Yen) Ann Arbor Science, Ann Arbor, 35 (1976).
15. Loughnan, F.C. "Rundle Oil Shale Mineralogical Analysis of Ore Types", Esso Australia Ltd. Report (1983).
16. Lynch, L.J., Webster, D.S. and Parks, T. Proc. First Australian Workshop on Oil Shales, Lucas Heights, 139 (1983).
17. Haddadin, R.A. and Tawarah, K.M. Fuel 59, 539 (1980).
18. Villey, M., Oberlin, A. and Combaz, A. Carbon 17, 77 (1979).
19. Oberlin, A., Villey, M. and Combaz, A. Carbon 18, 347 (1980).

**TABLE I**  
Analyses and Pyrolysis Data of Rundle Ore Types

Shale Ore Type <sup>1</sup>	F.A. Oil Yield (L/t) Shale	C (%w/w)		Ash (%w/w)		Temperature at Max. Rate of H Loss (K)		Hydrogen Volatile % (298-875K)	
		Shale	Shale	Shale	Demin.	Shale	Demin.	Shale	Demin.
LRC <sup>2</sup> I	137	17.50	72.2	16.9	725	725	90	95	
LRC II	134	17.18	71.2	19.5	725	725	93	95	
LRC III	29	6.71	84.0	37.9	725	725	88	91	
LRC IV	63	9.38	83.5	26.7	730	720	87	91	
LRC V	112	15.74	75.2	19.2	725	725	88	92	
LRC <sup>3</sup> VI	56	8.94	82.8	29.8	720	720	91	95	
BK <sup>3</sup> IX	95	14.09	77.1	-	725	725	90	92	
BK XI	56	8.81	82.7	-	720	725	86	92	

<sup>1</sup> Coshell (12)

<sup>2</sup> Lower Ramsay Crossing seam

<sup>3</sup> Brick Kiln seam

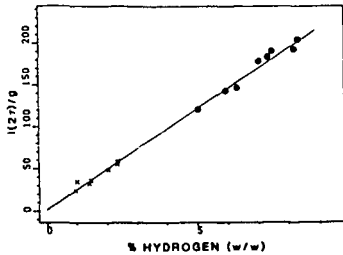


Figure 1.  $^1\text{H}$  NMR signal peak intensity ( $I(2\tau)$ ) per gram of specimen versus % elemental hydrogen for Rundle shales (x) and kerogen concentrates (•).

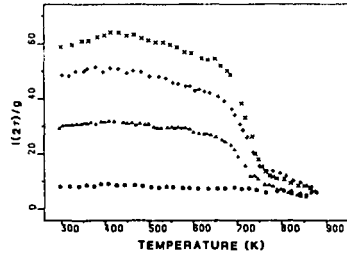


Figure 2. The apparent residual hydrogen per gram of specimen from  $^1\text{H}$  NMR measurements versus temperature for Rundle ore types I(x), IX(+), III(Δ) and montmorillonite (•).

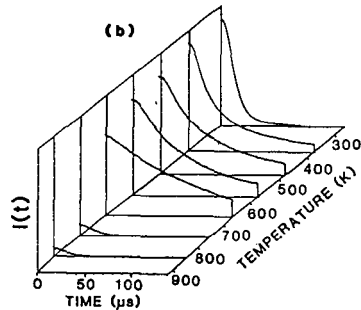
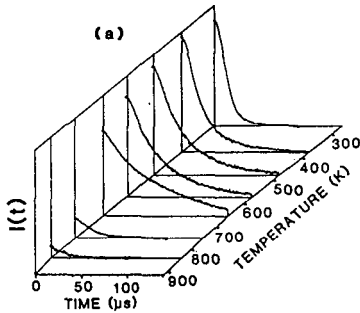


Figure 3.  $^1\text{H}$  NMR transverse relaxation signals,  $I(t)$ , recorded at various temperatures during pyrolysis of (a) the whole shale and (b) the kerogen concentrate of Rundle ore type II.

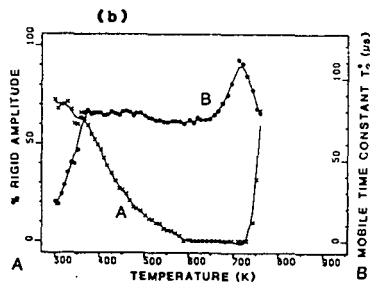
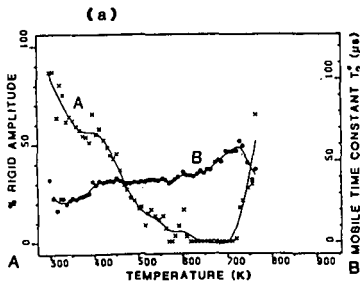


Figure 4. Pyrograms showing the temperature dependences of percentage rigid hydrogen (% Rigid) and the relaxation time constant ( $T_2$ ) of mobile hydrogen during pyrolysis of (a) the whole shale and (b) the kerogen concentrate for Rundle ore type II.

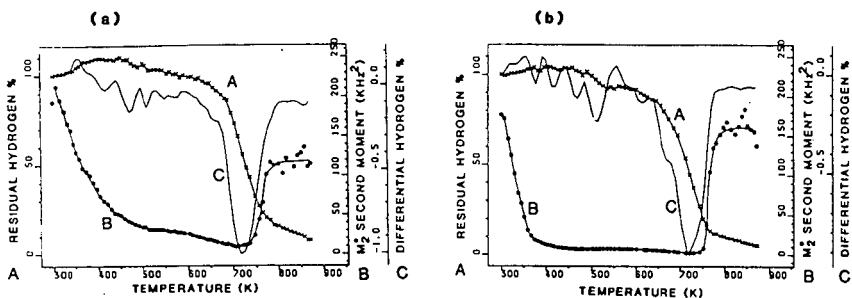


Figure 5. Pyrograms showing the temperature dependences of the apparent residual hydrogen (A), the differential hydrogen content (C) and the  $^1\text{H}$  NMR power spectrum second moment,  $M_2^*$ , (B) during pyrolysis of (a) the whole shale and (b) the kerogen concentrate of Rundle ore type II.

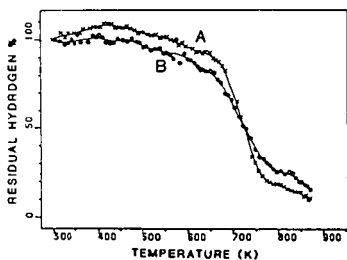


Figure 6. A comparison of pyrograms of the percent apparent hydrogen content for Rundle shale ore types (A) I and (B) XI.

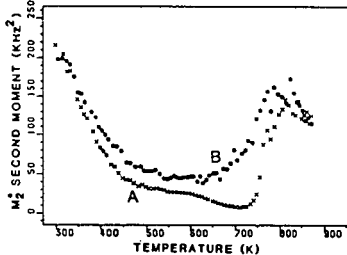


Figure 7. A comparison of the  $^1\text{H}$  NMR power spectrum second moment ( $M_2^*$ ) pyrograms for Rundle shale ore types (A) I and (B) XI.

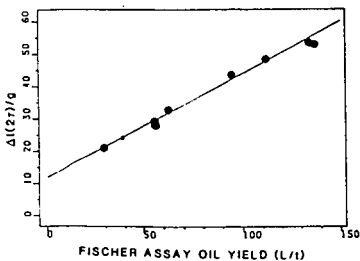


Figure 8. Loss of  $^1\text{H}$  NMR signal intensity ( $\Delta I(2\tau)$ ) on heating at  $4 \text{ K min}^{-1}$  from 298 to 875 K normalized per gram of shale versus Fischer Assay oil yield.

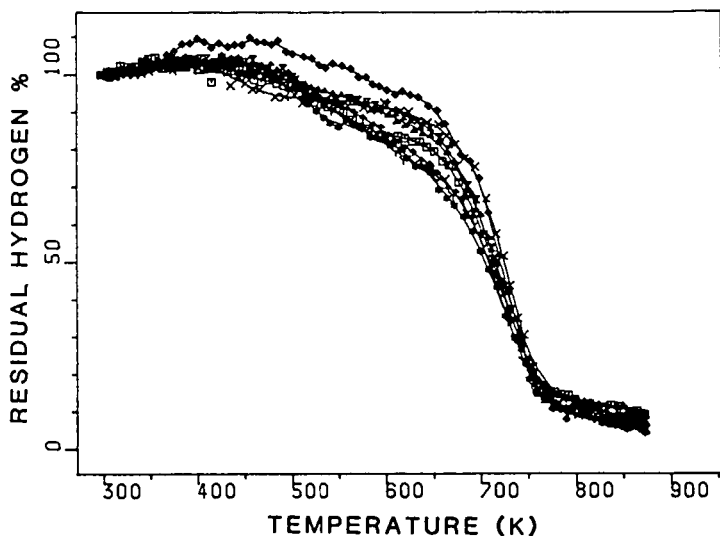


Figure 9. A comparison of pyrograms of the percent apparent residual hydrogen for demineralized specimens of eight Rundle oil shale ore types listed in Table I.

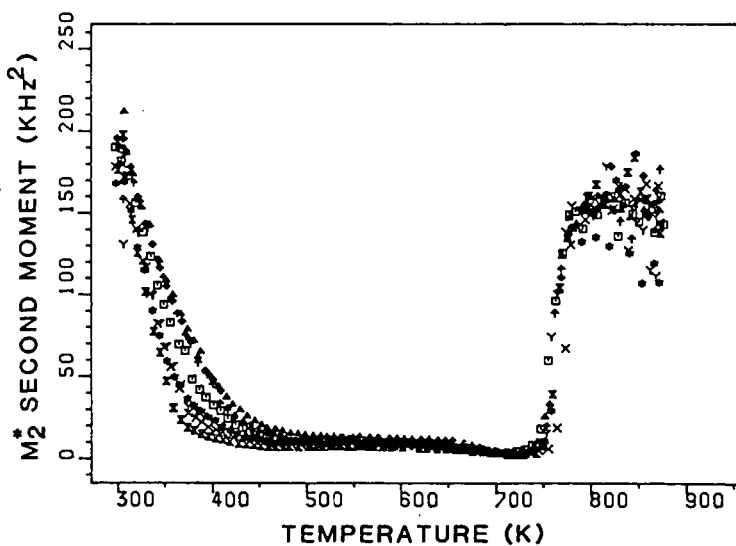


Figure 10. A comparison of the  $^1\text{H}$  NMR power spectrum second moment ( $M_2$ ) pyrograms for kerogen concentrates of eight Rundle oil shale ore types listed in Table I.

<sup>13</sup>C N.M.R. DIPOLAR DEPHASING AS A PROBE INTO THE STRUCTURE OF AUSTRALIAN OIL SHALE KEROGENS AND PYROLYSIS RESIDUES

D.E. Lambert and M.A. Wilson

CSIRO Division of Fossil Fuels, PO Box 136, North Ryde, NSW 2113, Australia

ABSTRACT

The solid state nuclear magnetic resonance (n.m.r.) technique of dipolar dephasing was applied to a range of Australian oil shale kerogens and pyrolysis residues of an aliphatic shale (Rundle, Queensland), in order to gain more information on chemical structure than can be obtained from a conventional cross polarization spectrum. From these measurements the proportion of aliphatic carbon that is methyl or non-protonated in an aromatic shale and the pyrolysis residues was estimated. Non-protonated carbon was found to be unimportant and thus it was shown that the methyl content varied according to shale type and/or thermal history. The proportion of aliphatic methyl carbon in residues, generated at a range of temperatures from 400-500°C, was found to increase with increasing reaction temperature. This trend indicates that the  $\beta$ -bond in alkyl chains attached to aromatic ring structures is cleaved in preference to the  $\alpha$ -bond during shale pyrolysis.

INTRODUCTION

Dipolar dephasing <sup>13</sup>C n.m.r has been extensively employed in determining the fraction of aromatic carbon that is protonated in a range of solid samples including model compounds, coals and other geochemical materials (1-17). In many heterogeneous samples the decay of aromatic signal intensity with increasing carbon magnetization holding time ( $t_1$ ) can be expressed, in terms of the decay constants  $T'_{2A}$  and  $T'_{2B}$ , as the sum of two exponential decays from protonated and non-protonated aromatic carbon, respectively. A separation of the aromatic signal intensity into two components is possible as the minimum  $T'_{2B}$  values for model aromatic ring compounds are five times the  $T'_{2A}$  values obtained for methane carbon (1). However, this was not found to be the case for oil shales (18). We have attributed this difference in relaxation behaviour to the intrinsic nature of the oil shale kerogen. Either the non-protonated carbons are in close proximity to protonated structures and thus have reduced  $T'_2$  values, which approach those of the protonated carbons, and/or there are significantly more protonated carbons present, which still dominate the total signal intensity at  $t_1 > 45 \mu s$ , when only signal from non-protonated carbon is normally observed.

Little work has been undertaken to investigate the chemical structure of the aliphatic components of fossil fuels by n.m.r. Some studies have been reported on coals (1), but data on oil shales are not currently available. Thus, in this work we have examined the potential of dipolar dephasing as a probe of the chemical structure of the aliphatic components in Australian shales and shale pyrolysis residues. The fraction of aliphatic carbon that is methyl in the most aromatic shale and the pyrolysis residues has been estimated. This is related to kerogen structure and the mechanism of shale pyrolysis.

THEORY

The technique of dipolar dephasing is based on the rapid loss of signal intensity from protonated carbons, when a time period ( $t_1$ ), in which the proton decoupler is turned off, is inserted before data acquisition in a conventional cross polarization program. The rate at which signal intensity is lost is dependent on the magnitude of the carbon-hydrogen dipolar interaction. Hence carbons bonded to protons experience stronger dipolar interactions than non-protonated carbons, unless the dipolar interaction is modulated by molecular motion, e.g. rapid rotation of

methyl groups. It has been shown for some compounds (19) that at a dipolar dephasing time of 50  $\mu$ s the signal intensity from methine and methylene carbons is almost completely eliminated from the conventional cross polarization spectrum. Resonances from quaternary carbons remain, although attenuated in intensity due to long range, weak interactions with protons. Methyl carbon resonances also remain if the methyl groups present are free to rotate at speeds sufficient to severely weaken the carbon-proton interaction. This is possible in almost all solids including coals (1).

For carbons that are weakly coupled to protons, model compound studies have shown that the decay of signal intensity is simply exponential with increasing dipolar dephasing time ( $t_1$ ) (5,7,20). However, for strongly coupled methylene and methine carbons, signal intensity decays as a function of time squared, i.e. a Gaussian decay pattern (5,7,20). In more complex systems such as coals the decay of aliphatic signal intensity is closer to exponential than Gaussian, however similar  $T_2'$  values are normally obtained from either Gaussian or exponential calculations (1).

For kerogen residues and highly aromatic shales (aromaticity ( $f_a$ ) > 0.60), which contain methine, methylene, quaternary and methyl carbons, our results (Figure 1) show that the decay of aliphatic signal intensity can be described as the sum of two decays given by Equation 1.

$$I_T = I_S^0 \exp[-t_1^2/2T_2'(S)^2] + I_W^0 \exp[-t_1/T_2'(W)] \quad 1)$$

where  $I_T$  is the total aliphatic signal intensity;  $I^0$  is the initial signal intensity of the strongly coupled aliphatic carbons ( $\text{CH}_2, \text{CH}$ );  $I_S^0$  is the initial signal intensity of the weakly coupled aliphatic carbons ( $\text{C}, \text{CH}_3$ );  $t_1$  is the delay period where the decoupler is gated off; and  $T_2'(S)$  and  $T_2'(W)$  are respectively the decay constants for the decay processes of strongly and weakly coupled carbon types.

If one approximates that the signal intensity of the strongly coupled carbons has decayed to a negligible amount after a delay period of 50  $\mu$ s, then Equation 1 simplifies to

$$I_T = I_W^0 \exp[-t_1/T_2'(W)] \quad 2)$$

$I_W^0$  can therefore be determined from the zero time extrapolated intercept of the graphed data for  $t_1 > 50 \mu$ s (see Figure 1).  $T_2'(W)$  is obtained from the reciprocal slope of the least-squares fit to the data. These parameters can then be used to obtain data on the decay of the strongly coupled carbons. The plot of  $\ln [I_T - I_S^0 \exp(-t_1^2/2T_2'(S)^2)]$  versus the square of  $t_1$  (1) yields a linear relationship and  $T_2'(S)$  is obtained from the slope.

The parameter,  $f_w(\text{Al}) = I_W^0 / (I_S^0 + I_W^0) = I_W^0 / I_T^0$ , gives the fraction of aliphatic carbon that is methyl or non-protonated.  $F_w(\text{Al})$  is related to the fraction of total carbon that is methyl or non-protonated ( $f_w$ ), by  $(1-f_a)$ , where  $f_a$  is the fraction of total carbon that is aromatic, i.e.

$$f_w = f_w(\text{Al}) \times (1-f_a) \quad 3)$$

Alternatively, when only a single exponential decay is observed (Figure 2), an estimate of  $f_w(\text{Al})$  can be made indirectly from the signal intensity of the aliphatic resonance at  $t_1 = 0 \mu$ s and a delay time at which all methylene and methine carbon has decayed completely (1). A delay of 50  $\mu$ s would be appropriate for the oil shale samples examined. However, as the  $T_2'$  values of the aliphatic kerogens are > 25  $\mu$ s, indicating that the methine and methylene groups in the kerogens are highly mobile, this approach is not applicable to oil shales.

## EXPERIMENTAL

### Sample Preparation

All samples were demineralized by hydrochloric/hydrofluoric acid treatment (18) prior to analysis by n.m.r.

Pyrolysis residues of Rundle shale (Queensland, Australia) were generated from pyrolysis experiments using a modification of the Fischer Assay method (ASTM D3904-80). Shale, crushed to -100 mesh, was heated to various temperatures between 400-500°C at a rate of 12.5°C/min, and held isothermally at temperature for the time specified between 10-40 min. The raw shale used in these experiments contained 13.35% organic C, 2.3% H, 1.3% S, 0.4 % N and 1.25% inorganic C on a dry weight basis. The major inorganic components were clay minerals (illite, kaolinite and montmorillonite), quartz, siderite, calcite and pyrite.

### N.M.R.

Solid-state  $^{13}\text{C}$  n.m.r. spectroscopic measurements were made on a Bruker CXP 100 instrument at 22.6 MHz. Kerogen was packed in a boron nitride rotor with a Kel-F base. The dipolar dephasing program chosen for this study used alternate phase inversion of the  $90^\circ$  r.f pulse to minimize baseline artifacts, and a refocusing  $180^\circ$  pulse along the spin locking co-ordinate was inserted in the middle of the  $t_1$  period to avoid linear phase distortions. The  $90^\circ$  pulse width was 4.5-8  $\mu\text{s}$ , with a recycle time of 0.8-1 s. Data were collected in 1 K of memory, zero filled to 4 K and Fourier transformed using line broadening factors of 30-100 Hz. Dipolar dephasing delays ( $t_1$ ) between 2-200  $\mu\text{s}$  were used and each experiment continued until 4,000-6,000 scans were acquired. Results were calculated from integrated signal intensities divided at the point of inflection between 80-100 ppm.

## RESULTS AND DISCUSSION

Results obtained from dipolar dephasing experiments of a selection of Australian kerogens, with a range of aromatic carbon contents ( $f_a$ ) are presented in Table 1. Figure 2 shows a typical plot of the logarithm of aliphatic signal intensity versus  $t_1$  for a kerogen of low aromaticity ( $f_a = 0.21$ ). Only an average  $T'_{2C}$  value ( $T'_{2C}$ ) can be determined for the decay process. A slowly decaying component with a  $T'_{2C} > 30 \mu\text{s}$  is not apparent in the plot; this indicates a very low concentration of methyl carbon in the kerogen. Figure 1 shows a similar plot for a highly aromatic kerogen ( $f_a = 0.60$ ). The decay process is clearly not exponential and two rate constants governing the decay,  $T'_2(S)$  and  $T'_2(W)$ , can be determined respectively from Gaussian (Figure 3) and exponential data calculations using Equations 1 or 2. Since two decay processes can be observed for the Condor carbonaceous shale and only one for the aliphatic shales then the aliphatic structures of the Condor carbonaceous kerogen contain large concentrations of methyl and/or non-protonated carbon whereas kerogens of lower aromatic content have relatively much lower concentrations of these species. The aliphatic moieties of the Glen Davis, Rundle, Condor brown and Nagoorin kerogens must consist mainly of chain methylene and methine carbons and an insignificant amount of quaternary carbon, whereas the highly aromatic kerogen must contain aromatic ring structures associated with relatively short alkyl chains and aliphatic cross-linking structures.

The  $T'_{2C}$  data calculated from dipolar dephasing experiments of shale pyrolysis residues from the Rundle deposit (Queensland) are listed in Table 2. The  $T'_{2C}$  values for the residues are greater than those of the aliphatic kerogens. However, the loss of aliphatic signal intensity is more appropriately described as a sum of two decays. The decay constants for strongly coupled carbon,  $T'_2(S)$ , lie near the lower limit for the time constants quoted for methylene and methine carbons (12-29  $\mu\text{s}$ )

TABLE 1  
DIPOLAR DEPHASING DATA FOR THE ALIPHATIC COMPONENTS  
OF AUSTRALIAN OIL SHALES<sup>a</sup>

Kerogen	$f_a$	Atomic H/C	$T'_{2C}$ ( $\mu s$ )	$T'_2(S)$ ( $\mu s$ )	$T'_2(W)$ ( $\mu s$ )	$f_w(AlI)$	$f_w$
Glen Davis	0.19	1.52	29	-	-	-	-
Rundle	0.21	1.55	26	-	-	-	-
Condor brown	0.25	1.41	26	-	-	-	-
Nagoorin	0.49	0.83	28	-	-	-	-
Condor carbonaceous	0.60	0.93	55 <sup>b</sup>	16 <sup>c</sup>	88 <sup>c</sup>	0.45	0.18

<sup>a</sup>  $T'_{2C}$  values are the average  $T'_2$  values determined from exponential fit to all  $t_1$  data points.

<sup>b</sup> Values obtained when data fitted to single exponential decay.

<sup>c</sup> Values obtained using Equation 1.

TABLE 2  
DIPOLAR DEPHASING DECAY DATA FOR THE ALIPHATIC COMPONENTS OF SHALE  
PYROLYSIS RESIDUES FROM THE RUNDLE DEPOSIT (QUEENSLAND)<sup>a</sup>

Pyrolysis conditions Temperature Time (°C) (min)	$f_a$	Atomic H/C	$T'_{2C}$ ( $\mu s$ )	$T'_2(S)$ ( $\mu s$ )	$T'_2(W)$ ( $\mu s$ )	$f_w(AlI)$	$f_w$
425 10	0.33	1.26	46	19	67	0.69	0.46
425 20	0.52	1.17	52	20	82	0.64	0.31
400 40	0.38	1.18	48	16	69	0.58	0.36
425 40	0.64	1.01	57	- <sup>b</sup>	76	0.78	0.28
450 40	0.81	0.74	52	-	-	-	-
475 40	0.85	0.64	65	-	-	-	-

<sup>a</sup>  $T'_{2C}$  values determined from exponential fit to all  $t_1$  data points.

<sup>b</sup> Insufficient points for accurate determination.

(20). The decay constants for weakly coupled carbons,  $T_2'(W)$ , are all less than 100  $\mu$ s suggesting a predominantly methyl contribution to the signal intensity. Hence the  $f_w(Al)$  estimates obtained for the residues reflect an increase in the proportion of aliphatic carbon that is methyl with increasing pyrolysis temperature.

The decay of aliphatic signal intensity from the highly aromatic residues could not be resolved into two components for a number of reasons. The aliphatic content of these residues is low, and there is a small contribution from spinning side bands to the total aliphatic signal intensity, owing to the greater chemical shift anisotropy of these samples. At  $t_1 > 45 \mu$ s these contribute most of the signal intensity in the aliphatic region and the small 'real' aliphatic signal becomes buried. Nevertheless chemical shift data (Figure 4) show that there is an upfield shift of the centre of the aliphatic resonance with increasing pyrolysis temperature of the shale residues. This resonance, centred at 31 ppm in the raw kerogen, approaches a value of 16 ppm, similar to the chemical shift expected for methyl carbon, in the high temperature residues. This progressive increase in methyl carbon content of the shale residues is more clearly illustrated by dipolar dephasing experiments. Figure 5 shows the spectra obtained after a dipolar dephasing delay of 2, 30 and 60  $\mu$ s from Rundle shale and a low (425°C) and high (475°C) temperature pyrolysis residue. The aliphatic peak of the raw shale is narrow, sharp and unsplit after a delay time of 60  $\mu$ s. In the 425°C residue set, a shoulder emerges from the central aliphatic resonance after a 30  $\mu$ s delay and a distinct separation of a methyl resonance is obvious after a 60  $\mu$ s delay. A marked upfield shift of the whole aliphatic resonance occurs after a 30  $\mu$ s delay in the high temperature residue. Thus our results indicate that the proportion of aliphatic carbon that is methyl increases significantly with increasing pyrolysis temperature.

These results allow some conclusions to be drawn about the mechanism of shale pyrolysis. Although the fraction of total carbon that is methyl or non-protonated in the residues ( $f_w$ ) appears to decrease with increasing pyrolysis temperature (Table 2), the aliphatic carbon of the pyrolysis residues contains a larger proportion of methyl groups than the parent shale (Rundle). Thus alkyl chains in the kerogen must be preferentially cleaved  $\beta$  to aromatic rings rather than  $\alpha$  to aromatic rings during pyrolysis. It is noteworthy that similar behaviour has been observed in residues from the flash pyrolysis of coals (21).

#### CONCLUSIONS

Dipolar dephasing studies on shales and shale residues can yield useful information about the structure of the aliphatic components present in these solids. It has been demonstrated that in an Australian shale (Condor carbonaceous) with a high aromatic carbon content ( $f_a = 0.60$ ) the aliphatic carbon consists of a high proportion of methyl groups whereas shales of lower aromaticity (Glen Davis,  $f_a = 0.19$ ; Rundle,  $f_a = 0.21$ ; Condor brown,  $f_a = 0.25$  and Nagoorin,  $f_a = 0.49$ ) all have very low methyl contents.

The dipolar dephasing behaviour of the aliphatic signal of the Condor carbonaceous shale can be resolved into a rapidly decaying component, with a signal intensity dependent on the square of the dipolar dephasing time and a slower exponentially decaying component. Similar behaviour has also been observed for pyrolysis residues from a highly aliphatic shale (Rundle). These results together with chemical shift data show that when shale is pyrolysed the proportion of aliphatic carbon that is methyl increases with increasing pyrolysis temperature up to 500°C. Hence during pyrolysis the  $\beta$ -carbon-carbon bond of alkyl chains attached to aromatic rings is cleaved in preference to the  $\alpha$ -bond, i.e. methyl groups are more stable.

#### ACKNOWLEDGEMENTS

Esso Australia Ltd and Southern Pacific Petroleum are thanked for financial support.

## REFERENCES

1. M.A. Wilson, R.J. Pugmire, J. Karas, L.B. Alemany, W.R. Woolfenden, D.M. Grant and P.H. Given. Anal. Chem. 1984, 56, 933.
2. M.A. Wilson, R.J. Pugmire and D.M. Grant. Org. Geochem. 1983, 5, 121.
3. F.P. Miknis, M. Sullivan, V.J. Bartuska and G.E. Maciel. Org. Geochem. 1981, 3, 19.
4. V.L. Weinberg, T.F. Yen, B.C. Gerstein and P. Dubois-Murphy. Am. Chem. Soc. Div. Pet. Chem. Prepr. 1981, 26(4), 816.
5. P. Dubois-Murphy, B.C. Gerstein, V.L. Weinberg and T.F. Yen. Anal. Chem. 1982, 54, 522.
6. B.C. Gerstein, P. Dubois-Murphy and L.M. Ryan. In "Coal Structure" Meyers, R.A., Ed: Academic Press, New York, 1982 pp. 87-129.
7. P. Dubois-Murphy, T.J. Cassady and B.C. Gerstein. Fuel 1982, 61, 1233.
8. V.A. Weinberg, T.F. Yen, P. Dubois-Murphy and B.C. Gerstein. Carbon 1983, 21, 149.
9. E.W. Hagaman and M.C. Woody. Proceedings of the International Conference on Coal Science, Dusseldorf, W. Germany, Sept 7-9, 1981, pp. 807.
10. D.W. Kuehn, A. Davis, R.W. Snyder, M. Starsinic, P.C. Painter, J. Havens and J.L. Koenig. Am. Chem. Soc. Div. Fuel Chem. Prepr. 1982, 27(2), 55.
11. J.R. Havens, J.L. Koenig and P.C. Painter. Fuel 1982, 61, 393.
12. M.J. Sullivan and G.E. Maciel. Anal. Chem. 1982, 54, 1606.
13. R.L. Dudley and C.A. Fyfe. Fuel 1982, 61, 651.
14. M.A. Wilson, P.J. Collin, R.J. Pugmire and D.M. Grant. Fuel 1982, 61, 959.
15. A.R. Palmer, and G.E. Maciel. Anal. Chem. 1982, 54, 2194.
16. R.J. Pugmire, W.R. Woolfenden, C.L. Mayne, J. Karas and D.M. Grant. Am. Chem. Soc. Div. Fuel Chem. Prepr. 1983, 28(1), 103.
17. M.A. Wilson, A.M. Vassallo and N.J. Russell. Org. Geochem. 1983, 5, 35.
18. M.A. Wilson, D.E. Lambert and P.J. Collin. Fuel 1985 (in press).
19. S.J. Opella and M.H. Frey. J. Am. Chem. Soc. 1979, 101, 5854.
20. M.A. Wilson and R.J. Pugmire. Trends Anal. Chem. 1984, 3, 144.
21. P.J. Collin, R.J. Tyler and M.A. Wilson. Fuel 1980, 59, 479.

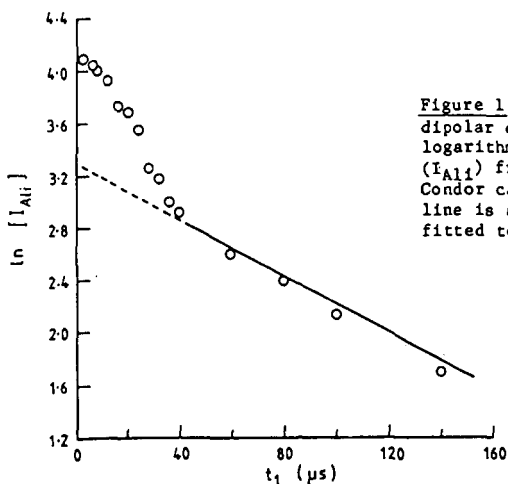


Figure 1 Effect of varying the dipolar dephasing time ( $t_1$ ) on the logarithm of the signal intensity, ( $I_{Aii}$ ) from aliphatic carbon in Condor carbonaceous kerogen. The line is an exponential function fitted to the data at  $t_1 > 40 \mu\text{s}$ .

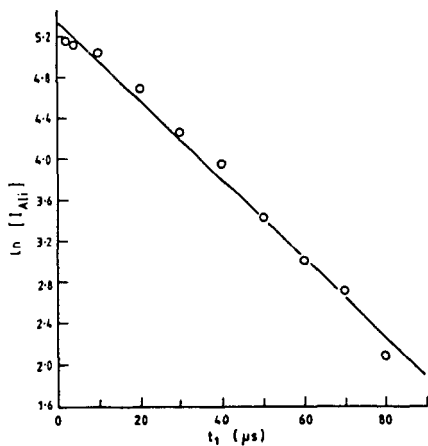


Figure 2 Effect of varying the dipolar dephasing time ( $t_1$ ) on the logarithm of the signal intensity ( $I_{Ali}$ ) from aliphatic carbon in Rundle kerogen.

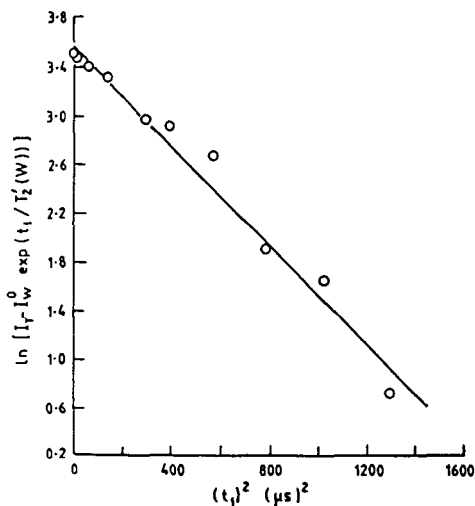


Figure 3 Plot of the square of the dipolar dephasing time (for  $t_1 < 40 \mu s$ ) against the logarithm of signal intensity from strongly coupled aliphatic carbon ( $CH_2, CH$ ) in Condor carbonaceous kerogen.

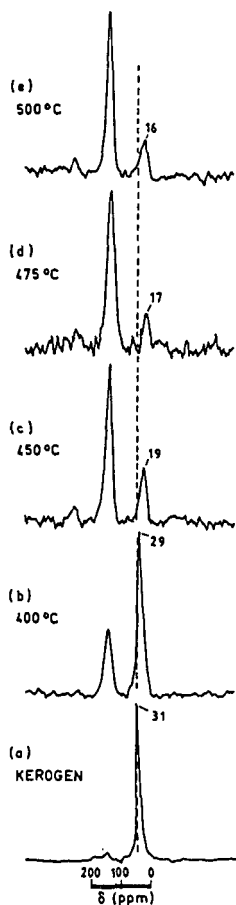


Figure 4 CP/MAS  $^{13}C$  n.m.r. spectra of Rundle kerogen and residues. a) kerogen; residue prepared at: b) 400°C, c) 450°C, d) 475°C, e) 500°C. Note that there is a decrease in chemical shift of the aliphatic resonance with increase in pyrolysis temperature.

DIPOLAR DEPHASING DELAY

(a) 2  $\mu$ s

(b) 30  $\mu$ s

(c) 60  $\mu$ s

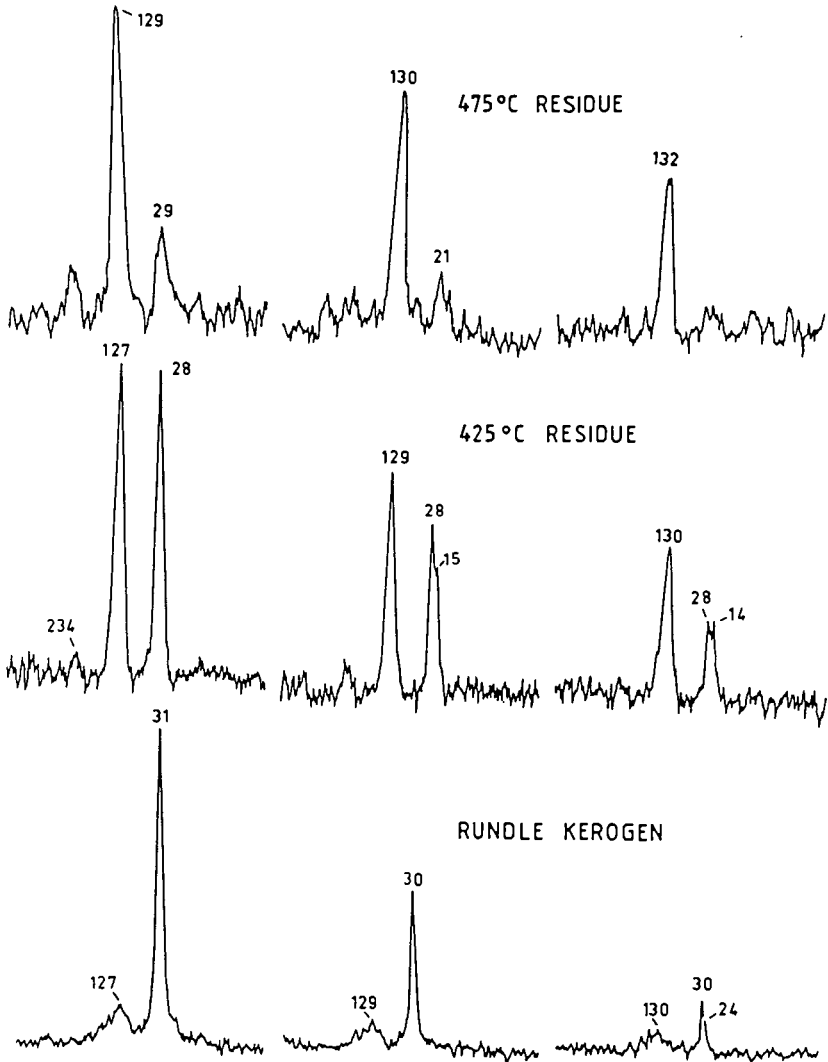


Figure 5 Dipolar dephased spectra of Rundle shale and residues prepared by pyrolysis at 425 and 475°C respectively. The dipolar dephasing times were a) 2  $\mu$ s, b) 30  $\mu$ s, c) 60  $\mu$ s.

SYMPOSIUM ON OIL SHALE REACTIVITY AND PROCESSING  
PRESENTED BEFORE THE DIVISIONS OF FUEL CHEMISTRY  
AND PETROLEUM CHEMISTRY, INC.  
AMERICAN CHEMICAL SOCIETY NATIONAL MEETING  
CHICAGO, ILLINOIS, SEPTEMBER 8-13, 1985

THE INFLUENCE OF TEMPERATURE UPON THE PYROLYSIS  
OF AUSTRALIAN OIL SHALES

By

N.V. DUNG and G.C. WALL

CSIRO Division of Energy Chemistry, Lucas Heights Research Laboratories,  
Private Mail Bag 7, Sutherland, NSW. 2232. Australia.

INTRODUCTION

Oil shale is one of the most prospective sources for the production of synthetic liquid fuels. Most of the Australian oil shale deposits are located in Queensland with the total in-situ resources in excess of  $4 \times 10^{12}$  L (25 billion barrels) of shale oil. This is more than 12 times the current Australian recoverable petroleum resources. The CSIRO Division of Energy Chemistry is undertaking a comparative study of the processing characteristics of seven oil shales from Condor, Duaringa, Lowmead, Nagoorin, Nagoorin South, Rundle and Stuart deposits which represent more than 80% of the current Australian shale oil resource.

A "fines" retorting process - arbitrarily defined as a process which accepts a feed particle size of minus 12 mm - is being investigated. The process consists of the fluidized bed pyrolysis of raw shale, fluidized bed combustion of spent shale, and recirculation of solids (spent shale and shale ash) between the combustor and the pyrolyser to supply heat to the retorting step. This process utilizes all the mined shale and is self-sufficient in process heat.

A fluidized bed pyrolyser provides, first, good mixing of the solids (raw shale and hot recycled shale ash) and good heat transfer, and hence rapid heating of oil shale and a uniform pyrolysis temperature; second, short residence time of oil vapor in the hot zones to give low oil cracking; and third, an environment of low partial pressure of oil vapor to enhance oil evaporation. These conditions give improved oil yields. Fluidized bed pyrolysis (FBP) gave oil yields in excess of the Fischer Assay (FA) for US oil shales (1,2) and Australian oil shales (3,4). The latter studies, using steam as the fluidizing gas, indicated that the yield enhancement was due to the effect of gas sweeping and that heating faster than  $12^\circ\text{C min}^{-1}$  had no additional effects on the oil yields from Rundle and Condor shales.

This paper presents results for the pyrolysis of Condor and Nagoorin oil shales in the temperature range 430 to  $600^\circ\text{C}$  using a laboratory-scale nitrogen fluidized bed pyrolyser. The Condor deposit (an in-situ shale oil resource of

1.3 x 10<sup>12</sup> L) is the largest Tertiary oil shale deposit in Australia and a potential candidate for the first new Australian shale oil production plant. The Nagoorin deposit is a carbonaceous oil shale which gives a high yield of oil of high aromatic content.

Small-scale fluidized beds severely dilute the product oil vapours with non-condensable fluidizing gases. Quantitative recovery of the diluted oil vapours presents problems with condensing the naphtha fractions and the formation of oil mists (1,3). A dichloromethane scrubber fitted with a series of shrouded turbine mixers was used to overcome these difficulties.

#### APPARATUS AND PROCEDURE

The pyrolyser, which had long solids and short (40.5 s) vapour residence times was designed to complete the kerogen decomposition and to minimize the oil loss due to the thermal cracking of oil vapor, and hence provided the ultimate yields and characteristics of the pyrolysis products. The final data will be used together with the data from pyrolysis kinetics (5) and oil cracking kinetics experiments to evaluate the performance of a large-scale continuous retort (6).

The FBP apparatus is shown in Figure 1. Metered high purity nitrogen was preheated to and controlled at the pyrolysis temperature in a coil of 9.5 mm o.d. tubing by an electric furnace before entering below a conical section at the base of the reactor vessel. The reactor was a stainless steel vessel (48 mm i.d. by 300 mm long) which was initially charged with 100 g of 0.5-1.0 mm roasted, acid-washed silica sand. The temperature of the fluidized bed was controlled to within  $\pm 1^\circ\text{C}$  by an electric heater wound around the bed section. The reactor axial temperature had a uniform profile from the bottom of the bed to a height of 220 mm. Temperature at the top of the reactor was about 30°C lower than the bed temperature. Reactor wall temperatures were recorded at three heights to monitor for hot spots. A superficial velocity of 1.35 times the minimum fluidizing velocity was used.

Samples of dried oil shale (100 g, particle size 0.6-1.4 mm) were added to the bed at the rate of 0.22 g every five seconds via an air-operated feed valve which was actuated by a cycle timer. Spent shale was accumulated in the reactor and a further retorting period of two to ten minutes after the completion of shale feeding was used to simulate an infinite solid residence time. The pyrolysis gases were passed through an internal 10 mm o.d. cyclone to remove fines from the product. The fines were then recovered, weighed and combined with the spent shale for each run. The hot gases and vapors entered a turbine scrubber (80 mm i.d. by 400 mm long), containing 1.2 L of rectified dichloromethane, via a sparger. Oil vapors condensed and dissolved in the dichloromethane which was kept at between 2 and 5°C by evaporation. The dichloromethane was refluxed through a condenser (-60°C) into the scrubber. Oil mists formed within gas bubbles were scrubbed by three shrouded turbines connected in series; big bubbles were sheared into smaller ones and then recirculated through one turbine many times before being released to the next. Before being metered, the off-gas passed through a bed packed with glass wool which trapped about 1 to 2% of the oil yield.

The oil/dichloromethane solution was pressure-filtered to remove traces of spent shale which were then weighed and included in the material balance. Dichloromethane was separated from the oil by atmospheric and vacuum distillation. The atmospheric fractionation column concentrated the solution to about 40 wt % of dichloromethane in the oil to keep the temperature of the solution below 60°C. The vacuum distillation was performed in a closed-system rotary evaporator. The equilibrium vacuum of the system was determined by the condenser temperature (0°C). The oil yield was corrected for the

dichloromethane content in the oil (1 to 3%) and the naphtha content in the vacuum distillate (1 to 4% of whole oil) which were determined using gas chromatography.

The Condor brown shale was supplied by Southern Pacific Petroleum N.L. and Central Pacific Minerals N.L. from 152 mm diamond drill No. 43 cores (from 60.65 to 68.25 m depth). The Nagoorin shale was the bulk sample from Unit Cc. The samples used in this study were split from the 0.6-1.4 mm fractions freshly crushed of 200 kg batches. Before each experiment, the shale was dried in nitrogen at 105°C for at least seven hours to a moisture content below 2 wt%.

Fischer Assays were done in accordance with ASTM standard D-3904-80 except that the particle size was 0.6 to 1.4 mm and the pyrolysis gases were collected and analysed. Raw and spent shales were analysed for total carbon, hydrogen and carbonate carbon (Australian Standard, AS 1038 part 6), and for moisture (Australian Standard AS 1038 part 3). Total sulphur in the raw and spent shales was determined by the high temperature combustion method (7) and sulphur in the oils by the reduction method (7). Simulated distillation of the oils was done on a Varian 3400 gas chromatograph according to the ASTM D-2887 method.

## RESULTS AND DISCUSSION

### Raw shale.

Table 1 shows the analyses and Fischer Assay yields of the Condor and Nagoorin oil shales. Compared to the Condor shale the Nagoorin shale is much richer in organic carbon, but lower in the H/C atomic ratio of the kerogen and carbonate carbon; also it produces double the oil, five times the pyrolysis water, eight times carbon monoxide, and much more hydrocarbon gas and carbon dioxide. The balances of the inorganic carbon for the shales indicated that the Condor carbon dioxide was from carbonate carbon (siderite) whereas the Nagoorin carbon dioxide was from the decomposition of kerogen (carboxyl group).

### Oil yields.

The results (ultimate yields, analyses of oil and spent shale, and recovery of organic carbon) for the FBP runs at various temperatures are given and compared with the FA data in Table 2 (Condor) and 3 (Nagoorin).

For Condor shale, the ultimate yield of the whole oil was constant in the range 450 to 525°C but decreased markedly from 525 to 600°C. The loss of the oil yield in the higher temperature range was caused mainly by thermal cracking in the oil vapor which correlated with the lower atomic H/C ratio, which for the 600°C oil was 1.49 compared to 1.60 for the 500°C oil. The cracking of oil vapor with a mean residence time of 0.5s at 600°C, estimated by the Burnham and Taylor equation (8), accounted for 71% of the oil yield loss.

Figure 2 shows the effect of pyrolysis temperature on the yields of oil fractions. The yields of naphtha (C<sub>5</sub> to 175°C) and kerosene (175 to 240°C) increased slightly with temperature. The yields of diesel (240 to 340°C) and gas oil (340 to 450°C) had maxima at about 550 and about 525°C, respectively. The yield of heavy gas oil (+450°C) decreased markedly with increase in temperature from 450 to 600°C. However, the reduction of temperature from 450 to 430°C reduced the yields of naphtha, kerosene, diesel and gas oil slightly, and the yield of heavy gas oil significantly. More than 50% of the oil yield loss at 430°C was accounted for by the loss of the heavy gas oil fraction which was believed to remain in the spent shale. This could be caused by the combination of the increased production and the decreased evaporation of the high boiling point oils at the lower temperature.

Figure 3 shows the influence of temperature upon the ultimate yields of the oils from the Nagoorin shale. The yield of the whole oil was constant (about 16.4 wt% dry basis) for temperatures from 450 to 550°C, except for 500°C where the yield reached the maximum of 17.1 wt%. Similar to the pyrolysis of the Condor shale, the yield of the whole Nagoorin oil decreased with temperatures from 550 to 600°C where the thermal cracking of oil vapor became significant. The general trend for the production of the oil fractions was also similar to that for the Condor shale, i.e. the yields of the low boiling point oil fractions (naphtha, kerosene and diesel) increased with temperature at the expense of the high boiling point gas oils.

The averages of the FBP oil yields at temperatures from 450 to 525°C for both the shales were about 10% greater than FAs. Table 4 compares the yields of naphtha, kerosene, diesel, gas oil and heavy gas oil from the FBPs and FAs. For both the shales, about 70% of the excess oils was heavy gas oil. This substantiates the claim that the increase in oil yield can be attributed mainly to enhanced evaporation of oil in a retort of low partial pressure of oil vapor (3).

#### Organic Carbon Conversion.

The organic carbon conversions to oils for both the shales were consistent with the oil yields (Tables 2 and 3). Compared to the FA results, the organic carbon conversions to oils increased at the expense of the conversions to spent shales. For the Condor shale, the organic carbon conversion to spent shale was independent of temperature (450 to 550°C), but for the Nagoorin shale, the conversion decreased with increase in temperature (450 to 600°C). This implied the continuing production of CO, CO<sub>2</sub> and hydrocarbon gases from the Nagoorin kerogen with temperature. When the shales were heated linearly at 3°C min<sup>-1</sup> to 850°C considerable amounts of carbon monoxide, carbon dioxide and methane from Nagoorin but not from Condor evolved at temperatures above 500°C, at which the production of oil ceased (9).

The Nagoorin spent shale had very high organic carbon content (about 50 wt%) which was more than ten times that of the Condor spent shale. Combustion of the Nagoorin spent shale will provide more than enough process heat for the retorting step; however, transferring the heat by recycling the hot shale ash would lead to a problem of balancing the recycled solids of suitable particle sizes.

#### Oil characteristics.

For both shales, the pyrolysis at the higher temperature gave oils of lower H/C atomic ratio. Figure 4 compares the short column gas chromatographs of the Nagoorin oils at 450 and 600°C. The 600°C oils had considerable more alkenes (peaks marked with 0 in Figure 4) and more light hydrocarbons (lower C<sub>16</sub>/C<sub>27</sub> height ratios) than the 450°C oil. This was evident from the thermal cracking of the 600°C oil vapor.

Compared to the FA whole oils, the FBP whole oils from both the shales were more aromatic (lower H/C atomic ratio). The increase in the aromaticity of the FBP whole oils was attributed entirely to the presence of the additional gas oils and heavy gas oils (see Table 4). These heavy oils were highly aromatic (10).

As was expected, the Condor oil shale produced oils (from FA and FBP) of better quality (higher H/C atomic ratio, and lower contents of heteroatoms and density) than the Nagoorin carbonaceous shale. However, the Condor oil contained more heavy gas oil (especially the fraction boiling above 550°C), as is shown in Figure 5.

## Carbonate Carbon.

By contrast with the shales from Green River formation, both shales contain small amounts of mineral carbonates (siderite). However, as is shown in Figure 6, the residual carbonate carbon in the Condor spent shale reduced sharply with increase in pyrolysis temperature, to 3% of the Condor shale carbonate carbon at 500°C. This implies that the heat of the decomposition of siderite has to be provided to the retorting step, hence the content of this mineral in the feed shale is vital to the retort heat balance.

### SUMMARY

The pyrolysis of Condor and Nagoorin shales was studied in the temperature range 430 to 600°C in a nitrogen fluidized bed retort with long solid and short vapour residence times.

The oil yields were constant from 450 to 525°C (Condor) and from 450 to 550°C (Nagoorin), and both were about 10% in excess of Fischer Assay. The additional oils were mainly high boiling point fractions. The distribution of oil fractions, namely naphtha, kerosene, diesel, gas oil and heavy gas oil were significantly influenced by temperature. Generally, increase in temperature reduced the high boiling point fractions (gas oil and heavy gas oil) and increased the low boiling point fractions (naphtha, kerosene and diesel).

The yields and quality of the oils decreased with temperature from 525 to 600°C where the thermal cracking of the oil vapors (having 0.5 s residence time) became significant.

### ACKNOWLEDGEMENTS

This work is partly funded through a collaborative research agreement with Southern Pacific Petroleum NL and Central Pacific Minerals NL (SPP/CPM) supported by a National Energy Research Development and Demonstration Program (NERDDP) grant. The Condor and Nagoorin oil shale samples were provided by SPP/CPM. The authors gratefully acknowledge the contributions of M. Chensee who conducted the Nagoorin experiments, P. Udaja and T.A. Noble who analysed the feed and product samples, G. Kastl who designed and operated the distillation units, S.J. Smith who conducted the simulated distillation analysis on the Nagoorin oils, and R.D. Pearse who did the Fischer Assays.

### LITERATURE CITED

1. M.J. Margolis, Proceedings of the 1981 Eastern Oil Shale Symposium, Lexington KY, 151 (1982).
2. A.M. Rubel and S.D. Carter, Preprints of Symposium on Characterization and Chemistry of Oil Shales, American Chemical Society, St. Louis, 202 (1984).
3. G.C. Wall, Proceedings of the First Australian Workshop on Oil Shale, Lucas Heights, 105 (1983).
4. G.C. Wall, Seventeenth Oil Shale Symposium Proceedings, Colorado School of Mines Press, 300 (1984).
5. G.C. Wall and N.V. Dung, Proceedings of the Second Australian Workshop on Oil Shale, Brisbane, 129 (1984).
6. N.V. Dung and G.C. Wall, *ibid*, 199.
7. P. Udaja, M.D. Chensee and T.A. Noble, *ibid*, 114, (1984).
8. A.K. Burnham and J.R. Taylor, Lawrence Livermore National Laboratory, Livermore, CA, UCID-18284 (1979).
9. A. Ekstrom, R.J. Hurst and C.H. Randall. American Chemical Society Symposium Series 230, 161 (1983).
10. J.A. Gray, C.J. Brady, J.R. Cunningham, J.R. Freeman and G.M. Wilson. Ind. Eng. Chem. Process Des. Dev., 22, 410 (1983).

TABLE 1  
PROPERTIES OF RAW SHALES

SHALE	CONDOR		NAGOORIN	
	Mean	s.d.	Mean	s.d.
Moisture, % as received	6.61		22.20	
<b>ANALYSIS, wt% dry basis</b> (4 observations)				
Organic carbon	10.84	0.03	50.70	0.13
Inorganic carbon	0.82	0.01	0.09	0.01
Hydrogen (total)	1.82	0.02	4.77	0.03
Sulphur	0.65	0.01	1.34	0.02
(a)				
Kerogen atomic H/C	1.41		1.02	
Inorganic hydrogen (b)	0.55		0.46	
<b>FISCHER ASSAY, wt% dry basis</b> (4 observations)				
Oil (C <sub>5</sub> +)	7.47	0.19	15.02	0.50
Water	0.97	0.03	6.28	0.33
Hydrogen	0.057	0.003	0.075	
Carbon monoxide	0.130	0.008	1.113	
Carbon dioxide	1.361	0.089	6.491	
Hydrogen sulphide	0.0	0.0	0.064	
Methane	0.163	0.009	0.900	
Ethane	0.132	0.007	0.442	
Propane	0.088	0.003	0.289	
n-Butane	0.063	0.003	0.126	
i-Butane	0.004	0.0	0.015	
Ethylene	0.042	0.003	0.131	
Propylene	0.080	0.006	0.213	
Butene	0.058	0.004	0.123	
Spent shale	89.06	0.09	68.78	0.48
TOTAL	99.68	0.14	100.06	0.43

(a) Data supplied by Southern Pacific Petroleum N.L. and Central Pacific Minerals N.L.

(b) Determined by the difference between the total hydrogen and the organic hydrogen which is calculated using the kerogen atomic H/C and the organic carbon of the shale.

TABLE 4  
OIL YIELDS : FBP v.s. FISCHER ASSAY

OILS	CONDOR			NAGOORIN		
	FBP <sup>(a)</sup> (500°C)	FA <sup>(a)</sup>	Distribution of additional oil <sup>(b)</sup>	FBP <sup>(a)</sup> (500°C)	FA <sup>(a)</sup>	Distribution of additional oil <sup>(b)</sup>
Naphtha (C <sub>5</sub> to 175°C)	9.9	9.6	3	6.2	7.5	-9
Kerosene (175 to 240°C)	10.7	10.6	1	12.8	13.9	-8
Diesel (240 to 340°C)	27.4	25.7	19	33.6	32.6	7
Gas oil (340 to 450°C)	33.4	32.8	7	39.2	33.8	39
Heavy gas oil (>450°C)	27.7	21.3	70	22.2	12.2	71
TOTAL	109.1	100.0	100	114.0	100.0	100

(a) % of the yield of FA whole oil

(b)  $100 \times (\text{yield of FBP oil} - \text{yield of FA oil}) / (\text{yield of FBP whole oil} - \text{yield of FA whole oil})$

TABLE 2  
RESULTS FROM CONDOR OIL SHALE

Temperature, °C	FA	FLUIDIZED BED PYROLYSIS							
		500	430	450	475	500	525	550	600
<b>YIELDS, wt% dry basis</b>									
Oil (C <sub>5</sub> +)	mean	7.0	7.2	8.2	8.1	8.0	8.0	7.7	7.0
	s.d.	0.2	-	0.0	0.1	0.1	-	0.1	-
	number of tests	4	1	2	3	3	1	2	1
Spent shale	mean	89.1	88.9	87.2	85.5	84.9	84.6	84.3	84.6
	s.d.	0.1	-	0.1	0.5	0.2	0.0	0.2	-
	number of tests	4	1	4	3	11	2	2	1
<b>ANALYSIS OF OIL</b>									
Carbon, wt%		84.1	83.87	82.20	82.57	84.08	84.11	83.85	83.39
Hydrogen, wt%		11.8	11.02	10.78	11.06	11.19	11.10	10.96	10.33
Sulphur, wt%		0.44	0.44	0.44	0.43	0.45	0.44	0.45	0.45
H/C atomic ratio		1.68	1.58	1.58	1.61	1.60	1.58	1.57	1.49
Density, 60°C g/cm <sup>3</sup>		0.84	0.89	0.89	0.88	0.88	0.91	0.87	0.90
<b>ANALYSIS OF SPENT SHALE wt% dry basis</b>									
Organic carbon		4.62	4.60	4.26	4.37	4.35	4.24	4.29	4.57
Inorganic carbon		0.45	0.63	0.48	0.13	0.02	0.01	0.00	0.00
Hydrogen		0.69	0.79	0.46	0.53	0.41	0.09	0.23	0.13
Sulphur		0.69	0.69	0.64	0.68	0.68	0.70	0.65	0.67
<b>RECOVERY OF ORGANIC CARBON, %</b>									
Oil,	mean	58.0	55.8	62.5	61.2	62.1	61.7	59.1	54.3
	s.d.	1.0	-	0.2	1.7	1.0	-	0.5	-
Spent shale,	mean	38.0	37.1	34.2	34.1	34.0	33.1	33.3	35.7
	s.d.	1.5	-	1.4	1.7	1.1	0.1	0.3	-
Gas,	mean	5.2	-	-	-	-	-	-	-
	s.d.	0.3	-	-	-	-	-	-	-
Not accounted for		-1.2	7.1	3.3	4.7	3.9	5.2	7.6	10.0

TABLE 3  
RESULTS FROM NAGOORIN OIL SHALE

Temperature, °C	FA	FLUIDIZED BED PYROLYSIS							
		500	450	475	500	525	550	575	600
<b>YIELDS, wt% dry basis</b>									
Oil (C <sub>5</sub> +)	mean	15.0	16.5	16.4	17.1	16.3	16.5	16.2	15.3
	s.d.	0.5	-	0.0	0.1	-	-	0.2	-
	number of tests	4	1	2	2	1	1	2	1
Spent shale,	mean	68.8	66.7	65.2	63.5	62.3	61.5	61.0	60.8
	s.d.	0.5	0.1	0.8	1.3	-	-	0.5	-
	number of tests	4	2	2	2	1	1	2	1
<b>ANALYSIS OF OIL</b>									
Carbon, wt%		82.60	81.94	81.79	81.00	81.51	81.78	81.70	81.28
Hydrogen, wt%		10.52	9.83	9.77	9.50	9.85	9.50	9.61	9.34
H/C atomic ratio		1.53	1.44	1.43	1.41	1.45	1.39	1.41	1.38
Density, 60°C, g/cm <sup>3</sup>		0.914	0.959	0.951	0.946	0.940	0.960	0.946	0.924
<b>ANALYSIS OF SPENT SHALE wt% dry basis</b>									
Organic carbon		50.05	47.92	49.10	49.19	50.58	50.25	50.16	48.71
Inorganic carbon		0.04	0.06	0.06	0.07	0.05	0.07	0.08	0.07
Hydrogen		2.49	2.82	2.03	2.07	1.39	1.51	1.44	1.36
Sulphur					1.48	1.50	1.30	1.20	1.42
<b>RECOVERY OF ORGANIC CARBON, %</b>									
Oil,	mean	24.4	26.7	26.5	27.3	26.2	26.6	26.1	24.5
	s.d.	0.7	-	0.1	0.1	-	-	-	-
Spent shale,	mean	67.9	63.1	63.1	61.6	62.1	60.9	60.4	58.4
	s.d.	0.6	-	0.1	0.1	-	-	-	-
Gas,	mean	7.9	-	-	-	-	-	-	-
	s.d.	0.1	-	-	-	-	-	-	-
Not accounted for		-0.2	10.2	10.4	11.1	11.7	12.5	13.5	17.1

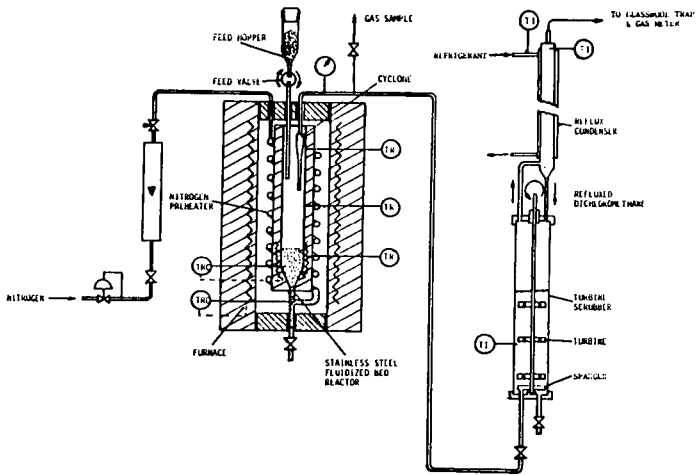


FIGURE 1. APPARATUS

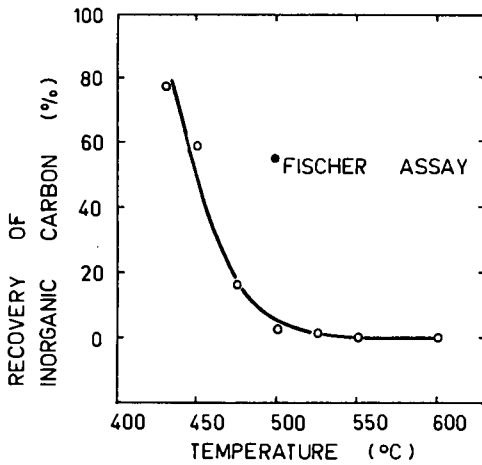


FIGURE 6. EFFECT OF TEMPERATURE ON RECOVERY OF INORGANIC CARBON IN CONDOR SPENT SHALE

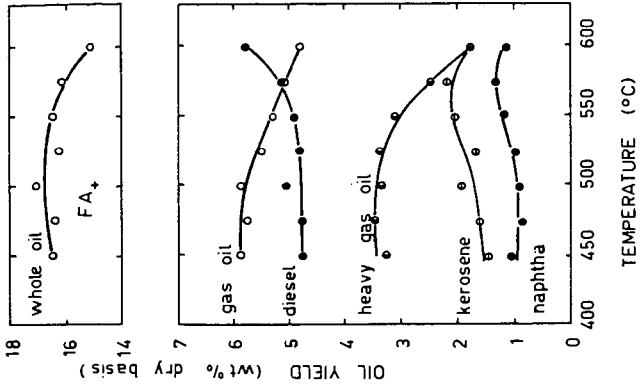


FIGURE 3. EFFECT OF TEMPERATURE ON YIELDS OF OILS FROM NAGORIN SHALE

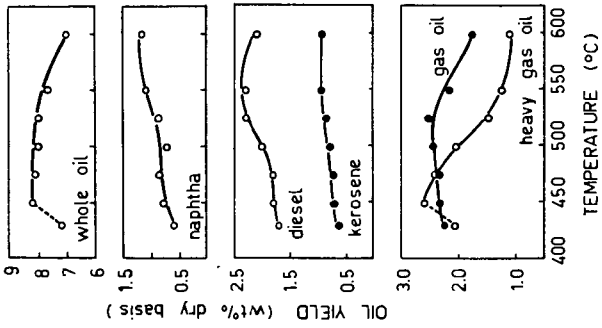


FIGURE 2. EFFECT OF TEMPERATURE ON YIELDS OF OILS FROM CONDOR SHALE

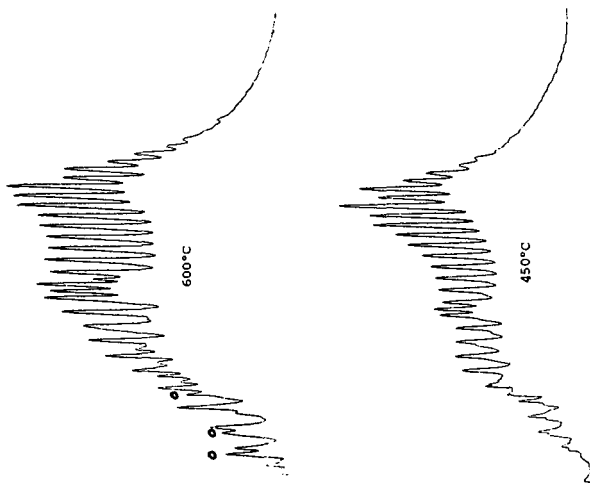


FIGURE 4. GAS CHROMATOGRAPHS OF NAGOORIN SHALE OILS AT 450 AND 600°C

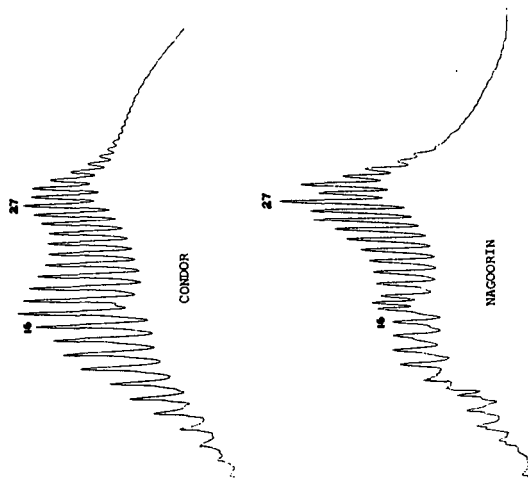


FIGURE 5. GAS CHROMATOGRAPHS OF CONDOR AND NAGOORIN SHALE OILS AT 450°C

CO-PYROLYSIS OF COAL AND OIL SHALE I: THERMODYNAMICS  
AND KINETICS OF HYDROGEN SULFIDE CAPTURE BY OIL SHALE

L. Johnson, M. Rostam-Abadi, I. Mirza, M. Stephenson, and C. Kruse

Illinois State Geological Survey  
Champaign, Illinois 61820

## Introduction

The potential for producing crude oil and a compliance char (less than 1.2 lb  $\text{SO}_2$ /MMBtu) by pyrolysis of Illinois Basin high volatile bituminous coals has been recognized for years but it has not been realized mainly because these coals agglomerate when pyrolyzed and because the chars have a relatively high sulfur content. The feasibility of using oil shale during pyrolysis of high sulfur coals and hydrodesulfurization of the resultant coal char is currently being investigated at the Illinois State Geological Survey (ISGS). Although still in the early stages of process development, three processes have been conceived which use oil shale with coal. In the first process, coal and oil shale, or coal and retorted shale are pyrolyzed in a fluidized bed reactor (FBR). In the second process, spent oil shale and coal are processed in a FBR. In the third process, coal and oil shale are pyrolyzed in a multistaged FBR with coal and oil shale occupying separate, alternating stages. The coal char product from these processes must be hydro-desulfurized to produce a compliance char.

Pyrolyzing coal and oil shale together could have many advantages over the pyrolysis of either material separately. First, preliminary ISGS data indicates that the inert minerals in oil shale dilute the coal-shale mixture, reducing the agglomeration of caking coals. Secondly, liquid and gaseous hydrocarbons are produced from both coal and oil shale. Thirdly, the carbonate minerals found in oil shale (calcite, dolomite) and their corresponding oxides formed during pyrolysis can act as scavengers of hydrogen sulfide during pyrolysis and hydrodesulfurization. Research efforts have recently been initiated at ISGS to obtain engineering data in the above areas. The results presented are the first phase of a larger thermodynamics and kinetics study of the reactions between oil shale and  $\text{H}_2\text{S}$ . The findings of this initial literature review provide the basis for the second phase of our research which will be presented in future publications.

## Decomposition Reactions

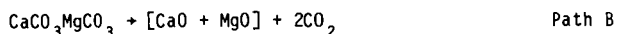
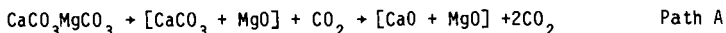
The most significant reactions of carbonate minerals which occur during the co-pyrolysis of coal and oil shale are shown in table 1. The extent and pathway of carbonate decomposition are significant because they determine which sorbent(s) are present during hydrodesulfurization or pyrolysis. The overall thermal efficiency of the process and the physical properties of the product oxide are also affected by the extent of carbonate decomposition.

Calcium carbonate in oil shale is found as calcite and dolomite. Dolomite ( $\text{CaCO}_3\text{MgCO}_3$ ) is a single phase of calcium and magnesium carbonate with its own unique crystal structure. During decarbonation of the magnesium component to form half-calcined dolomite,  $\text{CaCO}_3\text{MgO}$ , (hc-dolomite) small crystallites of  $\text{MgO}$  appear indicating a separation of the calcium and magnesium phases. This separation continues through the second decarbonation to form fully-calcined dolomite,  $\text{CaOMgO}$ , (fc-dolomite). Based on this observation, one would predict that the behavior of the solid more closely resembles an intimate mixture of its calcium and magnesium components as the calcination proceeds from dolomite to fc-dolomite.

Table 1. Shale Mineral Reactions Occurring During Pyrolysis and Hydrodesulfurization

Equation	H <sub>298</sub> (Kcal/mole)	Equation No
<u>Decomposition Reactions</u>		
CaCO <sub>3</sub> + CaO + CO <sub>2</sub>	43	1)
MgCO <sub>3</sub> + MgO + CO <sub>2</sub>	28	2)
CaCO <sub>3</sub> MgCO <sub>3</sub> + (CaCO <sub>3</sub> + MgO) + CO <sub>2</sub>	30	3)
CaCO <sub>3</sub> MgCO <sub>3</sub> + (CaO + MgO) + 2CO <sub>2</sub>	73	4)
<u>Desulfurization Reactions</u>		
CaCO <sub>3</sub> + H <sub>2</sub> S + CaS + CO <sub>2</sub> + H <sub>2</sub> O	28	5)
CaO + H <sub>2</sub> S + CaS + H <sub>2</sub> O	-15	6)
CaCO <sub>3</sub> MgO + H <sub>2</sub> S + (CaS + MgO) + H <sub>2</sub> O + CO <sub>2</sub>	28	7)
CaOMgO + H <sub>2</sub> S + (CaS + MgO) + H <sub>2</sub> O	-15	8)
CaCO <sub>3</sub> MgCO <sub>3</sub> + H <sub>2</sub> S + (CaS + MgO) + 2CO <sub>2</sub> + H <sub>2</sub> O	62	9)

Both the extent and mechanism of dolomite decomposition are affected by the partial pressure of CO<sub>2</sub>. Haul and Markus (1952) followed the decomposition of dolomite by thermogravimetric analysis of powdered dolomite at 500-900°C under various partial pressures of CO<sub>2</sub>. Their results, shown in figure 1, indicate that the decomposition occurs by two different pathways:



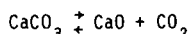
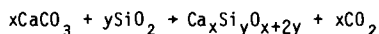
The decomposition followed Path A when the partial pressure of CO<sub>2</sub> was 12-24 mmHg while Path B prevails at higher CO<sub>2</sub> pressures. Since the equilibrium constant for the decomposition reaction is simply the partial pressure of CO<sub>2</sub>, the concentration of CO<sub>2</sub> affects both the mechanism and extent of decomposition. For processes in which a carbonaceous material (retorted shale or coal char) is oxidized to supply energy for the pyrolysis stage, the presence of CO<sub>2</sub> in the recycled combustion gases will inhibit the carbonate decomposition.

The onset of decomposition is affected by the presence of steam. MacIntire and Stansell (1953) report that calcium and magnesium components of dolomite decompose about 200°C lower than when air is used alone. The same effect was observed by Burnham et al. (1980) except dolomite was affected to a much greater extent than calcite.

Decomposition reactions are highly endothermic, thus they adversely affect the thermal efficiency of the process. Boynton (1980) described the heat balance for the calcination of limestone in a rotary kiln. Between 1.7 and 4.8 MMBtu/ton of CaCO<sub>3</sub> are expended depending on the heat recovery systems employed. The minimum heat for calcination at the dissociation temperature is 2.5 MMBtu/ton of calcite or 0.61 MMBtu/ton of shale to calcine an average western shale containing 33% carbonates. Chen et al. (1982) used the ASPEN computer simulation system to study the effect of calcite decomposition on the overall thermal efficiency of an oil shale retort.

Finally, the rate and the temperature of decomposition affect the pore structure of the carbonate mineral particles as well as the shale. Steen et al. (1980) reported an increase in porosity from 12 to 29% accompanied by an increase in surface area from 0.3 to 8.9 m<sup>2</sup>/g after half calcination of a dolomite sample. Surface area and porosity have a strong influence on the rate of sulfidation and absorbance capacity of the minerals.

Campbell (1978) and McCarthy et al. (1984) have shown that the under typical retorting conditions CaCO<sub>3</sub> also reacts with SiO<sub>2</sub>. The competing reactions are:



When a high CO<sub>2</sub> partial pressure and a slow heating rate were used, the carbonate reaction to form silicates increased because of the greater length of time required to reach the decarbonation temperature. Decomposition to CaO is very rapid once this temperature is reached. Oxide formation occurs at 600 to 750°C depending on the CO<sub>2</sub> partial pressure whereas silicate formation occurs at about 700-800°C. Therefore, this undesirable depletion of available carbonates would not be significant during pyrolysis (600°C) but may become a problem during hydrodesulfurization (750-850°C) or if the shale is retorted prior to mixing with the coal to be pyrolyzed.

#### Thermodynamics of Desulfurization Reactions

The IGS application of the minerals in oil shale differs markedly from fuel gas desulfurization by carbonates. During pyrolysis and hydrodesulfurization, H<sub>2</sub>O, H<sub>2</sub>, CO, CO<sub>2</sub>, and H<sub>2</sub>S influence the H<sub>2</sub>S adsorption equilibria, i.e. equations 5-9, table 1. Optimal temperatures, pressures, flowrates, etc. have been specified for pyrolysis and hydrodesulfurization processes, but these conditions may not be the most favorable for H<sub>2</sub>S adsorption. In the following discussion the thermodynamics of H<sub>2</sub>S adsorption by oil shale minerals are reviewed while taking into consideration the limited range of operating conditions typical of pyrolysis and hydrodesulfurization processes.

The reaction between calcium oxide and hydrogen sulfide (eqs. 6 and 8) has been studied by many researchers (Uno, 1951; Rosenquist, 1951; Curran et al., 1967). Pell (1971) summarized these experimental studies with the following least squares fit of their data:

$$\log K = \log \frac{P_{\text{H}_2\text{O}}}{P_{\text{H}_2\text{S}}} = 3519.2/T - 0.268 \quad 10)$$

Pell combined this expression with the data given by Hill and Winter (1956) for the decomposition of calcium carbonate to find the following equilibrium expression for the reaction between hc-dolomite and hydrogen sulfide (eq. 7):

$$\log K = \log \frac{P_{\text{H}_2\text{O}} \cdot P_{\text{CO}_2}}{P_{\text{H}_2\text{S}}} = 7.253 - 5280.5/T \quad 11)$$

Combining equation 11 with the data given by Stern and Weise (1969) on the decomposition of magnesium carbonate, the following expression for the equilibrium between dolomite and H<sub>2</sub>S (eq. 9) is obtained:

$$\log K = \log \frac{(P_{CO_2})^2 \cdot P_{H_2O}}{P_{H_2S}} = 16.19 - 10,553/T \quad (12)$$

Plots of  $\log K$  vs  $1/T$  derived from equations 10-12 are shown in figures 2 and 3. Plots from thermodynamic calculations based on the data of Barin et al. (1977) and Mills (1974) are also shown. A number of interesting observations can be made from these figures.

1. The efficiency of calcium oxide as an  $H_2S$  absorbent decreases at higher temperatures whereas the efficiency of calcium carbonate increases.
2. The thermodynamic calculations of the equilibrium constant for the reaction of  $H_2S$  and lime agree well with the experimental data. Since only thermodynamic data for dolomite exists, the calculations for the sulfidation of the full and half calcines were made as shown above, i.e., starting with dolomite calculations and combining them with decomposition data. Therefore, the good match between the thermodynamic and experimental values shown in figure 3 reflect accurate predictions of the extent of carbonate decomposition, not sulfidation.
3. As was mentioned earlier, the behavior of fc-dolomite is nearly the same as that of calcium oxide, and the reaction of hc-dolomite with hydrogen sulfide is similar to that of calcite. On the other hand, dolomite behaves completely different than calcite.

When coal is pyrolyzed, pyrite ( $FeS_2$ ) is converted to pyrrhotite ( $FeS$ ) and hydrogen sulfide. The hydrogen sulfide may then be removed with the off-gas or be captured in the carbon matrix of the coal or char (Huang and Pulsifer, 1977). Many studies of the reaction of  $H_2S$  with char, commonly referred to as the back-reaction, have been carried out (Robinson, 1976; Zielke et al., 1954; Jones et al., 1966). Depending on the temperature and nature of the char, the back reaction can occur at  $H_2S$  concentrations as low as 300 ppm. An acceptable scavenger should limit the  $H_2S$  concentration to this level to inhibit the back-reaction. Figure 4 shows that under typical pyrolysis conditions, calcium minerals are capable of maintaining this level if equilibrium is reached. The desired equilibrium partial pressure, i.e., below 300 ppm, is predicted at all temperatures of interest when  $CaO$  is present, at temperatures above  $400^\circ C$  when dolomite is present, and at temperatures above  $750^\circ C$  when  $CaCO_3$  is present. Data from the Lurgi-Rhurgas oil shale distillation process which recycles oxidized shale to the pyrolysis bed demonstrates the reactivity of  $CaO$  toward  $H_2S$ . At a recycle ratio of about 7/1 and at  $650^\circ C$ , hydrogen sulfide concentrations of ~1300 ppm and ~4000 ppm in the off gas have been reported by Schmalfeld (1975) and Weiss (1982), respectively. Sitrai (1984) has also shown that retorting a 1:1 mixture of oil shale and shale ash reduces the concentration of  $H_2S$  in the off-gas to less than 100 ppm.

The decomposition and desulfurization reactions of carbonates occur in parallel. Therefore, the competition between the two reactions should be considered. The FACT thermodynamics computing system (Bale et al., 1979) was used to develop the phase stability diagrams for  $Mg-C-H-O-S$  and the  $Ca-C-H-O-S$  systems shown in figures 5-7. Magnesium carbonate is unstable with respect to the oxide at  $327^\circ C$  and 10 atm.  $CO_2$ . As shown in figure 5, at hydrogen sulfide concentrations of 0.6% or higher, sulfidation is inhibited until about  $1227^\circ C$ . This result agrees with Westmoreland and Harrison (1980) who concluded that  $MgO$  is too stable to be used as an  $H_2S$  acceptor.

Phase diagrams for the  $Ca-O-H-S-C$  system at about  $500^\circ C$ , the maximum pyrolysis temperature, and  $750^\circ C$ , a typical hydrodesulfurization temperature for coal char, are shown in figures 6 and 7. At  $600^\circ C$  calcium oxide exists only at carbon dioxide

pressures lower than about 0.01 atm. Calcium oxide will react with  $H_2S$  at gas concentrations as low as 10 ppm whereas, depending on the  $CO_2$  concentration,  $H_2S$  concentrations from 100 to 1000 ppm are required before the carbonate will undergo sulfidation. At 750°C the reactivity of the oxide is nearly unchanged. However, at this temperature  $CaCO_3$  decomposes at  $CO_2$  pressures as high as 0.2 atm and will undergo sulfidation at  $H_2S$  concentrations as low as 100 ppm. Nonetheless,  $CaO$  still appears to be the most reactive. These results are in agreement with the observations of Harrison and Westmoreland (1980) who reported that the most efficient desulfurization occurred at the lowest temperature (about 880°C) at which  $CaO$  was first formed from  $CaCO_3$ .

An increase in the total pressure, with a corresponding increase in the  $CO_2$  and  $H_2O$  partial pressures, would inhibit desulfurization by the carbonates (eqs. 5, 7 and 9) but would not affect the equilibria between  $H_2S$  and calcium oxide (eqs. 6 and 8). However, at a higher  $CO_2$  partial pressure recarbonation of the oxide competes with sulfidation reaction. Under a 0.4 atmosphere pressure of  $CO_2$ ,  $CaO$  will recarbonate at temperatures below 827°C (Stern and Wiese, 1969). Thus  $H_2S$  adsorption by any of the sorbents considered is less efficient at higher pressure. However, most pyrolysis and hydrodesulfurization processes operate at or near atmospheric pressure.

#### Desulfurization Kinetics

Before any engineering decisions on the effectiveness of oil shale as hydrogen sulfide acceptor are made, detailed information on the thermodynamics and kinetics of reactions involved is required. However, thermodynamics only determine whether a given desulfurization reaction could occur, while the kinetics determine the degree of conversion of a thermodynamically allowable reaction. In particular, kinetic data are essential since in most engineering modeling calculations they are combined with transport equations to predict the performance of a given system.

The intrinsic rate constants for the reactions of calcium carbonate or calcium oxide with  $H_2S$  have been reported by a number of investigators. A summary of published work is presented in table 2. The experiments were conducted under conditions where transport effects were minimized. The reported activation energies for the reaction calcium oxide and  $H_2S$  range from 3.6 to 38 kcal/mole and those for the carbonate range from 17.3 to 60 kcal/mole. The low values of Westmoreland (1976) and Kamath and Petrie (1981) may be due to diffusion resistances. The activation energy values for the sulfidation of lime as reported by Attar (1978) and Borgwardt et al. (1984) are 37 and 31 kcal/mole. However, the former author believes that the reaction is controlled kinetically while the latter believes that diffusion through the  $CaS$  layer is the controlling step. The pre-exponential factors, shown in table 2, also vary by many orders of magnitude. It appears that the data available in the literature are inconclusive. The wide range of reactivities reported in the literature can be attributed either to differences in experimental methodology or in the physical characteristics of minerals employed.

The pore size distribution, porosity, and surface area of the sample as well as the presence of magnesium oxide have been shown to affect the reactivity of calcium minerals with  $H_2S$ . The work of Borgwardt et al. (1984) showed that the rate of reaction of lime with  $H_2S$  at 700°C is proportional to the 2.3 power of the B.E.T. surface area indicating product layer diffusion control at these conditions. Other authors, however, have observed that the reaction "stops dead" after 5 to 25% conversion due to the solid product layer (Attar, 1979; Squires, 1972). Harvey et al. (1976) concluded that the crystallites of  $MgO$  found in hc-dolomite increased the reactivity of the calcium carbonate by maintaining the porosity of the material and hindering the consolidation of the carbonate into larger crystals. Pell (1971) also found that the sulfidation of fc-dolomite particles occurred homogeneously throughout the solid. The inert minerals in oil shale could perform the same function as  $MgO$  in dolomite, thereby enhancing the reactivity of the  $CaO$  or  $CaCO_3$  in oil shale.

The rate of sulfation (reaction with  $\text{SO}_2$ ) of carbonates has also been shown to be highly sample dependent. Borgwardt and Harvey (1972) found the physical properties of the carbonate stones were much more important rate determinants than the composition of the carbonate. Similarly, Fee et al. (1982) found that the chemical composition, pore size distribution, and surface area of each individual limestone or dolomite must be considered before the performance of a solid as an  $\text{SO}_2$  acceptor could be predicted. The superior sulfation characteristics of oil shale carbonates over pure dolomite was demonstrated by Fuchs et al. (1978). They observed that the initial rate of sulfation for the hc-dolomite in shale is nearly six times that of pure hc-dolomite under identical experimental conditions. This was attributed to the fine-grained nature of carbonates in oil shale and the high surface area of the devolatilized shale among other factors. In the case of sulfidation, as in sulfation, we believe that the reaction kinetics will more likely depend on the physical properties of the solid than on the mineral itself. Therefore only rate measurements made with the oil shale sample will be useful for process design. Published work on the reactivity of the pure minerals is not a reliable substitute.

Since  $\text{H}_2$ ,  $\text{CO}_2$ , and  $\text{H}_2\text{O}$  are present during hydrotreatment and pyrolysis, their effect on the rate of sulfidation is important. Hydrogen concentrations as low as 3% have lowered the rate of sulfidation of the limestone (Borgwardt and Roache, 1984). The effect increases as the concentration of hydrogen is increased but levels off near 15%. Oddly enough, dolomite is unaffected. The effect of carbon dioxide is important because it is a common component of pyrolysis gas and a product of the sulfidation of carbonates. Ruth (1972) reported that not only the rate of reaction but also the extent of sulfidation of calcium carbonate were greatly increased when raising the  $\text{CO}_2$  level of the reactant gas from 3% to 60%. The reaction essentially stopped after 15% conversion when using 3%  $\text{CO}_2$  at 600°C whereas complete conversion was achieved at the 60%  $\text{CO}_2$  level. At 700°C the effect of the  $\text{CO}_2$  level was not particularly significant. The catalytic effect of steam on the rate of sulfidation has also been observed (Pell, 1971; Squires, 1972). Most authors theorize that the gas composition effects the growth and final crystalline structure of the calcium sulfide layer. This in turn enhances or inhibits the rate of hydrogen sulfide,  $\text{H}_2\text{O}$ , or  $\text{CO}_2$  diffusion through the solid layer, and changes the overall rate of reaction.

#### Concluding Remarks

A thorough understanding of the reactions between  $\text{H}_2\text{S}$  and carbonate minerals in oil shale is essential if this material is to be used effectively as an  $\text{H}_2\text{S}$  scavenger. Thermodynamics show that under typical conditions for coal-oil shale pyrolysis, dolomite and calcium oxide are capable of maintaining the desired  $\text{H}_2\text{S}$  concentration in the reactor. Additionally, under typical conditions of char desulfurization, calcium oxide will be an effective sorbent. However, because the gas residence time in an FBR is often on the order of a few seconds, the reaction rates must be high enough for the thermodynamically allowed reactions to reach equilibrium. Therefore, the kinetics of these reactions must be experimentally determined. In addition, a thorough understanding of the influence of the gas environment and the effects of the structural properties of the oil shale particles (raw, retorted, or spent) is essential. We have begun to obtain experimental data for the reactions between  $\text{H}_2\text{S}$  and carbonate minerals in oil shale under typical conditions for pyrolysis and hydrodesulfurization. In the near future, we intend to study the structural changes of oil shale particles during  $\text{H}_2\text{S}$  capture. This information will provide a basis for employing a gas-solid reaction model such as the changing grain size model to predict the behavior of a single oil shale particle during  $\text{H}_2\text{S}$  capture.

## References

- Attar, A., 1978, Reactions of sulfur in coal-gas reactions, *Fuel*, Vol. 57, p 209.
- Attar, A., and F. Dupius, 1979, The rate and fundamental mechanism of the reaction of hydrogen sulfide with basic minerals in coal, *Ind. Eng. Chem. Process Development and Design*, Vol. 18, No. 4, p. 607.
- Bale, C. W., A. D. Pelton, and W. T. Thompson, 1979, *FACT User's Guide*, McGill University.
- Barin, I., O. Knacke, and O. Kubaschewski, 1977, *Thermo-chemical properties of inorganic substances*, Springer-Verlag, Berlin.
- Borgwardt, R. H. and R. D. Harvey, 1972, Properties of carbonate rocks related to  $SO_2$  reactivity, *Environmental Science and Technology*, Vol. 6, p. 350-360.
- Borgwardt, R. H., N. F. Roache, and K. Bruce, 1984a, Surface area of calcium oxide and kinetics of sulfide formation, *Environmental Progress*, Vol. 3, No. 2, p. 129.
- Borgwardt, R. H. and N. F. Roache, 1984b, Reaction of  $H_2S$  and sulfur with limestone particles, *Ind. Eng. Chem Process Design Development*, Vol. 23, p. 742-748.
- Boynton, R. S., 1980, *Chemistry and Technology of Lime and Limestone*, 2nd ed., John Wiley, Inc.
- Burnham, A. K., C. T. Stubblefield, and J. H. Campbell, 1980, Effects of gas environment on mineral reactions in Colorado oil shale, *Fuel*, Vol. 59, p. 871-877.
- Campbell, J. H., 1979, The kinetics of the decomposition of Colorado oil shale II: carbonate minerals, UCRL - 52089.
- Chen, C. C., J. K. Floess, L. Fong, J. P. Longwell, and L. B. Evans, 1982, Modeling of an oil shale fluidized bed retorting process using ASPEN, *Energy Progress*, Vol. 2, No. 3, p. 147-150.
- Curran, G. P., C. E. Fink, and E. Gorin, 1967,  $CO_2$  Acceptor Gasification Process - studies of acceptor properties, *Advances in Chemistry Series*, No. 69, American Chemical Society, p. 141-165.
- Davidson, M. L., and D. P. Harrison, 1984, Evaluation of the changing grain size model, *Eng. Communication*, Vol. 25, p. 213-228.
- Fee, D. C., K. M. Myles, W. I. Wilson, L. S. Fan, G. W. Smith, S. H. Wong, J. A. Shearer, J. F. Lenc, and I. Johnson, 1980, Sulfur control in fluidized bed combustors; methodology for predicting the performance of limestone and dolomite sorbents, Report to DOE, ANL/FE-80-10.
- Harvey, R. D., G. Kan, R. A. Graff, and A. M. Squires, 1976, Behavior of dolomite in absorption of  $H_2S$  from fuel gas, *ISGS Reprint Series*, 1977C.
- Haul and Markus, 1952, *J. Appl. Chemistry*, Vol. 2, p. 298.
- Hill, K. J., and E. K. Winters, 1956, Thermal dissociation pressure of calcium carbonate, *J. Phys. Chem.*, Vol. 60, p. 1361-1362.
- Huang, E. T. and A. H. Pulsifer, 1979, Coal desulfurization during gaseous treatment, *ACS Symposium Series*, No. 64, American Chemical Society, p. 290-304.

- Jones, J. F., M. R. Schmid, M. E. Sacks, Y. C. Chen, C. A. Gray, R. T. Eddinger, 1966, COED final report, Jan.-Oct. 1966, OCR, Department of Interior.
- Kamath, V. S. and T. W. Petrie, 1981, Rate of reaction of hydrogen sulfide - carbonyl sulfide mixtures with fully calcined dolomite, SIU Carbondale, Environmental Science and Technology, Vol. 15, No. 8, p. 966.
- MacIntire, W., and T. Stansell, 1953, Ind. and Eng. Chemistry, Vol. 45, p. 1548.
- McCarthy, D. J. and H. J. Poynton, 1984, Formation of calcium silicates during processing of Julia Creek oil shale, Fuel, Vol. 63, p. 769.
- Mills, K. C., 1974, Thermodynamic data for inorganic sulfides, selenides and tellurides, Butterworths Inc., London.
- Pell, M., 1971, Reaction of hydrogen sulfide with fully calcined dolomite, PhD thesis, City University of New York.
- Robinson, L., 1976, Hydrodesulfurization of char, Fuel, Vol. 55, p. 193-201.
- Rosenqvist, T., 1951, A thermodynamic study of the reaction  $\text{CaS} + \text{H}_2\text{H}_2\text{S} + \text{CaO}$  and the desulfurization of liquid metals with lime, J. Metals Trans., Vol. 3, p. 535-40.
- Ruth, L. A., A. M. Squires, R. A. Graff, Desulfurization of fuels with half-calcined dolomite: first kinetic data, Environmental Science and Technology, Vol. 6, No. 12, p. 1009.
- Schmalfeld, P., 1975, The use of the Lurgi-Rhurgas process for the distillation of oil shale, Quart Colorado School of Mines, Vol. 670, No. 3, p. 129-145.
- Sitnai, O., 1984, Process concept for retorting of Julia Creek oil shale, Energy Progress, Vol. 4, No. 2, p. 100-104.
- Steen, C. L., K. Li, and F. Rogan, 1980, Half-calcination of dolomite at high pressures. Kinetics and structural changes, Environmental Science and Technology, Vol. 14, No. 5, p. 588.
- Stern, K. H. and E. L. Wiese, 1969, High temperature properties and decomposition of inorganic salts, part 2: carbonates, NSRDS - NBS30, p. 19.
- Squires, A. M., 1972, New systems for clean power, Int. J. Sulfur Chemistry, Pt B, Vol. 7, No. 1, p. 85.
- Uno, T., 1951, Tetsu To Hagana (Iron and Steel) Vol. 37, p. 14-17.
- Weiss, H., 1982, Retorting of oil shale - background, status, and potential of the Lurgi-Rhurgas process, ACS symposium, Oil shale retorting - Latest developments, March 28 - April 12, Las Vegas, Nevada.
- Westmoreland, P. R., J. B. Gibson, D. P. Harrison, Comparative kinetics of high-temperature reaction between  $\text{H}_2\text{S}$  and selected metal oxides, Environmental Science and Technology, Vol. 11, No. 5, p. 488.
- Westmoreland, P. R. and D. P. Harrison, 1976, Evaluation of candidate solids for high-temperature desulfurization of low-Btu gases, Environmental Science and Technology, Vol. 10, No. 7, p. 659.
- Zielke, C. W., G. P. Curran and G. E. Goring, 1954, Desulfurization of low temperature char by partial gasification, Ind. Eng. Chem., Vol. 46, No. 1, p. 53-56.

Table 2. Experimental Techniques and Results of Kinetic Studies, Part I

Reference	Kinetic Expression (Temperature range)	Reactor	$K_0$	$E_a$ (kcal/mole)
Atlar (1978)	Rate = $K[\text{Solid}][\text{H}_2\text{S}]$ (400-800°C)	Pulsed Differential Reactor, Packed bed design	-	$\text{CaCO}_3$ 17.3 $\text{CaO}$ 37.0 $\text{CaCO}_3/\text{MgCO}_3$ 18.9
Borgwardt (1984a)	Rate = $K[\text{CaO}][\text{H}_2\text{S}]$ (600-900°C)	Differential Reactor, Packed bed design	$1.2 \times 10^8$ L <sup>2</sup> cm/mole $\text{H}_2\text{S}^2 \text{min}^{-1}$ <sup>a</sup>	37
Borgwardt (1984b)	Rate = $\frac{K}{D_p} [\text{CaCO}_3][\text{H}_2\text{S}]$ (550-850°C)	Differential Reactor, Packed bed design	$8 \times 10^8$ L <sup>2</sup> cm/mole $\text{H}_2\text{S}^2 \text{min}^{-1}$ <sup>a</sup> at $D_p = 2.8 \mu\text{m}$	42.6
Davidson (1984)	Rate = $Ak[\text{H}_2\text{S}]$ ; where $A = \frac{K}{1 + K} \text{CaO}$ (625-950°C)	Thermobalance	$8.25 \times 10^4$ L <sup>2</sup> cm/mole $\text{H}_2\text{S}^2 \text{min}^{-1}$ <sup>b</sup>	27
Kamath (1981)	Rate = $K[\text{CaO}]$ (600-800°C)	Thermobalance	$K_{600} = 1.1 \times 10^{-4} [\text{H}_2\text{S}]^{0.76} \text{sec}^{-1}$ $K_{700} = 1.43 \times 10^{-4} [\text{H}_2\text{S}]^{1.01} \text{sec}^{-1}$ $K_{800} = 1.61 \times 10^{-4} [\text{H}_2\text{S}]^{1.22} \text{sec}^{-1}$	
Pell (1971)	Rate = $Ak[\text{H}_2\text{S}]$ ; where $A = \frac{K}{1 + K} \text{CaO}$ (700-900°C)	Thermobalance	$4.96 \times 10^5$ L/mole $\text{H}_2\text{S}^2 \text{min}^{-1}$	22.9
Ruth (1972)	Rate = $K'[\text{CaCO}_3]$ (550-800°C)	Modified Dupont TGA	-	60
Westmoreland and (1977)	Rate = $K'[\text{CaO}][\text{H}_2\text{S}]^N$ (300-800°C)	Thermobalance	$0.038$ L <sup>2</sup> cm/min <sup>2</sup> mg/mole	$N = 1$ 5.16

<sup>a</sup> Estimate from data given

<sup>b</sup> A recalculation of Pell's data

Table 2. Experimental Techniques and Results of Kinetic Studies, Part II

Reference	Material	Material Properties	Gas Composition & Flow Properties
Attar (1973)	Calcite, Lime, and Dolomite	-200 mesh, 0.1-0.5g sample	H <sub>2</sub> S pulse = $1 \times 10^{-6}$ mole/pulse in steady stream of He, flow rate not given but assumed to be low because gas diffusion was controlling at times
Borgwardt (1984a)	CaO from Calcined Limestone	2um limestone calcined at 700°C for 90 sec, 15 mg sample, surface area = 5.8 m <sup>2</sup> /g, BCR 2061	5000 ppm H <sub>2</sub> S, 70% CO <sub>2</sub> , balance N <sub>2</sub>
Borgwardt (1984b)	Limestone	Fredonia Valley White, Fredonia, KY, ratio Ca/Mg = 73/1, BC 2061 1-10 um limestone particles dispersed in quartz wool	5000 ppm H <sub>2</sub> S, 70% CO <sub>2</sub> , balance N <sub>2</sub> , 5 L/min at 25°C, 490 cm <sup>3</sup> /s at 750°C, gas diffusion was not a problem at this rate, exposure time = 30-55 min
Davidson (1984)	Fully-calcined Dolomite	surface area = 14 m <sup>2</sup> /g, 124-380 mg samples, sphere diameter = 0.277 to 0.406 cm	5% H <sub>2</sub> S, 7.5% H <sub>2</sub>
Kamath (1981)	Fully-calcined Dolomite	-30+50 mesh, Dp = 400um, Pfizer Corp., Gibsonville, Ohio, ratio Ca/Mg = 0.84	0.5-5% H <sub>2</sub> S, 20% H <sub>2</sub> , 30% CO, balance N <sub>2</sub> , 500 SCCM used, no difference at 1000 SCCM
Pell (1971)	Fully-calcined Dolomite	-80+325 mesh, ratio Ca/Mg = 1.09	0.5-20% H <sub>2</sub> S, 7.5% H <sub>2</sub> , balance N <sub>2</sub> , H <sub>2</sub> O used at times, flowrate = 0.5 L/min (STP), Reynolds number = 1
Ruth (1972)	Half-calcined Dolomite	Greenfield formation, 25mg sample, -250+270 mesh, dolomite calcined immediately before reaction in TGA, BCR 1337 and 1930	0.5-20% H <sub>2</sub> S, various levels of CO <sub>2</sub> , H <sub>2</sub> , and N <sub>2</sub> , flow rate = 100-300 mL/min
Westmoreland (1977)	Pure CaO	100 mesh heated to 500°C in an inert gas, surface area = 17.3 m <sup>2</sup> /g	1.9-7% H <sub>2</sub> S, ratio H <sub>2</sub> /H <sub>2</sub> S = 5:1, balance N <sub>2</sub> , volumetric flowrate set to eliminate external mass transfer resistance

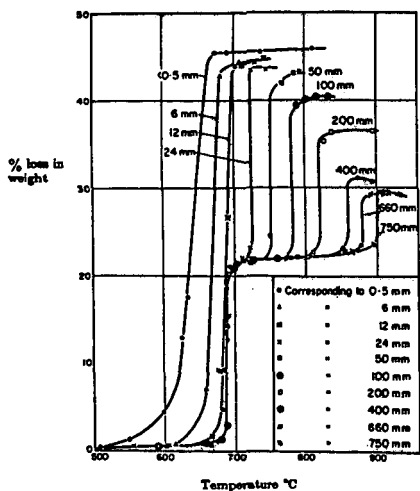


Figure 1. The thermogravimetric analysis of dolomite at various temperatures and  $\text{CO}_2$  pressures.

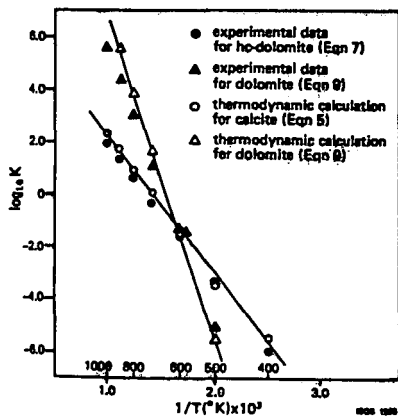


Figure 3.  $\text{Log} K_{eq}$  vs  $1/T$  for the adsorption of  $\text{H}_2\text{S}$  by various forms of  $\text{CaCO}_3$ .

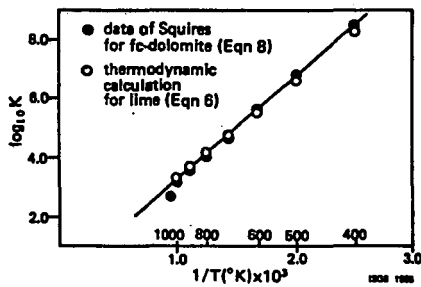


Figure 2.  $\text{Log} K_{eq}$  vs  $1/T$  for the adsorption of  $\text{H}_2\text{S}$  by  $\text{CaO}$ .

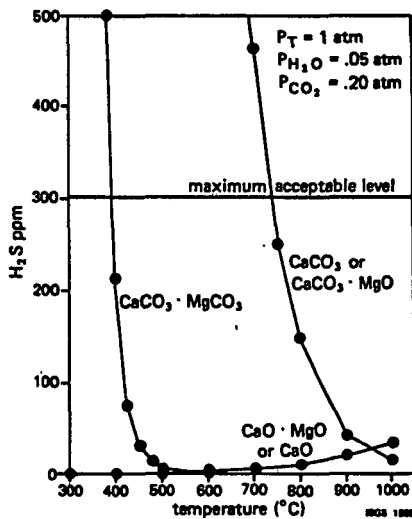


Figure 4. Equilibrium partial pressure of  $\text{H}_2\text{S}$  in the presence of oil shale minerals.

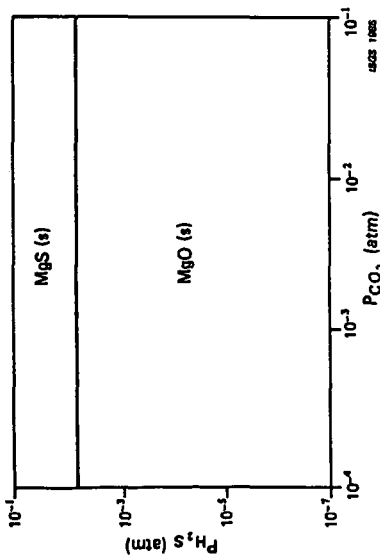


Figure 5. Phase stability diagram for the Mg-H-O-S-C system,  $T=1227^{\circ}\text{C}$ ,  $P_{\text{H}_2\text{O}} = 0.05$  atm.

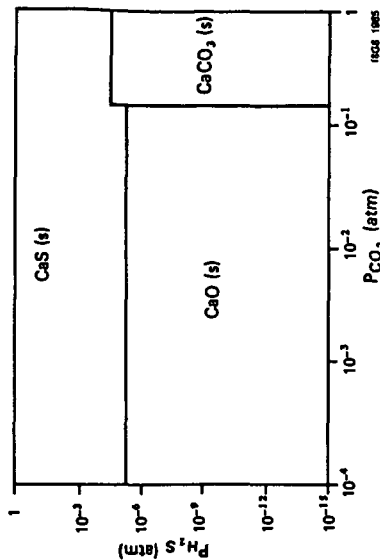


Figure 7. Phase stability diagram for the Ca-H-O-S-C system,  $T=750^{\circ}\text{C}$ ,  $P_{\text{H}_2\text{O}} = 0.05$  atm.

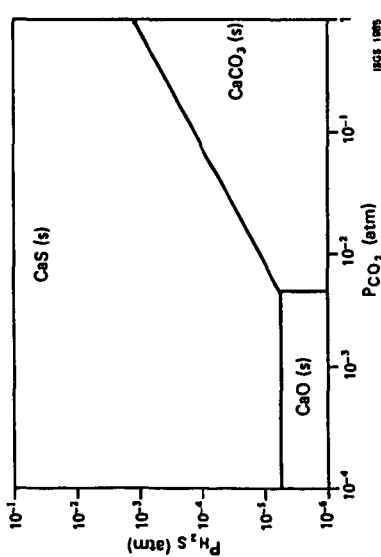


Figure 6. Phase stability diagram for the Ca-H-O-S-C system,  $T=600^{\circ}\text{C}$ ,  $P_{\text{H}_2\text{O}} = 0.05$  atm.

## ENHANCED OIL RECOVERY FROM PYROLYSIS OF VARIOUS AUSTRALIAN SHALES

Vetkav Parameswaran, Mark Polasky and Sunggyu Lee

Department of Chemical Engineering  
The University of Akron.  
Akron, Ohio 44325.

### ABSTRACT

The oil yields from retorting Stuart, Rundle and Condor shales have been optimized with respect to their process operating conditions using a statistical experimental design technique. A three factor, two level factorial design of experiments was adopted to determine the main and interaction effects of variables on the yield of oil from these shales. The three variables are the particle size, the type of sweep gas and the sweep gas flow rate.

It was found that retorting with carbon dioxide as the sweep gas enhances the oil yield from Stuart shale by up to 24 percent. The strongest effect was observed from the sweep gas flow rate and the optimal condition for this variable was found through out-layer experiments. For each of the significant effects, transport processes such as the combined heat and mass transfer were explained and design criteria for a retorting system were found for scale up purposes.

### INTRODUCTION

Extensive deposits of oil shale, bearing enormous amounts of equivalent synthetic fuel exist in the U.S.A., Australia, Canada, China and various other parts of the world. However, these deposits are far from uniform and there are wide variations in the physical and chemical structure of the rocks even within the same general location. As a result, engineering and fundamental data are required even for preliminary design and economic feasibility analysis. The need for data is even more vital during the detailed industrial process development. In order to maximize the yield, the kinetics as well as the physical and chemical properties of the shale and shale oil must be known. An extensive review of oil shale technology covering the historical development and the kinetics of oil shale retorting as well as the properties of oil shale has been presented by Branch (1). This paper aims at finding the optimum operating conditions for the retorting of Australian Tertiary shales. The shale samples studied were taken from the Kerosene Creek member of the Stuart deposit, the Ramsey crossing member of the Rundle deposit, and the Brown oil shale unit of the Condor deposit, all of which are located along the coastline of Queensland, Australia.

## APPROACHES

Optimization studies generally involve either the solution of differential equations or the discrete techniques of linear algebra. In either case, it is necessary to have a mathematical description of the system. The physical and chemical complexity of oil shale renders such a rigorous mathematical treatment extremely difficult.

For engineering purposes however, an experimental exploration of the range of interesting process conditions can be coupled with the methods of statistical experimental design to arrive at optimum operating parameters with the minimum of experimental cost and effort. Therefore a three factor, two level design of experiments for each type of oil shale was adopted for this study.

### IDENTIFYING THE CRITICAL VARIABLES

In order to ensure the reproducibility of experimental results, standard retorting procedures must be adopted without stifling the degree of freedom necessary to optimize the operating conditions. Twenty grams of oil shale were charged into the retort which was then heated at the rate of 10 C/min from 25 C to 700 C at atmospheric pressure. The details of the retorting apparatus have been published elsewhere (2). The apparatus consists essentially of a 15.75 inch long x 1 inch diameter stainless steel tube which is placed inside an electric furnace. The shale sample is loaded into the retort through a ball valve at the top of the tube. The sweep gas (which is preheated in a gas preheater following the reactor preheating schedule) flows down through the sample bed into an oil collection tube which is kept cool in a water bath.

The variables studied were the particle size (-8 +10 mesh and -20 +40 mesh (Tyler)), sweep gas type (carbon dioxide and nitrogen) and sweep gas flow rate (2 ml/sec and 5 ml/sec (STP)). The levels of these variables have been chosen based on preliminary experiments as well as prior experience (2).

The mechanism by which the oil is released from the pores of the shale is not very clear. The influence of the particle size on the retorter yield seems to depend on the type of oil shale being retorted. As the oil shales are fairly non-porous (very often below 5 % porosity), it is to be expected that crushing the oil shale would improve the process of oil evolution. However, there seems to be a minimum particle size below which the influence on the yield tends to be negative. This is due to the loss of kerogen entrapped in macropores while crushing. Therefore, two different sizes were tested, viz, -8 +10 mesh and -20 +40 mesh (Tyler).

It has been found by Lee (3), that carbon dioxide sweep gas conditions enhance the oil recovery from Colorado oil shales. Therefore tests were conducted with two types of sweep gas, i.e., nitrogen and carbon dioxide.

The flow rate of sweep gas is very important from an engineering point of view. This influences the heat and mass transfer conditions within the reactor and scale up and scale down of commercial reactors would be disastrous if the mass transfer conditions were not kept uniform in the scaled models. Therefore experiments were made with two different sweep gas flow rates, viz, 2 ml(STP)/sec and 5 ml(STP)/sec. This corresponds to vapor space velocities (calculated at STP) of 720 and 1800 per hour (superficial linear velocities of 0.4 and 1.0 cm/sec) respectively in the retort.

The influences of these three variables were studied on three different Australian Tertiary oil shales identified as Rundle, Stuart and Condor oil shales and the results were critically compared with those obtained with the Eastern and Western U.S. oil shales in terms of their yield, effects and optimal process conditions.

## RESULTS AND DISCUSSION

The results of the various experiments conducted on Stuart, Rundle and Condor oil shales are presented in Table 1. The yields obtained were analyzed using Yates' algorithm (4) to determine the effects of the various treatment combinations on the yield. These effects are also summarized in Table 1. For the purpose of comparison, similar data are also included in Table 1 for the Colorado (5) and Ohio #2 (6) oil shales.

For the purpose of determining the significant effects, three replications were carried out and the effects that were larger than twice the standard deviation in these runs were identified as the significant effects. Accordingly, the minimum effects for the determination of significance were 4.80, 6.38, 2.34, 4.10, and 1.90 for the Stuart, Rundle, Condor, Colorado and Ohio # 2 shales respectively.

### Stuart Shale

Of the three Australian shales tested, the Stuart shale gave the largest oil yield (Fischer Assay of 101 ml/kg) comparable to the yields obtained from most Colorado shales.

The sweep gas flow rate had the largest influence on the oil yield. This predominant effect was observed with all the oil shales so far tested. The influence in all cases was negative in the range of the variable studied indicating thereby that an increase in the flow rate from 2 ml(STP)/sec to 5 ml(STP)/sec reduces the yield. This strongly suggests that mass transfer

TABLE 1. Summary of Yields and Effects

Shale Type	Tertiary	Tertiary	Tertiary	Tertiary	Eocene	Devonian				
Treatment Combination	Yield Effect	Yield Effect	Yield Effect	Yield Effect	* COLORADO	* OHIO # 2				
	STUART	RUNDLE	CONDOR		Yield Effect	Yield Effect				
(1)	105	110.94	80	63.13	65	51.72	94.2	92.94	32	25.75
a	125	- 4.38	82.5	1.25	67.5	- 0.31	95.8	0.57	31	2.50
b	130	5.63	65	- 5.00	60	- 2.81	105.9	8.72	29	2.00
ab	120	- 8.13	72.5	0	61.3	- 1.56	98.0	- 1.37	30	2.00
c	107.5	- 18.13	50	- 23.75	40	- 23.44	81.0	- 11.07	17	- 9.50
ac	95	- 9.38	50	- 3.75	40	- 2.19	83.3	3.72	19	2.50
bc	110	- 4.38	55	7.50	42.5	2.81	89.5	1.77	20	4.00
abc	95	6.88	50	- 2.50	37.5	- 0.94	95.8	3.37	28	1.00

Units of Yield are ml/kg

The significant effects are underlined

The Factors and the Levels are as follows:

Factor	+ Level	- Level
(a) Particle size	-8 +10 mesh -4 + 8 mesh(*)	-20 +40 mesh
(b) Sweep Gas Type	Carbon Dioxide	Nitrogen
(c) Sweep Gas Flow	5 cc/sec	2 cc/sec
Heating Rate	----- 10 C/min -----	

Note:(\*) Particle size of -4 + 8 mesh was used for the + Level for the Colorado (5) and Ohio # 2 (6) shales.

plays an important role in shale oil extraction. Based on similar situations in gas-solid reaction systems, this implies that beyond a certain limit in the sweep gas flow rate, an increase in the flow rate adversely affects the total yield. Therefore, either a corner test or outlayer experiments have to be conducted to determine the optimal flow rate. In the corner test, the sweep gas flow rate was varied while keeping the other variables at their optimal values. The results show that the best yield is obtained with a sweep gas flow rate of 2 ml(STP)/sec.

On the other hand, the type of sweep gas used also has a significant effect on the yield. As the effect is positive, it can be concluded that carbon dioxide retorting enhances the yield. This was also the case with the Colorado and some Eastern U.S. Devonian shales (2,5). The role of carbon dioxide in enhancing the yield from such shales while having negative effects on the yield from other shales is not completely understood. However, the trend indicates that carbon dioxide enhances the retorting yield from shales with a large kerogen content. This influence is much less or even negative when the kerogen content is low (Fischer Assay below 30) or medium (Fischer Assay of the order of 60 to 70). It has been known among various investigators that kerogen swells better in a carbon dioxide medium than in a nitrogen medium. This should normally result in an improved yield; however, it also enhances the probability of caking or agglomeration inside and outside the shale particles. Therefore highly caking shales, such as the North Carolina lacustrine shale do not exhibit an increase in oil yield and this caking phenomenon is also observed.

The influence of the particle size on the oil yield was insignificant. However, the interaction effect of the gas flow rate and the particle size was negative and significant. This also shows that mass transfer plays an important role in the process. Even though improved mass transfer conditions around the shale particle should directly result in a smoother transport of oil and vapor products out of the sample bed, complex, semi-macroscopic phenomena such as the blockage of pore mouths, gel or liquid entrapment within the pores, formation of new pores, agglomeration of particles, etc., are not easily accounted for. Therefore, it can be said that the total yield of oil from oil shale is not only directly related to the heat and mass transfer conditions, but also to the morphological changes and the swelling of kerogen.

The largest yield was indeed obtained with small size particles and low sweep gas flow rates coupled with the use of carbon dioxide. The significance of carbon dioxide is also indicated by the large positive abc interaction effect.

It can therefore be concluded that the optimal operating conditions for retorting Stuart shale are:

1. Use carbon dioxide as the sweep gas.
2. Operate at low sweep gas flow rates, i.e., 2 ml(STP)/sec.
3. Use smaller particles, i.e., -20 +40 mesh.

### Rundle Shale

The oil yield from Rundle shale was in the moderate range. The only significant main effect was from the sweep gas flow rate.

The influence of sweep gas flow rate in depressing the oil yield was most pronounced with the Rundle shale. Hence a corner test was performed by varying only the sweep gas flow rate while holding the particle size, type of sweep gas and the heating rate constant. The results show (Figure 1) that the optimal sweep gas flow rate is between 1 and 2 ml(STP)/sec.

It is interesting to note that even though carbon dioxide depresses the oil yield to a relatively insignificant extent, the interaction effect of the sweep gas type and flow rate is positive. This result also supports the prior conclusion that the oil yield is influenced not only by the mass transfer conditions, but also by the process of kerogen swelling and other morphological changes that occur during pyrolysis. The large interaction effect is shown schematically in a three-dimensional plot in Figure 2.

The optimal retorting conditions for the Rundle shale are therefore:

1. Use a sweep gas flow rate of 1.5 ml(STP)/sec.
2. Use nitrogen as the sweep gas, and
3. Use the larger size particles, i.e., -8 +10 mesh.

### Condor Shale

The Condor shale yielded the smallest amount of oil per kilogram of sample. It was observed in this case also that the sweep gas flow rate had a large negative influence on the oil yield. Moreover, the use of carbon dioxide also depresses the yield. The standard experimental error calculated by conducting replicate experiments was smaller in this case than in the other two cases. Such an influence was also observed in the case of Ohio shale. The accuracy of experimentation is improved with smaller yields. It should be noted here that in the case of Ohio shale, the quantity of sample used was larger in order to improve the resolution of the experiments (6).

As in the case of Rundle shale, the optimal retorting conditions are:

1. Use lower sweep gas flow rate, i.e., 2 ml(STP)/sec.
2. Use smaller size particles, i.e., -20 +40 mesh.
3. Use nitrogen as the sweep gas.

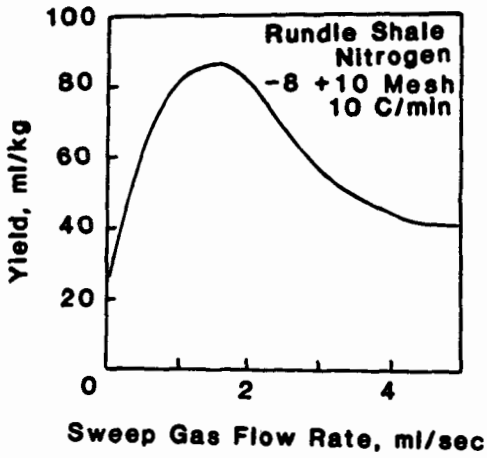


Figure 1. Optimization of Sweep Gas Flow Rate (ml (STP) of  $N_2$  / Second).

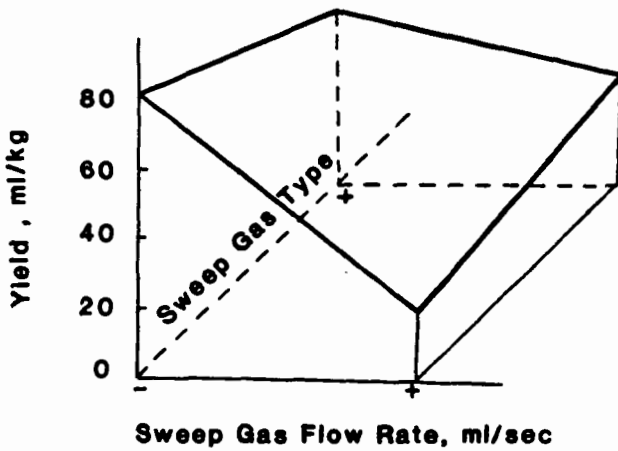


Figure 2. Schematic Representation of the Interactive Influence of Sweep Gas Type and Flow Rate on the Yield from Rundle Shale.

## CONCLUSION

A statistical experimental approach was used to determine the optimal retorting conditions for three Australian oil shales. The optimal conditions are summarized below:

Particle size:	Stuart -20 +40 mesh	Rundle -8 +10 mesh	Condor -20 +40 mesh
Sweep Gas Type:	Carbon dioxide	Nitrogen	Nitrogen
Gas Flow Rate:	2 ml(STP)/sec	1.5 ml(STP)/sec	2 ml(STP)/sec

It is also concluded that the yield from oil shale pyrolysis is influenced by many mechanistic factors such as the heat and mass transfer conditions, the swelling of kerogen in the rock matrix, morphological changes during pyrolysis, agglomerating properties etc. Therefore, the factors investigated in this statistical optimization study represent a set of process variables that are most important for the successful design and operation of retorting equipment. The vapor hourly space velocity of the sweep gas was also calculated for scale up purposes.

## REFERENCES

1. Branch M.C., Prog. Energy Combust. Sci., 5, pp 193 (1979).
2. Joshi R. and S. Lee, Liquid Fuels Technology, 1, pp 17 (1983).
3. Lee S., U.S. Patent No: 4,502,942. (1985).
4. Box G.E.P., W.G. Hunter, J.S. Hunter, Statistics for Experimenters, John Wiley and Sons, New York (1978).
5. Joshi R., Kinetic Study of Eastern Oil Shale Pyrolysis, Masters Thesis, The University of Akron (1983).
6. Lee S., M. Polasky, R. Joshi, Proceedings of 1983 Eastern Oil Shale Symposium, pp 225-233, University of Kentucky, Institute for Mining and Minerals Research (1984).

PYROLYSIS KINETICS OF VARIOUS AUSTRALIAN OIL SHALES  
IN NITROGEN AND CARBON DIOXIDE ATMOSPHERES

Mark E. Polasky and Sunggyu Lee

Department of Chemical Engineering  
The University of Akron  
Akron, Ohio 44325

ABSTRACT

The kinetics of oil generation from retorting of various Australian shales have been investigated under both nitrogen and carbon dioxide sweep gas conditions. Experiments were conducted both isothermally and nonisothermally with linear temperature control, in a unique fixed bed retorting system. The kinetics of these shales were directly compared with those of eastern and western U.S. shales, previously studied on the same experimental system.

The pyrolysis of the investigated Australian shales was found to comply with first-order global kinetics within the limits of experimental error. The activation energies calculated were: 217.2 kJ/gmole ( $\text{CO}_2$ ) and 114.8 kJ/gmole ( $\text{N}_2$ ) for Condor shale; 252.2 kJ/gmole ( $\text{CO}_2$ ) and 190.1 kJ/gmole ( $\text{N}_2$ ) for Rundle shale; 154.0 kJ/gmole ( $\text{CO}_2$ ) and 127.4 kJ/gmole ( $\text{N}_2$ ) for Stuart shale. The average Fisher assay of these shales are 62 cc/kg for Rundle, 63 cc/kg for Condor, and 100 cc/kg for Stuart shale.

INTRODUCTION

An experimental study has been performed in order to obtain the retorting kinetics of oil generation from various Australian Tertiary oil shales under both nitrogen and carbon dioxide sweep gas conditions. The carbon dioxide retorting has been investigated first by Lee et al. and proven efficient for the western U.S. type oil shale (1). Therefore, the rather nonconventional carbon dioxide retorting as well as the conventional nitrogen retorting has been applied to Australian shales.

The shale samples studied were taken from the Kerosene Creek member of the Stuart deposit, the Ramsey Crossing member of the Rundle deposit, and the Brown oil shale unit of the Condor deposit, all of which are located along the coastline of Queensland, Australia.

In order to obtain an unbiased comparison and to eliminate unaccountable systematic errors, a unique fixed bed retorting system was used to determine the kinetic parameters of each shale (2). Both the isothermal and nonisothermal retorting techniques were employed for the kinetic measurements, and the results compared favorably with each other. The pyrolysis of the Australian shales under investigation were found to comply with global first-order kinetics within the limits of experimental errors.

## THEORY

Three experiments for each shale under different isothermal conditions were carried out and the global power-law type rate expression was applied to analyze the data:

$$\frac{dx}{dt} = A[\exp(-E/RT)](1-x)^n \quad (1)$$

where  $x$  is the kerogen conversion based on the Fisher assay oil yield,  $E$  is the activation energy, kJ/gmol,  $A$  is the Arrhenius frequency factor, 1/sec, and  $n$  is the reaction order.

The nonisothermal technique eliminated the uncertainty of the initial heat-up period which had been an inherent problem with a fixed bed type retorter for an isothermal measurement. The kinetic parameters were obtained for the condition that a linear heating rate be maintained. The choice of a linear heating rate is to facilitate an easier mathematical analysis. For an overall first-order reaction, one obtains the following equation by integration (1):

$$-\ln(1-x) = \frac{AE}{CE} [e^{-u}u^{-2} - 2e^{-u}u^{-3}] \quad (2)$$

where  $C$  is the heating rate ( $dT/dt$ ) in C/min and  $u=E/RT$ . Rearranging equation (2) yields

$$\frac{-\ln(1-x)}{T^2} = \frac{AR}{CE} [(1 - 2RT/E) \exp(-E/RT)] \quad (3)$$

Taking natural logarithms on both sides of equation (3) gives

$$\ln \frac{-\ln(1-x)}{T^2} = \ln \left( \frac{AR}{CE} (1 - 2RT/E) \right) - E/RT \quad (4)$$

A plot of  $\ln[-\ln(1-x)/T^2]$  vs.  $1/T$ , which turns out to be a linear plot for  $RT/E \ll 1$ , gives the activation energy and the kinetic frequency factor for a first-order kinetics from the slope and intercept, respectively. The goodness of fit was a good indication of the validity of the assumed reaction order. A similar analysis can be done for an  $n$ -th order kinetics using successive approximation of exponential integrals and the best fitting order can be found by a regression technique (3).

## EXPERIMENTAL SYSTEM AND PROCEDURE

A schematic diagram of the apparatus used for this study and a detailed design of retorter internals are published elsewhere (2). Some of the features of this retorting system are considered to be special or unique. These features include the use of a stainless steel wire mesh distributor plate, so that a well-defined fluid dynamic condition is achieved with a minimal pressure drop, the use of a quick opening and closing ball valve which permits the instantaneous loading of a sample in addition to permitting the application of both isothermal and nonisothermal techniques to the same retorter, introducing a chromel-alumel thermocouple directly into the shale bed to obtain good temperature control and measurements, and by connecting two specially designed graduated U-tubes in series which allows the condensable product to settle in the bottom of the tubes while the noncondensable product to pass through a bridge across the tube arms.

A 20 gram sample of -35+40 mesh Australian oil shale was used for each experiment. For an isothermal measurement the retorter was preheated to a temperature about 100 C higher than the reaction temperature to facilitate an easy and fast control of the temperature. For a nonisothermal measurement the retorter was heated up at a linear heating rate of 10 C/min, which was found to be ideal for kinetic measurement. The sweep gas was sent into the retorter at the nominally same temperature as the shale samples for both isothermal and nonisothermal measurement. The flow rate used was 2 cc(STP)/sec and is equivalent to the vapor hourly space velocities of 720 hour<sup>-1</sup>. Since the length of the connecting line between the retorter and the collection tube was kept short and the temperature was kept high enough to keep the product as a vapor and the liquid holdup in the retort was negligible.

## DATA AND ANALYSIS

Nitrogen Retorting Kinetic parameters for the pyrolysis of Australian and eastern and western U.S. oil shales, under nitrogen sweep gas conditions are summarized in Table 1. As shown in the table, the relative rates obtained from isothermal and nonisothermal methods are nearly the same at 450 C. However, the kinetic parameters obtained from nonisothermal retorting may give a more realistic set of engineering information of the overall kinetic parameters for the design of efficient and economical retorting processes, since it comes closer to actual retorter conditions. It should be noted that the lower relative reaction rate for North Carolina shale was due to the fact that the retorting of this shale required a much higher initial retorting temperature than those for the other shales studied. Therefore, the practical retorting temperatures under nitrogen sweep gas conditions ranges from 400 to 500 degrees Celcius for all three types of Australian shales which matches the practical retorting conditions of most of the western U.S. shales.

Table 1. Kinetic Parameters for Nitrogen Retorting of  
Australian and Eastern United States Shales

Shale Type		Activation Energy, KJ/mol	Arrhenius Frequency Factor, (sec) <sup>-1</sup>	Relative Rates at 450°C
Rundle	N	190.09	4.17x10 <sup>12</sup>	1.000
	I	180.89	9.10x10 <sup>11</sup>	1.008
Stuart	N	127.36	9.05x10 <sup>7</sup>	0.739
	I	116.79	1.74x10 <sup>7</sup>	0.825
Condor	N	114.83	9.92x10 <sup>6</sup>	0.652
	I	104.08	1.94x10 <sup>6</sup>	0.762
Ohio	N	170.62	3.54x10 <sup>10</sup>	0.217
	I	185.32	3.53x10 <sup>11</sup>	0.187
West Virginia	N	203.11	5.74x10 <sup>12</sup>	0.158
	I	201.37	5.74x10 <sup>12</sup>	0.173
North Carolina	N	193.40	6.92x10 <sup>8</sup>	1.50x10 <sup>-5</sup>
	I	204.62	4.74x10 <sup>9</sup>	1.01x10 <sup>-4</sup>
Colorado	N	182.58	5.62x10 <sup>11</sup>	0.471

N denotes nonisothermal run

I denotes isothermal run

Table 2. Kinetic Parameters for Carbon Dioxide Retorting of  
Australian and Eastern United States Shales

Shale Type		Activation Energy, KJ/mol	Arrhenius Frequency Factor, (sec) <sup>-1</sup>	Relative Rates at 450°C
Rundle	N	252.17	1.39x10 <sup>17</sup>	1.000
	I	243.33	3.48x10 <sup>16</sup>	1.090
Stuart	N	154.01	1.21x10 <sup>10</sup>	1.076
	I	141.02	1.61x10 <sup>9</sup>	1.243
Condor	N	217.24	5.92x10 <sup>14</sup>	1.422
	I	209.17	1.65x10 <sup>14</sup>	1.518
Ohio	N	141.23	4.45x10 <sup>8</sup>	0.332
	I	136.07	2.33x10 <sup>8</sup>	0.410
West Virginia	N	183.56	2.27x10 <sup>11</sup>	0.148
	I	178.32	1.11x10 <sup>11</sup>	0.173
North Carolina	N	211.37	8.43x10 <sup>9</sup>	5.38x10 <sup>-5</sup>
	I	202.91	2.13x10 <sup>9</sup>	5.55x10 <sup>-5</sup>
Colorado	N	189.96	6.89x10 <sup>12</sup>	1.548

N denotes nonisothermal run

I denotes isothermal run

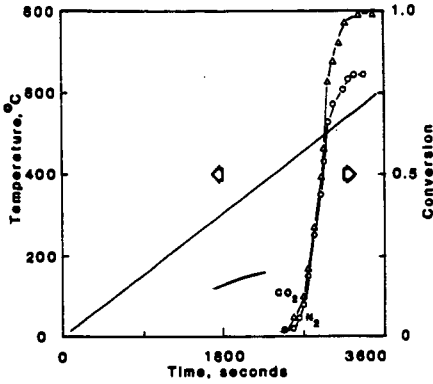


Figure 1.

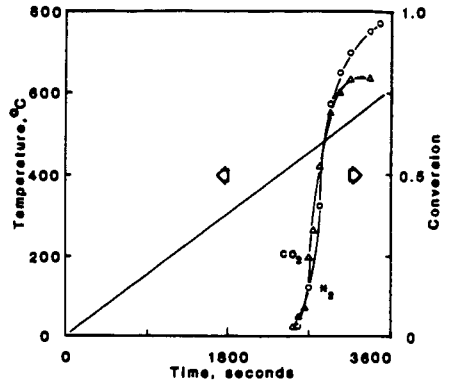


Figure 2.

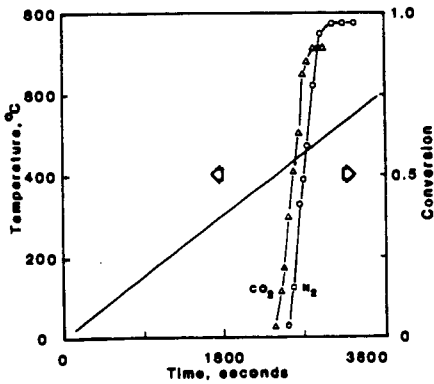


Figure 3.

Figure 1. Nonisothermal Kinetic Measurement of Stuart Shale under  $N_2$  and  $CO_2$ . -35+40 mesh; 10  $^{\circ}C/min$ ; 2 cc(STP)/sec.

Figure 2. Nonisothermal Kinetic Measurement of Rundle Shale under  $N_2$  and  $CO_2$ . (same conditions as Figure 1.)

Figure 3. Nonisothermal Kinetic Measurement of Condor Shale under  $N_2$  and  $CO_2$ . (same conditions as Figure 1.)

Carbon Dioxide Retorting Kinetic parameters for the pyrolysis of Australian and eastern and western oil shales under carbon dioxide sweep gas conditions are summarized in Table 2. Figures 1, 2, and 3 show the experimental data for nonisothermal kinetic measurement of pyrolysis of Stuart, Condor, and Rundle shales under nitrogen and carbon dioxide sweep gas conditions. It is interesting to note the difference in kinetic parameters between nitrogen and carbon dioxide retorting conditions. This is believed to be due to the difference in kerogen swelling in both gases and/or the differences in molecular penetration into pores between nitrogen and carbon dioxide. It has been known among the researchers that the kerogen in oil shale swells better in the carbon dioxide medium than the nitrogen medium. This is why carbon dioxide retorting is always kinetically faster than nitrogen retorting at nominally identical process conditions.

#### SUMMARY

The pyrolysis kinetics of various Australian oil shales were experimentally obtained using both isothermal and nonisothermal retorting techniques. The results from the two methods compared favorably with each other over a practical range of retorting temperatures. The pyrolysis reaction of the investigated Australian oil shales followed a global first-order kinetics very closely and the activation energies range from 110 to 250 kJ/gmole, depending on the type of shale. These values closely followed those for eastern and western U.S. oil shales retorted using the same experimental system. Every possible effort has been made to eliminate the internal and external mass transfer influence on the kinetics obtained, viz., using finely ground shales as well as providing optimal heat and mass transfer conditions.

In addition, the pyrolysis kinetics of various Australian shales were investigated both under nitrogen sweep gas conditions and under carbon dioxide sweep gas conditions and the results were directly compared. It was found that the carbon dioxide retorting process exhibits a kinetically faster rate of oil evolution from all the Australian shales. This result was true regardless of its impact on the overall yield from the shale and was equally valid for other types of oil shales including the Eastern and Western U.S. oil shales.

#### REFERENCES

1. Lee S. and Joshi R., U.S. Patent, No. 4,502,942 , (1985).
2. Joshi R. and Lee S., Liquid Fuels Technology, 1, 17, (1983).
3. Polasky M. E., ' Pyrolysis Kinetics and Process Optimization of Eastern United States and Australian Oil Shales ', Master's Thesis, The University of Akron, (1985).

# THE RETORTING OF SELECTED AUSTRALIAN OIL SHALES UNDER HIGH PRESSURE HYDROGEN AND NITROGEN

By

A. EKSTROM\*, C.J.R. FOOKES, K. WONG

CSIRO Division of Energy Chemistry, Lucas Heights Research Laboratories,  
Private Mail Bag 7, Sutherland, NSW 2232, Australia.

## INTRODUCTION

There is increasing interest in the effects of gas pressure on the retorting properties of oil shales, both as a means of increasing the oil yield and as an aid to developing a better understanding of the chemical processes involved in oil shale retorting. In the presence of hydrogen at pressures up to 7 MPa, significant increases in oil yield have been reported for some shales(1-5), and the technique forms the basis of the HYTORT process under development in the USA(6,7). Although the small increase in oil yield observed(8) when Green River shale was retorted under 2.7 MPa hydrogen was accompanied by a slight increase in the aromaticity(8-10), the changes in the composition of the oils produced from shales, which under higher hydrogen pressures gave very much greater oil yields (up to 500%), have not been reported.

The present work was undertaken to investigate the effects of hydrogen and nitrogen pressure at 6 MPa on the yields and composition of the oils produced from three Australian oil shales. These included Rundle as representative of the Tertiary shales of lacustrine origin found in Queensland, and Nagoorin as typical of the highly aromatic and organic rich shales of mixed lamossite/lignite origin(11). The extent of the Mt Coolon deposit, located approximately 200 km west of the city of Mackay in Queensland is at present unknown. The shale was formed in the early Miocene, is unusually rich in parts, and is probably best regarded as an immature torbanite(12).

## EXPERIMENTAL

Samples of the shales were crushed and sieved to  $-2.8 +1.4$  mm. Retorting was carried out at various pressures in a fixed bed reactor using a heating rate of  $6^{\circ}\text{C}/\text{minute}$  to  $550^{\circ}\text{C}$  followed by a 30 minute soak period. The gas flow rates were adjusted to give a constant residence time of 30 seconds at all pressures. This required very high gas flow rates at the higher operating pressures. The oils (condensed at  $-10^{\circ}\text{C}$ ) were analysed by gas chromatography/mass spectrometry (GC/MS: JEOL DX300) and nuclear magnetic resonance (NMR: JEOL GX400) techniques. Solution  $^{13}\text{C}$  spectra were determined in the presence of chromium relaxation reagents with an inverse gated decoupling and a recycle time of five seconds. Proton spectra were recorded with a recycle time of 20 seconds.

## RESULTS AND DISCUSSION

### (a) Properties of Shales

Table 1 illustrates the diversity of the shales used in this study with respect to their organic carbon content, atomic H/C ratio, aromaticity and retorting properties. Of particular interest are the very poor conversions of organic carbon in the shale to oil obtained under normal (Fischer Assay) retorting for the Mt Coolon and Nagoorin shales, indicating that for these shales conventional retorting procedures are not particularly effective.

#### (b) Effect of Pressure on Oil Yields

For all three shales, increasing nitrogen pressure resulted in only minor decreases in oil yields (Figure 1) and organic carbon conversions (Figure 2). Increasing hydrogen pressure had no effect on the oil yield from the aliphatic Rundle shale, although a reduction in the organic carbon remaining in the char was observed, presumably reflecting the conversion of the carbonaceous residue to methane, as has been previously observed for Green River shale(8).

However, increases of 150 and 350% of Fischer Assay oil yields were observed for the Mt Coolon and Nagoorin shales, equivalent to oil yields of 390 and 290 L t<sup>-1</sup> respectively, assuming an oil density of 0.9 g cm<sup>-3</sup>. These large increases are matched by corresponding decreases in the organic carbon remaining in the char (Figure 2) which, in the case of Nagoorin decreased from 58 to 24% at 6 MPa hydrogen. Increased hydrogen pressure resulted in only small changes in the conversion of organic carbon to gaseous products.

As shown in Figure 3, the oil yields determined for three Australian(13) aromatic shales retorted in 6 MPa hydrogen compared favourably with similar results(3) for a variety of other shales. Data on the importance of the total oil yield on the economics of HYTORT type processes do not appear to have been published, but it appears that the three Australian shales are particularly suited to retorting in high pressure hydrogen.

#### (c) Effect of Pressure on Oil Composition

Although increased oil yields are obviously important, the composition of the oil is equally significant from the viewpoint of the subsequent hydro-treatment and refining of the crude product.

Increasing nitrogen pressure had no effect on the <sup>1</sup>H and <sup>13</sup>C aromaticities of the whole shale oils (Figure 4), but large changes were observed with increasing hydrogen pressure, particularly for the Mt Coolon and Nagoorin shales. For example, the Nagoorin oil formed in 6 MPa hydrogen had carbon and proton aromaticities of 68 and 29% respectively. The data indicate that for the Mt Coolon and Nagoorin shales a substantial part of the additional oil formed in the presence of hydrogen is aromatic.

Examination of the whole oils by gas chromatography (GC) and gas chromatography/mass spectrometry (GC/MS) showed (Figure 5) that phenol, the cresols and dimethyl/ethyl phenols were prominent components of the oils retorted under high pressure hydrogen from the Mt Coolon and Nagoorin shales. These compounds also completely dominate the <sup>13</sup>C NMR spectra of these oils in the aromatic region but were absent in the oils retorted from the Rundle shale in both nitrogen and hydrogen.

Nitrogen had virtually no effect on the yield of any of the various molecular groups determined by proton NMR spectroscopy (Figure 6), as was expected from the absence of any corresponding effect on the total oil yield. However, large increases in the proportions of particularly polycyclic aromatics were observed for the Mt Coolon and Nagoorin shales retorted in the presence of hydrogen. Very much smaller increases in the relative proportions of these compounds were observed in oils retorted from the aliphatic Rundle shale.

Taken together, the results obtained for the Nagoorin and Mt Coolon oils retorted under hydrogen suggest that these are not normal shale oils, but more closely resemble coal-derived liquids, no doubt reflecting the partial lignitic origin of these shales. The results also indicate that for these shales in the

absence of hydrogen, a major coke forming process involves the decomposition of aromatic compounds, particularly phenols.

An unusual aspect of these results is the lack of any effects of shale composition and retorting conditions on the alkene yields. Proton NMR measurements showed that 3.2% of the protons in the Rundle oil were present as alkenes, 2.8% in Nagoorin oil and 2.4% in Mt Coolon oil. Similarly, the alkene content of Green River shale oil has been reported as 3.1%(8). Furthermore, the total alkene yield and the ratio of internal/terminal alkenes were not significantly affected by the presence of high pressure hydrogen or nitrogen. Similar results have been reported for Green River shale(8).

A possible source of alkenes is the disproportionation of alkane-free radicals produced in turn from the primary decomposition of the kerogen(14). However, it is not at all clear why quite different kerogens should give almost identical yields of alkenes. Further, it is difficult to accept that a hydrogen pressure of 6 MPa does not reduce the above disproportionation reaction, and even hydrogenate the newly formed alkenes.

#### (d) Model for Kerogen Decomposition

Published models for the decomposition of kerogen(8-10) are based on work with Green River shale which is highly aliphatic, produces an oil of low aromaticity with a yield and composition which are only marginally affected by hydrogen pressure, and which thus generally resembles the shale from the Rundle deposit. Our work has shown that the aromatic Mt Coolon and Nagoorin shales can be retorted under conditions which give oils containing large amounts of phenols and polycyclic aromatics and thus resemble coal pyrolysis liquids. For these shales, the reactions of the dominant aromatic components of the kerogen are at least equally as, and possibly even more important than those of the aliphatic components, whose behaviour dominates the retorting chemistry of shales from Rundle or Green River. For these aromatic shales, the following retorting model is proposed:

- (i) The organic matter in these shales is composed of material of algal (predominantly aliphatic) and lignitic (predominantly aromatic) origin. Varying amounts of wax and material derived from leaf cuticles may also be present and, for the Mt Coolon shale, these may be major components(12).
- (ii) The aliphatic components of the organic matter decompose to give largely aliphatic products. As shown by the work of Regtop et al.,(15) some of the aliphatic oil may be converted to aromatics by reactions catalysed by the spent shale surfaces. The contribution of such reactions to the total aromatic yield must however be small because of the very short residence times.
- (iii) The aromatic components of the shale organic matter decompose to aromatic and reactive products which, under normal retorting conditions, rapidly decompose to give coke and gas. Under certain circumstances, e.g. high pressure hydrogen or very short residence times, these compounds survive and appear in the oil as phenols and other aromatic compounds. The decomposition of these compounds during normal retorting serves as a preliminary clean-up of the oil, at the expense of the organic carbon conversion.
- (iv) The coke formed during pyrolysis of the aromatic shales can undergo further aromatisation reactions, as is shown by the loss of hydrogen

and methane at temperatures significantly higher than those normally required for retorting(16).

#### ACKNOWLEDGEMENTS

The authors thank Southern Pacific Petroleum NL/Central Pacific Minerals NL (Mr. J. Gannon) and the International Mining Corp. (Mr. D. Hawley) for the samples of shale used in this work. The assistance of Mr. C.H. Randall, Miss C. Walters and Mr. I. Liepa with the experiments, Mr. G.C. Wall who arranged the Fischer Assays and Ms. P. Udaja who carried out some of the analytical work is also gratefully acknowledged.

#### LITERATURE CITED

1. Janka, J.C. and Rex, R.C., The HYTORT Process, presented at the Oil Shale Symposium, Rabat, Morocco, April 1984.
2. Roberts, M.J., Feldkirchner, H.L., Punwani, D.V. and Rex, R.C., American Chemical Society Fuel Division Preprints, 29, 194 (1984).
3. Lynch, P.A., Janka, J.C., Lace, F.S., Feldkirchner, H.L., and Dirksen, H.A., American Chemical Society Fuel Division Preprints, 29, 71 (1984).
4. Rex, R.C. and Roberts, M.J., Paper presented at the 1983 Eastern Oil Shale Symposium, Lexington, Kentucky, 13-16 November, 1983.
5. Furimsky, E., Synnott, J., Boormen, R.S. and Salter, R.S., Fuel Process. Technol., 8, 293 (1984).
6. Anon. Synthetic Fuels from US Oil Shales, A Technical and Economic Verification of The HYTORT Process. DOE/ET/14102 (1981).
7. Falk, A.F., Garey, M.P. and Rosemary, J.K., Final Technical Report Application of Hydropyrolysis to the Hydroconversion of Eastern Oil Shale. ESC-DOE-13406 (1983).
8. Hershkowitz, F., Olmstead, W.N., Rhodes, R.P. and Rose, K.D., American Chemical Society Symposium Series 230, 301 (1983).
9. Burnham, A.K. and Singleton, M.F., *ibid.*, 335.
10. Burnham, A.K. and Happe, J.A., Fuel (in press)
11. Hutton, A.C., - Organic Petrology of Oil Shales. Ph.D. Dissertation, University of Wollongong, NSW, Australia (1983).
12. Chaffee, A., Ekstrom, A., Fookes, C.J.R., Glickson, M. and Loeh, H., Proceedings of the Second Australian Workshop on Oil Shale, Brisbane, 6-7 December, 1984, p.56.
13. Data for the Yaamba shale are taken from unpublished work by Ekstrom and Wong (1985).
14. Fookes, C.J.R. and Johnson, D.A., This symposium.
15. Regtop, R., Ellis, J., Crisp, P.T., Ekstrom, A. and Fookes, C.J.R., Proceedings of the Second Australian Workshop on Oil Shale, Brisbane, 6-7 December, 1984, p. 170.

16. Ekstrom, A., Hurst, H.J. and Randall, C.H., American Chemical Society Symposium Series 230, 317, (1983).

TABLE 1  
PROPERTIES OF OIL SHALE

PROPERTY <sup>a</sup>	RUNDLE	MT COOLON	NAGOORIN
<u>ANALYSIS</u>			
Weight loss on drying (%)	10	50	25
Inorganic carbon (%)	0.89	-	0.14
Organic carbon (%)	13.9	45.9	44.8
Hydrogen (%)	2.1	4.3	3.1
Nitrogen (%)	0.4	0.4	2.1
Sulphur (%)	0.6	3.1	1.5
H/C ratio	1.84	1.12	0.81
<sup>13</sup> C Aromaticity	0.20	0.33	0.48
<u>RETORTING</u>			
Fischer Assay (wt % dry shale)	11.0	24.6	7.6
Organic carbon in char (%)	14.8	45.2	41.6
Conversion of organic carbon to oil (%)	50	35	10

<sup>a</sup> Based on dry shale.

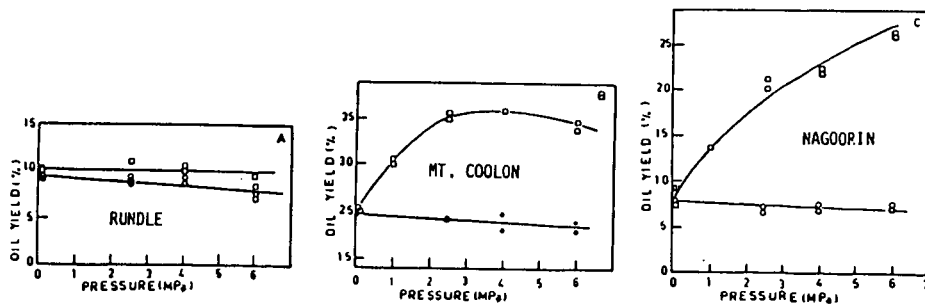


FIGURE 1. Effect of pressure on oil yields  
○ nitrogen, □ hydrogen

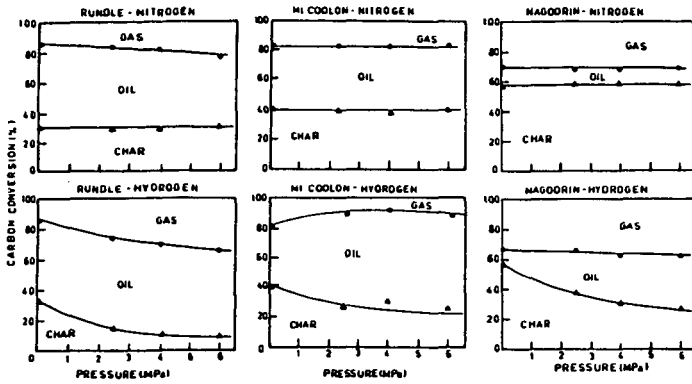


FIGURE 2. Effect of pressure on organic carbon distributions

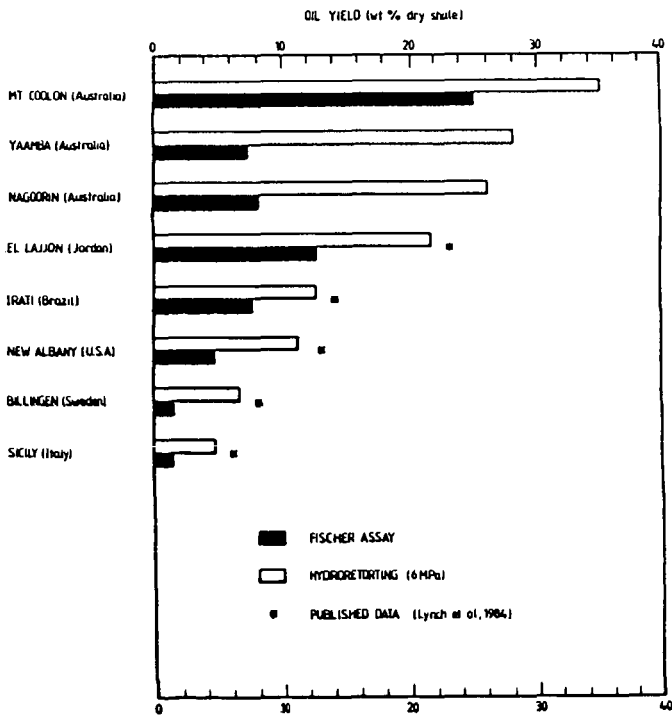


FIGURE 3. Comparison of the effects of hydrogen pressure on oil yields.

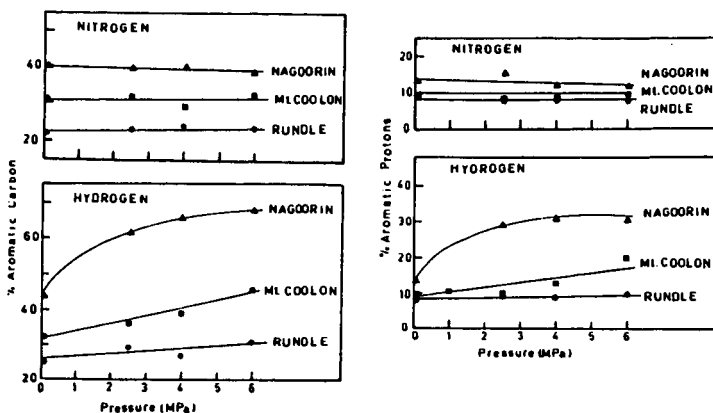
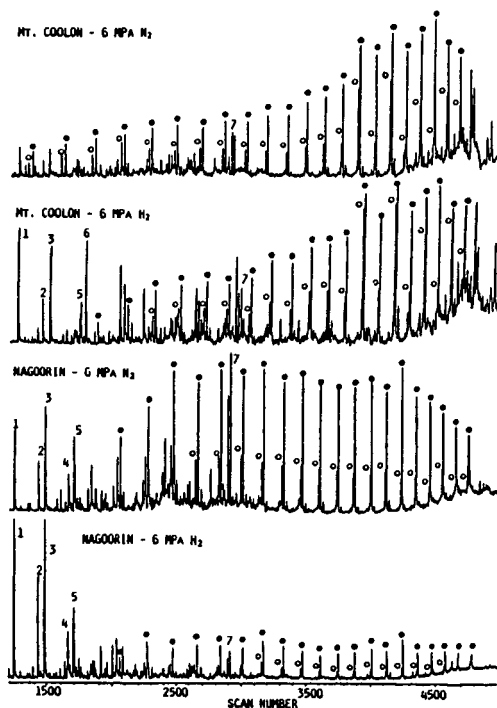


FIGURE 4 Effect of retorting pressure on carbon and proton aromaticities.

FIGURE 5. Total ion chromatograms of whole oils retorted in hydrogen and nitrogen.

- 1 phenol
- 2 o-cresol
- 3 m&p cresol
- 4 & 5 dimethyl and ethyl phenols
- 6 naphthalene
- 7 pristenes



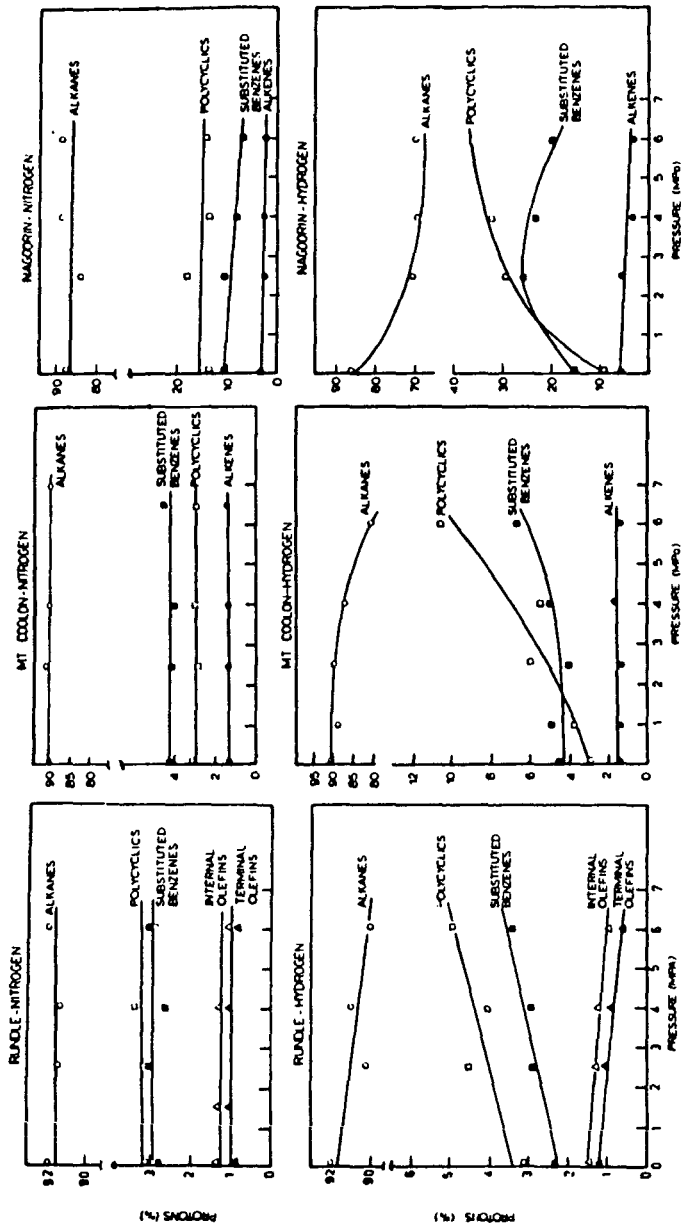


FIGURE 6. Effects of retorting pressure on the proton distributions in the shale oils.

## PYROLYSIS AND HYDROPYROLYSIS OF KENTUCKY OIL SHALE IN SUPERCRITICAL TOLUENE UNDER RAPID HEATING CONDITIONS

R.M. Baldwin and J.A. Manley  
Chemical Engineering Department  
Colorado School of Mines, Golden, CO 80401

### ABSTRACT

Oil shale from the Cleveland member of the Ohio shale, Montgomery County, Kentucky has been pyrolysed in supercritical toluene in the presence and absence of gas-phase molecular hydrogen. Data have been collected in a 300-cc stirred tank autoclave at residence times of 0<sup>+</sup>, 5, and 30 minutes, temperatures from 653 to 733 K, and total pressures (at temperature) ranging from 15.1 to 20.6 MPa. The reactor was equipped with a gas-driven sample injector so that shale could be injected into the pre-heated dense gas at reaction conditions. Heating rates of approximately 500 C/min were obtained with this configuration. Results for conversion of organic carbon to oil have been computed based on a carbon balance on the reaction system.

The objectives of the experimental program were:

- 1: investigate the use of toluene as a dense gas medium;
- 2: elucidate the reaction kinetics and the effect of hydrogen and heating rate on the rate and extent of oil formation. The data have shown toluene to be an excellent dense-gas media for facilitating supercritical pyrolysis and hydrolysis. Carbon conversions and oil yields of in excess of 185% of Fischer Assay were achieved in the presence of gas-phase molecular hydrogen at very short (<2 minute) residence times. Carbon conversion to oil was found to be a function of final temperature, hydrogen partial pressure, and heating rate.

### INTRODUCTION

Oil shale represents one of the largest hydrocarbon reserves in the world (1). Of the various techniques available for recovery of oil from oil shale, processes based on thermal decomposition of the organic matter in shale have received, by far, the most attention (2). Thermal decomposition or retorting technologies have been developed to a high degree of sophistication as evidenced by the TOSCO II, Union B, and Chevron. Unfortunately, retorting processes are plagued by inefficiencies in oil recovery which are inherent to the pyrolytic chemical reactions taking place. Principally, these inefficiencies result in low carbon conversion to oil due to free radical reactions such as cracking and condensation. In the case of cracking, a high gas make is promoted at the expense of oil while the oil product remaining is correspondingly high in olefin content. Regressive reactions due to condensation promote formation of coke. Both cracking and coking may be reduced to some extent by operation at low temperature and/or short residence times, or by processing in the presence of hydrogen and/or hydrogen transfer agents that act as free radical scavengers. It is the latter phenomenon that gives rise to interest in alternate oil shale processing schemes based on

reactions in dense gas media.

Kerogen in oil shale is known to be relatively insoluble in most organic solvents at or below their normal boiling points, but when oil shale is heated to temperatures above 600 K, the organic matter may be extracted in high yield (3,4). Several early patents describe solvent processing of torbanite and other shale-like materials at elevated temperatures both with and without hydrogen gas atmospheres (5,6,7,8). Jensen et al. (9) have reported on hydrogenation of Green River oil shale in vehicle oils, while Gregoli (10), Patzer (11), and Greene (12) have all recently been issued patents for hydrogenation of oil shale in hydrogen donor and non-donor solvents in the presence and absence of gas phase molecular hydrogen. Recently, McKay et al. (13) and Baldwin et al. (14) have reported on investigations using dense (supercritical) gases and subcritical fluids for extraction of shale oil from oil shale under a wide variety of processing conditions.

This paper presents the results of pyrolysis and hydrolysis of oil shale from the Cleveland Member of the Ohio shale group from Montgomery County, Kentucky. The objective of the research described was to investigate the effect of temperature, hydrogen partial pressure, time, and heating rate on carbon conversion and oil yield using toluene as the dense gas vehicle.

#### EXPERIMENTAL APPARATUS AND METHODS

All experiments were carried out in a 300-cc autoclave reactor, manufactured by Autoclave Engineers. The reactor was interfaced to an Apple II+ microcomputer for data acquisition and control of heating rate. A schematic of the system is shown in Figure 1. The as-received shale was processed by crushing (to 100 $\mu$  -200 mesh) and vacuum drying at 40 C. Dried shale was stored in a vacuum dessicator until used. A Fischer Assay of the feed shale is shown in Table 1. Also shown in this table are data on organic carbon conversion to oil for the Fischer Assay analysis, computed from quantitative analysis of the spent shale and retort gases for carbon, and a forced ash balance on the feed and spent shale. For the supercritical gas extraction experiments, helium and hydrogen were used as the reaction process gases, with a 1% krypton tracer employed so that gas make could be readily quantified. Spent shale recovered from the reactor was extracted with acetone and methylene chloride to remove adsorbed shale oil. Samples of the feed and spent shale were analyzed for total and inorganic carbon on a Coulometrics system.

#### DISCUSSION OF RESULTS

Experimental runs were made at temperatures between 653 and 733 K (380 and 460 C) in 20 degree increments, and at reaction times of 0 $\frac{1}{2}$ , 5, and 30 minutes. Prior to initiating heating of the reactor, 2.06 MPa (300 psi) of either helium or hydrogen was added to the reactor. This initial pressure plus the autogeneous pressure of the solvent (toluene) resulted in a total pressure at reaction temperature of between 15.1 and 20.6 MPa (2200 to 3300 psi). At these conditions, toluene (critical temperature 593.9

K, critical pressure 4.07 MPa) was present in the reactor as a dense gas. After heating to reaction conditions with only gas and toluene present in the reactor, the shale was injected into the vessel with an overpressure of helium. The reaction temperature rapidly rebounded to the desired temperature (generally within one minute). Following the desired reaction time, the reactor was quenched by forced convection. Samples of the spent shale were analyzed for total and inorganic carbon, and ashed in a muffle furnace. Carbon conversion to oil plus gas was then calculated based on a forced ash balance, while carbon conversion to gas was calculated from an analysis of the reaction product gases. Carbon conversion to oil, and thus oil selectivity, was then finally computed by difference. In the following discussion, oil selectivity refers to the fraction of carbon converted that is converted to oil.

Two baseline runs in helium and hydrogen atmospheres were performed at 698 K in order to establish the thermal reactivity of the shale in supercritical toluene. These runs were, however, done with the reactor used in the true batch mode of operation where the entire reaction mass was heated slowly (approximately 8 C per minute) to the final temperature, and then held at this level for one hour. Results of this run are shown in Table 2. As may be seen, an organic carbon conversion of 44.0% and oil selectivity of 91.6%, resulting in an overall conversion of carbon to oil of only 40.3% was achieved in the absence of hydrogen. This conversion level is consistent with the results obtained in standard Fischer Assay pyrolysis (viz. Table 1). Pyrolysis under these conditions in the presence of hydrogen however raises the carbon conversion to oil to 68.9%, thus demonstrating the well-recognized benefits attendant to hydrolysis of aromatic oil shales. Clearly, hydrogen in the reaction gas atmosphere greatly enhances carbon conversion. This is primarily accomplished by inhibiting condensation reactions which lead to formation of coke, as the oil selectivities differ by only about 10%. This observation is consistent with a radical quenching mechanism, promoted by the presence of gas phase molecular hydrogen.

Results for pyrolysis and hydrolysis in supercritical toluene under rapid heating conditions (c.a. 500 C/min) are shown in Figures 2, and 3. Figure 2 presents the kinetic data for organic carbon conversion obtained with hydrolysis under rapid heating conditions at an initial (cold) hydrogen pressure of 300 psi. As may be seen, the low temperature isotherms (653, 673, and 693 K) exhibit the expected time/temperature behavior. Hydrolysis at 713 and 733 K however shows an entirely different behavior, with the organic carbon conversion reaction becoming essentially instantaneous at the highest temperature studied (733 K). Oil selectivity (the fraction of carbon reacted that is converted to oil) at the highest temperature and shortest residence time is 95.6%. This, coupled with the 61.3% organic carbon conversion achieved at this combination of reaction conditions gives rise to an overall oil yield in excess of 185% of Fischer Assay. Perhaps more interesting however, is the effect of hydrogen on the reaction that is indicated in Figure 3. As illustrated, under conditions of rapid heating and low final

temperature (673 K), the organic conversion is insensitive to the presence of hydrogen in the reaction gas atmosphere over a wide range of residence times as shown by the essentially identical results for pyrolysis (helium atmosphere) and hydrolypyrolysis. This is in direct contrast to the slow heating data shown in Table 2, where hydrogen has a marked effect on the ultimate yield of oil. At 713 K, the presence of hydrogen has a small beneficial effect at the short residence time (5 minutes), and a substantial beneficial effect at the extended residence time of 30 minutes. At 733 K, the effect of hydrogen is pronounced over the entire range of reaction times studied, and is especially pronounced at 30 minutes. Considering these data in light of the previous data from the slow heating rate experiments serves to indicate that a complex mechanism involving both radical quenching and oil evolution rate processes is operative in this reaction system. Under conditions of rapid heating but at low final temperatures (673 K or less) the secondary condensation reactions leading to decreased oil yield are apparently sufficiently slow such that the carbon conversion reactions are not sensitive to the presence of added hydrogen. Reaction at high heating rates but higher final temperatures (713 K and above) however shows a significant sensitivity to the presence of gas-phase molecular hydrogen, especially at extended residence times. Apparently, under these conditions, regressive (coke-forming) reactions are sufficiently rapid that inhibition of condensation by radical quenching becomes significant, thus leading to enhanced organic carbon conversions. At high heating rates, significantly higher organic carbon conversions can be obtained with inert atmosphere pyrolysis when compared to the Fischer Assay as shown by a comparison of the high temperature helium atmosphere data in Figure 3 and the data in Table 1. This enhanced yield is, however, only present at short residence times (<5 minutes). This is undoubtedly due to the well documented effect of "flash pyrolysis", where the rapid rate of volatiles evolution is successful in preventing secondary reactions which decrease carbon conversion (15). At higher reaction severity (time/temperature combinations), some form of hydrogen activity is required to prevent the onset of regressive reactions with the resultant loss of carbon conversion.

#### ACKNOWLEDGEMENTS

The authors wish to acknowledge the financial support of Southern Pacific Petroleum, N.L. of Sydney, Australia. Conversations with Carl S. Minden and John Gannon were also helpful in execution and interpretation of the research.

#### LITERATURE CITED

1. Dickson, P.F., Oil Shale, Kirk-Othmer Encyclopedia of Chemical Technology, Vol. 16, Third Edition, 1981.
2. Baughman, G.L., Synthetic Fuels Data Handbook, second edition, Cameron Engineers, Inc., 1978.
3. Gavin, M.J., and Aydelotte, J.T., "Solubilities of Oil Shales in Solvents for Petroleum", Bureau of Mines R.I. 2313, 1922.
4. Dulhunty, J.A., "Solvent Extraction of Torbanite", Proc.

- Linnean Soc., New South Wales, vol. 67, 1942.
5. Ryan, H.D., "Bituminous Material from Oil Shale", U.S. Patent 1,327,572, Jan. 6, 1920.
  6. Hampton, H., "Hydrocarbons from Bituminous Shale-Like Material", U.S. Patent 1,668,898, May 8, 1928.
  7. Fisher, A., "Pyrolytic Conversion and Coking of Finely Divided Bituminous Material and Hydrocarbon Oil", U.S. Patent 2,073,367, March 9, 1937.
  8. Buchan, F.E., "Processing Oil Shale", U.S. Patent 2,487,788, November 15, 1949.
  9. Jensen, H.B., Barnet, W.I., and Murphy, W.I.R., "Thermal Solution and Hydrogenation of Green River Oil Shale", U.S. Bureau of Mines Bulletin 533, 1953.
  10. Gregoli, A.A., "Fluidized Bed Hydroretorting of Oil Shale", U.S. Patent 4,075,081, February 21, 1978.
  11. Patzer, J.F., "Recovery of Oil from Oil Shale", U.S. Patent 4,238,315, December 9, 1980.
  12. Greene, M.I., "Process for Hydrogenation/Extraction of Organics Contained in Rock", U.S. Patent 4,325,803, April 20, 1982.
  13. McKay, J.F., "Characterization of Organic Matter from Supercritically Treated Green River Oil Shale", CONFAB '84, Saratoga, Wyoming, July, 1984.
  14. Baldwin, R.M., Frank, W.L., Baughman, G.L., and Minden, C.S., "Hydroprocessing of Stuart A (Australian) Oil Shale", Fuel Processing Technology, 9, 1984.
  15. Anthony, D.B. and Howard, J.B., "Coal Devolatilization and Hydrogasification", AIChE Journal, vol. 22, no. 4, July, 1976.

FIGURE 1

Batch Reactor Schematic

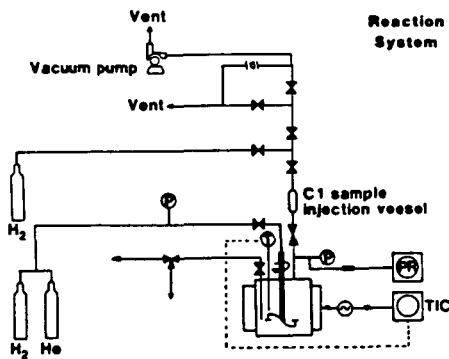


FIGURE 2

Organic Carbon Conversion Isotherms

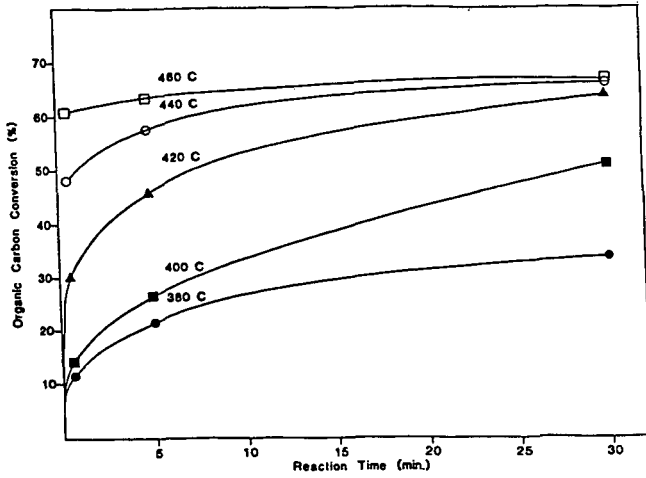


FIGURE 3

Inert Gas and Hydrogen Atmosphere Comparisons

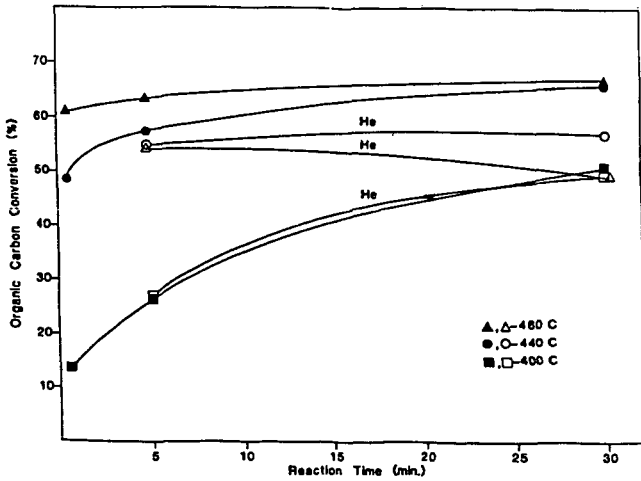


TABLE 1  
Analysis of Feed Shale

%spent shale	Fischer Assay <sup>1</sup>			oil, GPT	OCC <sup>2</sup>
	%oil	%water	%gas+loss		
91.6	4.6	1.5	2.3	11.6	42.9

1. Analysis by Commercial Testing and Engineering Co., Golden, CO
2. % organic carbon conversion to oil

TABLE 2  
Results under Slow Heating Rate Conditions<sup>1</sup>

	H <sub>2</sub>	He
OCC <sup>2</sup>	72.6	44.0
OY <sup>3</sup>	95.9	91.6

1. Reactions carried out in true batch mode, heating rate of approximately 8 C/min, 425 C final temperature, 300 psi initial hydrogen charge, 60 minutes residence time.
2. Organic carbon conversion to oil+gas, wt%.
3. Percent of organic carbon converted that is converted to oil.

## CHARACTERIZATION AND STABILITY PROPERTIES OF POLAR EXTRACTS DERIVED FROM A RECENT SHALE LIQUID

John V. Cooney\*, George W. Mushrush and Erna J. Beal

Naval Research Laboratory, Code 6180, Washington, D.C. 20375-5000

### INTRODUCTION

Recent studies into the mechanisms of storage instability with middle distillate fuels have indicated that the presence of polar compounds, particularly nitrogen heterocycles, is frequently related to the deterioration of aged fuel samples [1-5]. In certain instances, direct autoxidation of nitrogen containing species is indicated, which may be subject to catalytic effects made possible by trace fuel components [6,7]. At other times, the organic nitrogen compounds themselves assume the role of catalyst in the oxidation of other fuel molecules. One approach to the problem of nitrogen compound induced storage instability has involved model compound dopant studies [8,9]. A second approach involves the study of the stability properties of actual high-nitrogen middle distillate fuels [10,11]. In this paper we discuss the second approach which was applied to a recently refined high-nitrogen shale liquid. Thus, polar extract components were isolated, characterized and studied in the context of accelerated storage stability tests.

### EXPERIMENTAL

The high-nitrogen shale liquid which was examined in this study was refined from Geokinetics crude shale oil refined at the Caribou-Four Corners Refinery (Utah). The sample which was studied had been distilled and partially hydrotreated, and was designated at NRL as "fuel 83-65". Fuel 83-65 is identical to processing intermediate 1-HTR-3 recently studied by Thompson and Holmes [12]. Fuel 83-65 was separated into three polar extracts using a reported procedure involving extraction with acid (1.0 N HCl) followed by batch adsorption onto silica gel, which was subsequently back-washed with methylene chloride and methanol [10,11]. The three extracts thus provided were: (a) BNC ("basic nitrogen compound" extract, the acid-extractable material, in methylene chloride), (b) NBNC(CH<sub>2</sub>Cl<sub>2</sub>) ("non-basic" extract in methylene chloride), and (c) NBNC(CH<sub>3</sub>OH) (methanolic wash of the silica gel). The polar extracts were examined by capillary GC/MS using reported conditions [10].

The accelerated storage stability test method used has been described in detail [4]. In summary, 300 ml samples of filtered fuel were thermally stressed in the dark in 500 ml screw-cap borosilicate Erlenmeyer flasks (Teflon-lined caps). Replicate samples were run, with both filterable sediment and adherent gum values determined after storage. Peroxide numbers (ASTM D1583-60) were also determined in samples of filtered fuel before and after stress. Extract-doping experiments employed a very stable Navy Shale-II process shale diesel fuel, fuel D-11, as diluent. Fuel

D-11 has been well-characterized and contains AO-30 (2,4-dimethyl-6-t-butylphenol) as the sole additive [4]. All extracts were stripped of their solvent (verified by GC) by gentle rotary evaporation prior to being added to fuel D-11. Nitrogen concentration levels in fuel samples were determined by a chemiluminescent technique with an Antek Model 720 instrument [4,10].

### RESULTS AND DISCUSSION

Preliminary accelerated storage stability tests at 43°C and 80°C indicated that shale fuel 83-65 possessed marginal stability (Table I). The fuel was found to be relatively high in nitrogen content, containing 2290 ppm N (w/v). It was consequently of interest to us to examine the polar components of this shale liquid as part of an effort to relate fuel composition to stability behavior [10]. The high nitrogen content of fuel 83-65 permitted the convenient extraction of a significant amount of polar material for use in the subsequent doping experiments. In addition to these preliminary tests, the shale liquid was subjected to a simulated distillation analysis. Fuel 83-65 was found to be a broad-cut fraction. By ASTM D2887, IBP was 120°C, 50% was 299°C, 95% was 421°C and FBP was 485°C. Correlation to ASTM D86 gave IBP of 190°C, a 50% value of 306°C and a 95% value of 423°C. No hydroperoxide was detected in fuel 83-65 prior to or following storage stability testing (i.e., peroxide numbers were 0.0 by ASTM D1583-60).

Table I

Accelerated Storage Stability Results for Fuel 83-65  
(unvented - mg/100 ml)

<u>Storage Conditions</u>	<u>Filtered Sediment</u>	<u>Adherent Gum</u>	<u>Total Insolubles</u>		
			<u>Duplicate</u>	<u>Mean</u>	<u>Std.Dev.</u>
80°C-7 days	2.3	0.6	2.9		
	1.7	1.1	2.8		
	1.8	1.0	2.8	2.8	±0.1
80°C-14 days	4.5	2.6	7.1		
	3.7	4.9	8.6		
	3.5	2.9	6.4	7.4	±1.1
43°C-49 days	1.6	0.6	2.2		
	1.8	1.1	2.9		
	0.8	1.6	2.4	2.5	±0.4
43°C-91 days	2.5	2.2	4.7		
	2.4	2.2	4.6		
	2.1	3.2	5.3	4.9	±0.4

### Extraction of Nitrogen Compounds

The separation scheme which was used for the removal of polar extracts was patterned after an earlier procedure [10]. A single, mild acid extraction (using 3.67 equiv. of 1.0 N HCl) was selected to minimize the opportunity for chemical changes in the fuel. The BNC extract was obtained in methylene chloride following neutralization of the acid wash. Subsequent treatment of the acid extracted fuel with active silica gel afforded two NBNC extracts (in methylene chloride and methanol). The fuel and extracts were analyzed for soluble nitrogen content in order to assess a nitrogen balance (Table II). It was possible (within analytical error) to account for nearly all of the nitrogen originally present in fuel 83-65. The accelerated storage stability of fuel 83-65 was improved by the acid/silica treatment, with only ca. 2.4 mg/100 ml of total insolubles resulting after 14 day - 80° stress (cf. 7.4 mg/100 ml before extraction).

Table II

#### Nitrogen Analyses for Extracted Fuel 83-65

<u>Sample</u>	<u>N Concentration (ppm w/v)</u>
1. Original	2290
2. After acid extraction	700
3. Isolated in CH <sub>2</sub> Cl <sub>2</sub> wash of silica	490
4. Isolated in CH <sub>3</sub> OH wash of silica	75
5. After acid and silica treatment	130

### Examination of Polar Fuel Extracts

Components of the BNC, NBNC(CH<sub>2</sub>Cl<sub>2</sub>) and NBNC(CH<sub>3</sub>OH) extracts were examined by GC/MS by a procedure which has been reported [10]. The results for the acid extractable material (BNC) and the NBNC(CH<sub>3</sub>OH) extract are given together in Table III. Table III indicates that both of these extracts were rich in nitrogen heterocycles, principally alkyipyridines. The pyridines which were in the BNC extract were characterized by long alkyl chains (unbranched) while the NBNC(CH<sub>3</sub>OH) extract pyridines were highly branched and generally of a higher molecular weight. Table IV compares the identifications of the ten largest peaks found in these two extracts. The presence of a substantial amount of tetrahydroquinolines (ca. 29%) in the BNC extract is a reflection of the hydrotreatment used during processing. For all three polar fuel extracts, over 95% of the total sample peak area was identified, so that the peaks which were examined were representative of the samples.

Table III

Examination of BNC and NBNC(CH<sub>3</sub>OH) Extracts from Fuel 83-65

Compound Class*	BNC Extract		NBNC(CH <sub>3</sub> OH) Extract	
	n	Area %	n	Area %
A. Pyridines	(175)	(60.2)	(213)	(88.6)
<C <sub>4</sub>	12	0.7	6	0.6
C <sub>4</sub>	5	0.6	7	1.5
C <sub>5</sub>	19	0.6	15	0.6
C <sub>6</sub>	10	0.2	1	<0.1
C <sub>7</sub>	14	9.8	3	0.1
C <sub>8</sub>	20	16.4	6	0.1
C <sub>9</sub>	24	14.6	6	0.1
C <sub>10</sub>	22	9.9	10	0.8
C <sub>11</sub>	43	6.3	15	1.9
C <sub>12</sub>	6	1.2	28	5.5
C <sub>13</sub>	-	-	34	27.9
C <sub>14</sub>	-	-	39	26.4
C <sub>15</sub>	-	-	34	12.7
C <sub>16</sub>	-	-	9	10.3
B. Tetrahydroquinolines	(134)	(29.0)	(114)	(5.7)
<C <sub>3</sub>	6	0.6	2	0.2
C <sub>3</sub>	13	2.9	9	0.5
C <sub>4</sub>	19	12.8	2	0.1
C <sub>5</sub>	23	6.6	3	0.1
C <sub>6</sub>	29	3.2	5	0.1
C <sub>7</sub>	35	2.2	32	1.7
C <sub>8</sub>	8	0.6	17	1.0
C <sub>9</sub>	1	0.2	25	0.8
C <sub>10</sub>	-	-	12	0.5
C <sub>11</sub>	-	-	7	0.7
C. Quinolines	(54)	(7.9)	(12)	(0.2)
<C <sub>3</sub>	2	0.4	-	-
C <sub>3</sub>	7	2.1	-	-
C <sub>4</sub>	12	1.6	-	-
C <sub>5</sub>	18	3.2	-	-
C <sub>6</sub>	13	0.7	-	-
C <sub>7</sub>	2	<0.1	-	-
D. Indoles	(40)	(2.2)	(20)	(1.3)
<C <sub>7</sub>	10	0.7	-	-
C <sub>7</sub>	9	0.5	-	-
C <sub>8</sub>	18	0.8	-	-
C <sub>9</sub>	3	0.1	-	-
E. Carbazoles	(-)	(-)	(98)	(3.2)
<C <sub>4</sub>	-	-	8	0.1
C <sub>4</sub>	-	-	22	0.5
C <sub>5</sub>	-	-	38	1.1
C <sub>6</sub>	-	-	22	1.3
C <sub>7</sub>	-	-	5	0.1
C <sub>8</sub>	-	-	3	0.1
F. Other N Compounds	(16)	(0.8)	(16)	(0.4)
G. Other Compounds	(-)	(-)	(19)	(0.6)

\*"C<sub>x</sub>" denotes the no. of carbon atoms in substituents on the heterocyclic ring, "n" is the number of isomers observed, "Area %" is based on the total ion count from mass of 45 through 450.

Table IV

A. Ten Largest Peaks - BNC Extract From Fuel 83-65

<u>Rank</u>	<u>Rel. Area</u>	<u>Main Component</u>	<u>Retention Time (min)</u>
1	1000	Dimethylhexylpyridine	27:16
2	913	Methylpropyltetrahydroquinoline	26:26
3	870	Trimethylpentylpyridine	26:15
4	854	Dimethylheptylpyridine	30:32
5	825	Dimethylhexylpyridine	28:10
6	775	Dimethylpentylpyridine	23:51
7	676	Trimethylhexylpyridine	29:30
8	660	a C <sub>4</sub> Tetrahydroquinoline	25:59
9	472	Trimethylhexylpyridine	28:58
10	413	a C <sub>8</sub> Pyridine	27:07

B. Ten Largest Peaks - NBNC(CH<sub>3</sub>OH) Extract From Fuel 83-65

<u>Rank</u>	<u>Rel. Area</u>	<u>Main Component</u>	<u>Retention Time (min)</u>
1	1000	a C <sub>13</sub> Pyridine	37:48
2	549	Trimethyltridecylpyridine	47:12
3	544	a C <sub>13</sub> Pyridine	38:09
4	495	a C <sub>16</sub> Pyridine	47:15
5	375	Trimethylundecylpyridine	42:26
6	317	Trimethyldecylpyridine	39:53
7	281	Dimethyltridecylpyridine	45:19
8	260	Trimethylundecylpyridine	40:49
9	251	Dimethylundecylpyridine	40:14
10	238	Trimethylundecylpyridine	43:29

The methylene chloride NBNC extract was found to be very complex, consisting primarily of hydrocarbons. Most of the nitrogen in this extract appeared in the form of substituted indoles. The compound classes present are summarized in Table V.

Table V

Examination of NBNC(CH<sub>2</sub>Cl<sub>2</sub>) Extract From Fuel 83-65

<u>Compound Class</u>	<u>No. Isomers</u>	<u>Area %</u>
A. <u>Hydrocarbons</u>	(294)	(91.3)
Alkanes	33	44.8
Cycloalkanes	35	2.1
Benzenes	80	10.7
Naphthalenes	22	8.5
Tetralins	53	11.1
Indanes	15	2.8
Fluorenes	15	4.2
Phenanthrenes	9	3.8
Biphenyls	11	2.1
Other Hydrocarbons	21	1.2
B. <u>Nitrogen Compounds</u>	(37)	(8.7)
Indoles	27	6.0
Other Nitrogen Compounds	10	2.8

Results of Doping Experiments

The polar components of each of the three extracts were added as dopants to a stable shale diesel fuel (fuel D-11). Stress conditions employed temperatures of 80°C and 43°C for periods of time ranging up to 14 and 154 days respectively [8,10]. The results of the doping experiments are given in Table VI. In the table, the amount of total insoluble material is reported as the mean of three experimental trials.

Table VI

Total Insolubles for D-11 with Added Polar Extracts

<u>Extract</u>	<u>Storage Conditions</u>	<u>N Added (ppm-w/v)</u>	<u>Total Insolubles(mg/100 ml)</u>	
			<u>Mean</u>	<u>Std. Dev.</u>
BNC	80°C-7d	337	1.6	±0.2
	80°C-14d	337	1.3	±0.6
	43°C-77d	337	0.5	±0.0
	43°C-154d	337	0.7	±0.1
NBNC(CH <sub>2</sub> Cl <sub>2</sub> )	80°C-7d	264	4.3	±0.6
	80°C-14d	264	4.7	±0.6
	43°C-70d	264	4.1	±0.2
NBNC(CH <sub>3</sub> OH)	80°C-14d	163	63.7	±22.5
undoped D-11	80°C-14d	0	0.0	±0.1
	43°C-52d	0	0.1	±0.2
	43°C-154d	0	0.4	±0.0

The results of the dopant experiments indicated that the methanolic NBNC extract was by far the most active sediment promoter in the D-11 fuel, about as active as 2,5-dimethylpyrrole on a ppm N (w/v) basis [4]. This is the most active fuel extract we have yet isolated; it is considerably more reactive than the NBNC(CH<sub>3</sub>OH) extracts obtained from other shale fuels in earlier work [10]. Notable constituents of the methanolic NBNC extract were branched alkylpyridines as well as alkylcarbazoles, which have yet to be studied as model dopants in well-defined systems [4]. We speculate that these species may be involved in the oxidation reactions of storage instability. It was surprising to isolate such a reactive extract from fuel 83-65, since the fuel is actually quite a bit more stable than other shale fuels which we have studied (cf. Table I and ref. 10). This clearly indicates the importance of complex "interactive effects" present in a given fuel in controlling and allowing the expression of oxidative lability of sensitive molecules [7]. Thus, it is possible that natural antioxidants present in fuel 83-65 normally suppress the tendency of the components of extract NBNC(CH<sub>3</sub>OH) to oxidize or initiate oxidation processes.

The NBNC(CH<sub>2</sub>Cl<sub>2</sub>) extract was found to be a mild promoter of instability, while the BNC extract had little effect despite the fact that some 337 ppm N (w/v) had been added to the D-11 base fuel. The inertness of the BNC extract may be a result of reduced oxidizability of straight-chain alkylpyridines (relative to branched) or may be due to inhibition as a result of the high tetrahydroquinoline content [10]. Instability promoted by the NBNC(CH<sub>2</sub>Cl<sub>2</sub>) extract may be a consequence of the presence of modest amounts of olefins and alkylindoles in this extract.

#### CONCLUSIONS

Polar fractions have been isolated and characterized from a recently refined shale-derived liquid. When the extracts were added as dopants to a stable shale diesel fuel and stored at elevated temperatures, the formation of insoluble material was observed. The most active extract in promoting instability consisted primarily of branched alkylpyridines (not acid-extractable) together with modest amounts of tetrahydroquinolines and alkylcarbazoles.

#### ACKNOWLEDGEMENT

This work was funded by the Department of Energy under an interagency agreement, contract no. DE-AI-19-81-BC10525. References to brand names were made for identification only and do not imply endorsement by DOE or NRL.

#### LITERATURE CITED

- (1) Frankenfeld, J.W., Taylor, W.F. and Brinkman, D.W., U.S. Department of Energy Report No. DOE/BC/10045-12 (1981).
- (2) Frankenfeld, J.W., Taylor, W.F. and Brinkman, D.W., Ind. Eng. Chem. Prod. Res. Dev., 22, 608, 615, 622 (1983).
- (3) Goetzinger, J.W., Thompson, C.J. and Brinkman, D.W., U.S. Department of Energy Report No. DOE/BETC/IC-83/3 (1983).
- (4) Cooney, J.V., Beal, E.J. and Hazlett, R.N., Liq. Fuels Tech., 2, 395 (1984).
- (5) Dahlin, K.E., Daniel, S.R. and Worstell, J.H., Fuel, 60, 477 (1981); Worstell, J.H. and Daniel, S.R., Fuel, 60, 481 (1981); Worstell, J.H., Daniel, S.R. and Frauenhoff, G., Fuel, 60, 485 (1981).
- (6) Frankenfeld, J.W., Taylor, W.F. and Brinkman, D.W., U.S. Department of Energy Report No. DOE/BC/10045-23 (1982).
- (7) Cooney, J.V., Beal, E.J. and Beaver, B.D., Preprints, Div. of Fuel Chem., ACS, 30, in press (1985).
- (8) Cooney, J.V., Beal, E.J. and Hazlett, R.N., Preprints, Div. of Petro. Chem., ACS, 28, 1139 (1983).
- (9) Cooney, J.V., Beal, E.J., Wechter, M.A., Mushrush, G.W. and Hazlett, R.N., Preprints, Div. of Petro. Chem., ACS, 29, 1003 (1984).
- (10) Cooney, J.V., Beal, E.J. and Hazlett, R.N., Preprints, Div. of Petro. Chem., ACS, 29, 247 (1984).
- (11) Cooney, J.V., Beal, E.J. and Hazlett, R.N., Ind. Eng. Chem. Prod. Res. Dev., in press (1985).
- (12) Thompson, L.F. and Holmes, S.A., Fuel, 64, 9 (1985).